STUDY OF BEAM INJECTION, BEAM OPTICS AND INSERTION DEVICES FOR SYNCHROTRON RADIATION SOURCE: A CASE STUDY OF INDUS-1 AND INDUS-2

By

ALI AKBAR FAKHRI
Enrolment No. PHYS 03201004015

Raja Ramanna Centre for Advanced Technology, Indore

A thesis submitted to the

Board of Studies in Physical Sciences

In partial fulfillment of requirements

for the Degree of

DOCTOR OF PHILOSOPHY

of

HOMI BHABHA NATIONAL INSTITUTE

August 2016

Homi Bhabha National Institute

Recommendations of the Viva Voce Committee

As members of the Viva Voce Committee, we certify that we have read the dissertation prepared by **Ali Akbar Fakhri** entitled " **Study of Beam Injection, Beam Optics and Insertion Devices for Synchrotron Radiation Source: A case study of Indus-1 and Indus-2**" and recommend that it may be accepted as fulfilling the thesis requirement for the award of Degree of Doctor of Philosophy.

S B Roy	7.2.17
Chairman - Prof. S. B. Roy	**Date:**
Arup Banerjee	07/02/2017
Guide / Convener - Prof. Arup Banerjee	**Date:**
V Nanal	
Examiner - Prof.V. Nanal	**Date:** 7/2/17
for V.K. Senecha	07/02/2017
Member 1- Prof.P. Singh	**Date:**
S R Mishra	07.02.2017
Member 2 -Prof. S.R.Mishra	**Date:**
Vinit Kumar	7.02.2017
Member 3- Prof.Vinit Kumar	**Date:**
	7.2.17
Member 4 -Prof. T. K. Sharma	**Date:**
Anand Moorti	
Member 5 -Prof. Anand Moorti	**Date:** 7/2/2017.

Final approval and acceptance of this thesis is contingent upon the candidate's submission of the final copies of the thesis to HBNI.

I/We hereby certify that I/we have read this thesis prepared under my/our direction and recommend that it may be accepted as fulfilling the thesis requirement.

Date: 7th February, 2017

Place: Indore

Arup Banerjee

Dr. Arup Banerjee

Guide

STATEMENT BY AUTHOR

This dissertation has been submitted in partial fulfillment of requirements for an advanced degree at Homi Bhabha National Institute (HBNI) and is deposited in the Library to be made available to borrowers under rules of the HBNI.

Brief quotations from this dissertation are allowable without special permission, provided that accurate acknowledgement of source is made. Requests for permission for extended quotation from or reproduction of this manuscript in whole or in part may be granted by the Competent Authority of HBNI when in his or her judgment the proposed use of the material is in the interests of scholarship. In all other instances, however, permission must be obtained from the author.

Ali Akbar Fakhri

DECLARATION

I, hereby declare that the investigation presented in the thesis has been carried out by me. The work is original and has not been submitted earlier as a whole or in part for a degree / diploma at this or any other Institution / University.

Ali Akbar Fakhri

List of publications arising from the thesis

A.1 Papers in refereed Journals

[1] **Ali Akbar Fakhri**, A.D.Ghodke, and Gurnam Singh, “Effect of wavelength shifter on Indus-1”, Nuclear Instruments and Methods in Physics Research A, 613 (2010) 169-176.

[2] **Ali Akbar Fakhri**, S.K. Prajapati, A.D.Ghodke, and Gurnam Singh, “Studies of beam injection with a compensated bump and uncompensated bump in a synchrotron”, Review of Scientific Instruments, 84, 083303 (2013).

[3] **Ali Akbar Fakhri**, Pradeep Kant, Gurnam Singh and A.D.Ghodke, “An analytical study of double bend achromat lattice”, Review Of Scientific Instruments, 86, 033304 (2015).

[4] **Ali Akbar Fakhri**, Pradeep Kant, A.D.Ghodke and Gurnam Singh, “Beam emittance reduction during operation of Indus-2”, Review of Scientific Instruments, 86, 113305 (2015).

A.2 Papers published in conferences

[1] **Ali Akbar Fakhri**, P. Kant, A. D. Ghodke and G.Singh, “Low emittance electron beam optics commissioning in Indus-2”, InPAC2011, Paper ID 171, IUAC, Delhi, Feb., 15-18, 2011.

[2] **Ali Akbar Fakhri** and A.D.Ghodke, “Electron Beam Optics Of Indus-2 In Presence Of Insertion Devices”, InPAC2013, Paper ID 74, VECC, Kolkata, Nov., 19-22, 2013.

A.3 RRCAT Newsletters

[1] **A.A. Fakhri**, A.D. Ghodke, “Commissioning of low emittance electron beam optics in Indus-2”, RRCAT Newsletter, Vol. 25, Issue 2, 2012.

Ali Akbar Fakhri

I dedicate this dissertation to my doting parents,

Late Mr. Husain (Maqbool Husain) Barkat Ali Fakhri

&

Late Mrs. Samina (Suraiyya) Fakhri

ACKNOWLEDGMENT

By the grace of Allah, Vasila-e-Panjaetan Pak AS and with kind benedictions of Syedna Mohammed Burhanuddin (R.A.) and Syedna Aali Qadar Mufaddal Saifuddin (T.U.S), I am able to do research studies.

I would like to express my sincere gratitude to my technical advisor Sh. Gurnam Singh for the continuous support, patience, motivation and immense knowledge to conduct the research work. I have benefited a lot from his wide vision and innovative ideas which helped me in all the time of research and writing of this thesis.

I am thankful to Dr. Arup Banerjee (Head, BARC training school at RRCAT) who kindly agreed to be my guide for the PhD work. He reviewed my research work and gave very useful advice during the entire course of my PhD work.

I would like to thank Doctoral Committee Dr. S. B. Roy, Dr. P. Singh, Dr. Vinit Kumar, Dr. S. R. Mishra, Dr. T.K. Sharma and Dr. Anand Moorti for critically reviewing the progress of my work which helped me to put more efforts in this task. It is a pleasure to gratefully acknowledge the valuable suggestions received from Sh. A. D. Ghodke.

I am extremely thankful to colleagues from Indus accelerator program and operation crew member for the help in carrying out the experiments in Synchrotron and in Indus-2.

It is a pleasure to thank Dr. P. D. Gupta, Ex-Director, RRCAT, Shri A. C. Thakurtta Head Power Supply and Industrial Accelerator Division and Shri T. A. Puntambekar, Head, Indus Operations, Beam Dynamics and Beam Diagnostics Division for continuing to provide full support to this work.

I am very thankful to Shri Pradeep Kant and Shri S. K. Prajapati, who have been involved in this work with me since the beginning.

I sincerely thank Dr. Amalendu Sharma, Dr. M. H. Modi, Dr. Pradeep kumar, Sh. K. Saifee, Sh. Y. Kelkar, Sh. Y. Singh, Smt. S. Gangopadhyay, Sh. Y. M. Sheth, Sh. D. Baxy, Sh. P. Mohania, Sh. J. Musuku, Dr. M Borage, Sh. Akash Deep, Sh. S. Yadav, Dr. Gautam Sinha, Sh. R. K. Agrawal and all my colleagues in Beam Dynamics Laboratory, who provided me help during my research work.

Above all, it would have not been possible for me to achieve this milestone in my research career without encouragement and support from my all family members who have dreamed and prayed for my all around success. My late parents for their grace, who hold exceptional concerned about my success and imparted a great enthusiasm in my life. Without active support of my wife Tasneem and daughters, I couldn't imagine to triumph over different landmarks during my research career. I am also thankful to my parents in laws, sister, brothers, and sister in laws, who have prayed for my success.

CONTENTS

Homi Bhabha National Institute

SYNOPSIS OF Ph. D. THESIS

1.	**Name of the Student:**	**Ali Akbar Fakhri**
2.	**Name of the Constituent Institute:**	**RRCAT, Indore**
3.	**Enrolment No.:**	**PHYS 03201004015**
4.	**Title of the Thesis:**	**Study of Beam Injection, Beam Optics and Insertion Devices for Synchrotron Radiation Source: A case study of Indus-1 and Indus-2**
5.	**Board of Studies:**	**Physical Sciences**

SYNOPSIS

Synchrotron radiation is the electromagnetic radiation emitted by highly relativistic charged particles, when they are radially accelerated. Electron storage rings, which are designed specifically for the production of synchrotron radiation, are termed as synchrotron radiation sources. In these storage rings, synchrotron radiation is produced using dipole magnets and insertion devices. Dipole magnets are used to bend the electron beam imparting above mentioned radial acceleration to electrons. Insertion devices are devices having periodic arrangements of dipole magnets, and are classified as wigglers and undulators. Synchrotron radiation is widely used because of its unique characteristics such as high spectral flux and brightness, broad band spectrum from infrared to hard X-ray, highly collimated and polarized, pulsed time structure and its uninterrupted availability for several hours. The spectral characteristics of the radiation are decided by the energy, emittance and current of the stored electrons, dipole-magnet field and configuration of insertion devices.

An important parameter for synchrotron radiation users is the spectral brightness of emitted photon beam, which is governed by the electron beam emittance. Smaller the beam emittance, higher is the spectral brightness [1] of the emitted photon beam. This is achieved by choosing a suitable magnetic lattice and a large number of cells of the chosen lattice. The magnetic lattice is a periodic arrangement of magnets namely dipole, quadrupole and sextupole magnets, which are arranged in a closed loop. In addition to this, a storage ring has long straight sections preferably dispersion free for installation of insertion devices. The twiss parameters (β, α governing width and divergence of the electron beam at various locations) in these sections are also chosen such that the effect of insertion devices on the beam dynamics is minimum. The commonly used magnetic lattice structures include double bend achromats, triple bend achromats, multiple bend achromats and FODO lattices [2-8] (alternate arrangement of focusing and defocusing quadrupole magnets).

An injector, which is normally either a linear accelerator or a synchrotron, is required for injecting an electron beam into the storage ring. The beam energy from the injector may be either equal to or less than the final beam energy in the storage ring. The storage ring, in which the beam is injected at lower beam energy, a higher beam current from the injector is required to reduce the filling time of the ring.

Raja Ramanna Centre for Advanced Technology (RRCAT) in Indore (India) is house for two synchrotron radiation sources, known as Indus-1[9] and Indus-2[10]. Indus-1 is a 450 MeV small storage ring, which is designed to produce radiation in vacuum ultraviolet region mainly from its dipole magnet (critical wavelength 31A^{o}). The magnetic lattice of the Indus-1 is a combined function lattice, consisting of 4 superperiods, each having one dipole magnet and two doublets of quadrupole~~s~~ magnets. On the other hand, Indus-2 is a 2.5 GeV energy machine classified as third generation x-ray synchrotron radiation source. This has a double bend achromat lattice and which has been designed to operate with a beam emittance of 58 nm.rad at 2.5 GeV. Both storage rings have a common injector which is a synchrotron with a microtron as the pre-injector. The microtron is the accelerator in which electrons are produced and accelerated to 20 MeV. These electrons are, then injected into the synchrotron at a repetition rate of 1Hz. In this, electrons are accelerated from 20 MeV to 450/550 MeV with the help of an RF cavity and by synchronously ramping the magnetic fields of its dipole, quadrupole and steering magnets. After acceleration to the required beam energy, the beam is extracted from the synchrotron for its injection to Indus-1 and Indus-2. In Indus-1, electron beam is injected at the peak energy of the ring i.e. at 450 MeV, whereas in Indus-2 electrons are injected at 550 MeV and after storage of required beam current, they are accelerated to 2.5 GeV.

The objective and scope of thesis is to study beam injection, beam optics and insertion devices for synchrotron radiation sources. To this end in this thesis, we focus on the following aspects of synchrotron radiation sources.

1) Beam injection dynamics of the synchrotron.
2) Beam optics of double bend achromat lattice and their application to Indus-2 and a scheme for reducing beam emittance in Indus-2.
3) Effect of insertion devices like a wavelength shifter on the beam dynamics of Indus-1.

In the synchrotron, a three kicker magnets multi turn compensated bump injection scheme [11] has been employed for beam injection. The beam is injected in the horizontal plane with the help of an injection septum magnet, which is kept close to the focusing quadrupole magnet. In this case, at the injection septum magnet location, twiss parameters (β and α) have a large values. The high value of horizontal β-function helps in maximizing horizontal beam acceptance of the synchrotron, which is desirable for beam injection. The high value of α-function plays an important role in deciding the amplitude of residual oscillations during and after beam injection. The performance of the synchrotron in terms of accelerated beam current was found better (from ~1.3 mA to ~3.2 mA), when all the three kicker magnets are operated at the same current than the situation when kicker magnets are operated at currents required to generate the compensated bump. The first topic listed above involves study of beam dynamics by tracking of electrons for a large number of turns to understand this phenomenon.

In the second topic of the thesis, beam optics of the double bend achromat lattice has been studied. The double bend achromat structure contains two dipole magnets and the drift space between two dipole magnets contains either a single focusing quadrupole magnet or combination of focusing and defocusing quadrupole magnets to form the achromat. Here, the dispersion function and its derivative of an electron entering the first dipole magnet and that of the beam coming out of second dipole magnet are zero. The achromat structure plays an important role in deciding the beam emittance and dynamic aperture. The beam emittance in a lattice is proportional to the cube of bending angle of the dipole magnet. Thus the beam emittance can be reduced significantly by reducing the bending angle of the dipole magnet. In this case, dynamic aperture is reduced due to higher strengths of sextupole magnets, needed for chromaticity correction, which is a consequence of smaller dispersion function. In a storage ring with a smaller number of unit cells, bending angle is relatively large as compared to the rings with a higher number of unit cells. In the former case, beam emittance is higher, and consequently sextupole strengths are lower. The beam emittance in a given lattice can also be optimized with a proper choice of the achromat structure. In the literature, no analytical approach is available for providing guidance on how to choose quadrupole magnets in the achromat part of a double bend achromat to obtain theoretical minimum beam emittance. In a double bend achromat, Chasman-Green lattice [2] represents the basic structure for low emittance synchrotron radiation sources. In this lattice, single focusing quadrupole magnet (QF) is used to form an achromat. In this thesis work, we carry out study of this structure assuming quadrupole magnets to be thin lenses and derive an analytical expression, showing the limitation of this lattice in achieving the theoretical minimum beam emittance. From the point of view of achieving the theoretical minimum emittance, analytical expressions are derived for the achromats having two, three and four quadrupole magnets. In a two quadrupole magnet structure, two focusing quadrupole magnets are used. The three- and four-quadrupole magnet structures consist of three and four quadrupole magnets respectively and have different combinations of focusing (QF) and defocusing (QD) quadrupole magnets. The magnetic lattice configuration of Indus-2 is a double bend achromat in which its achromat part has QF-QD-QF structure. This analytical study is extended for Indus-2 and the issue of achromat length chosen for it is addressed.

Beam optics studies carried out during the thesis work also include the scheme evolved and implemented to reduce the beam emittance in Indus-2 at final beam energy. The storage ring of Indus-2 was commissioned with a moderate optics in which beam emittance was 135 nmrad (~2.4 times of the design beam emittance). This was done to overcome difficulties faced in the storage of electron beam at the design beam emittance, which were attributed to injection errors arising from the mismatch of kicker magnets [12] and small dynamic aperture. In the moderate optics, dynamic aperture in transverse planes is higher and the effects of injection errors are smaller in comparison to the low emittance optics. These are attributed to reduced strengths of sextupole magnets with a higher dispersion function at their locations, which is achieved by breaking the achromatic condition. The effect of injection error is further reduced in the moderate optics with the help of off-momentum beam injection. An analysis is presented to explain why it is easier to inject the beam with an off-momentum beam injection as compared to the on-momentum beam injection.

In order to operate Indus-2 with a low emittance optics, avoiding difficulties arising during the beam injection, a scheme has been discussed, in which electron beam is injected (at 550 MeV) using the moderate optics with higher beam emittance (135 nmrad) in comparison to the design beam emittance (58 nmrad) and after beam storage and its acceleration to 2.5 GeV, the emittance is reduced by changing the strengths of quadrupole and sextupole magnets. Here, the emittance is reduced to one third (45 nmrad) of the present operating value. In addition, the vertical β-function at the center of the long straight sections used for insertion devices, is also reduced by ~60% (from 3.6 m to 1.4 m), which helps to reduce the effect of insertion devices on beam dynamical parameters. The above procedure is implemented in presence of finite distortion of closed orbit and betatron functions [13]. In order to ensure a smooth switch over from the moderate to low emittance optics, a procedure is evolved and executed in a step by step manner. In each step, storage ring's sensitivity to linear and nonlinear imperfections is controlled in a well-defined way to avoid any fast decay of beam current.

The third topic of the thesis is devoted to the effect of insertion devices on beam dynamical parameters [14] such as tune, β-asymmetries (β- beat) and dynamic aperture. Here, the effect of a wavelength shifter on beam dynamics of Indus-1 is addressed. In an electron storage ring, a wavelength shifter is used to reduce the critical wavelength of the emitted radiation spectrum. The peak magnetic field of a wavelength shifter is much higher than that of a dipole magnet. Effects of the wavelength shifter on beam dynamical parameters depend upon the trajectory of electron beam and profile of the magnetic field. The linear and non-linear forces, which are generated by the wavelength shifter, may excite resonances that can lead to a severe degradation of the dynamic aperture. To estimate these forces, a Hamiltonian for wavelength shifter is derived. In Indus-1, the available length for installation of insertion devices is very small. In view of this, a wavelength shifter with a peak field of 3 T is considered to shift its critical wavelength. Using this Hamiltonian, the effect of a 3 T-wavelength shifter in Indus-1 is studied. The organization of the thesis is given below

Chapter 1: Overview of synchrotron radiation sources is presented in which a brief description of Indus-1 and Indus-2 synchrotron radiation sources is discussed. A brief description of accelerator physics of synchrotron/storage ring is presented. In this chapter, we discuss equation of motion, radiation damping, beam emittance, chromaticity correction and transverse beam acceptance. Besides, different types of magnetic lattices, injection schemes and effects of insertion devices on beam dynamical parameters are also discussed.

Chapter 2: This chapter discusses the description of compensated and uncompensated injection schemes for the synchrotron. During beam injection, α-function plays an important role in the injection dynamics and its effect is highlighted in this chapter. It is shown that the performance of the synchrotron, in terms of accelerated beam current, is improved by injecting a short pulse (pulse duration equal to few times the revolution period of the synchrotron) with small residual oscillations. For this, the bump shape, bump reduction rate as well as injection angle with respect to the bump slope are optimized. It is possible to do so by employing an uncompensated bump scheme in which the strengths of the kicker magnets are not correlated to one another unlike in the compensated bump scheme and with the adjustment of injection angle from turn to turn. Tracking and experimental results of compensated and uncompensated injection scheme are presented, highlighting the advantage of uncompensated bump scheme. In the uncompensated bump scheme, increase in the beam current is also achieved when the injection beam angle is regulated during beam injection by injecting the beam on the rising part of the septum magnet pulse.

Chapter 3: In this chapter, a study for the double bend achromat is carried out. The phase advance requirement for the minimum beam emittance is derived. To achieve this phase advance requirement, different arrangements of quadrupole magnets consisting of single QF, two QFs, three quadrupole magnets (having different combination of QFs and QDs) and another having four quadrupole magnets (two QFs and two QDs or four QFs) are studied. Using the analytical expressions, parameters of the chosen structures (strength of quadrupole magnets and length of drift space) are varied and their effects are evaluated on beam emittance.

It is shown that in single QF structure, the required phase advance cannot be achieved, thus in this structure, minimum beam emittance is not achievable. A formula for the minimum achievable beam emittance for this configuration is derived. In QF-QF structures, the condition of phase advance for minimum beam emittance is satisfied. However, it is found that in this structure, the drift space between two focusing quadrupole magnets becomes prohibitively long and besides, there is no way to control vertical β-function. Thus the above structure is not suitable for minimum beam emittance. For three and four quadrupole magnet structures, following arrangement of quadrupole magnets QF-QF-QF/QF-QD-QF/QD-QF-QD and QF-QD-QD-QF/QF-QF-QF-QF/QD-QF-QF-QD are studied with the objective of achieving minimum beam emittance. Among these structures QF-QD-QF/ QF-QD-QD-QF are shown to be more suitable for obtaining minimum beam emittance.

The achromat of Indus-2 consists of QF-QD-QF configuration. In this lattice, the length of drift space between QF and QD i.e. l_2 of the achromat part is varied and for each length, tunability of the lattice under the given constraints on beam emittance and lattice parameters is studied. For minimum beam emittance, lattice parameters are beyond the given constraints. The tunability of the lattice is optimum, if l_2 is chosen in between 2.5 m to 3 m. In Indus-2, l_2 is chosen 2.66 m, in which beam emittance is ~55 nm.rad, which is ~1.5 times of the minimum beam emittance.

Chapter 4: Indus-2 ring was commissioned with the moderate optics to overcome with the difficulties faced with the design beam emittance. In this chapter, commissioning experience of Indus-2 ring with the moderate optics is discussed. It is shown that in the presence of mismatch between injection kicker magnets, injection of the electron beam with the moderate optics is easier as compared to low emittance optics. The effect of off-momentum beam injection is also highlighted.

To carry out transition of optics from the moderate to low emittance, an objective function employing least square method with Lagrangian multiplier is defined. This function is used to calculate the strengths of quadrupole and sextupole magnets. The objective function is evolved and executed in a step by step manner in a well-defined way to avoid any fast decay of the stored electron beam. With this method, the beam emittance in Indus-2 at 2.5 GeV is successfully reduced to one third (from 135 nmrad to 45 nmrad) without any additional loss of beam current. The results of switch over process from the moderate to low emittance optics are also discussed in this chapter.

Chapter 5: The effect of insertion devices on beam dynamics was studied by L. Smith, in which equations of motion were obtained from the Hamiltonian with Halbach's magnetic field model for sinusoidal electron beam trajectory transformation. To understand the effect of a wavelength shifter, these equation of motions are derived for the compensated electron beam trajectory transformation. The modified equations of motion give extra terms of the quadrupole, sextupole and octupole force components, which are not present in undulators and wigglers. These force components arise due to profile of the magnetic field and electron beam trajectory in the wavelength shifter.

This model was used to study the effect of 3T-wavelength shifter in Indus-1. As the beam lifetime is short in Indus-1, it is desirable to keep the wavelength shifter operational during the beam injection. In this ring, amplitude of the injected and stored beam oscillation is large due to injection scheme followed. The studies carried out show that there is a degradation in dynamic aperture, which may make it difficult to accumulate the beam. For its smooth operation, a correction scheme is developed to correct the tune and β-asymmetries leading to a significant improvement in dynamic aperture, which is sufficient for beam injection

The work carried out in the thesis is summarized and further scope of above studies is also discussed in **Chapter 6**.

References for synopsis

[1] H. Winick, G. Brown, K. Halbach, and J. Harris, “Synchrotron Radiation: Wiggler and Undulator Magnets,” Physics Today 34, No. 5 (1981) 50.

[2] R. Chasman, G. K. Green and E. M.Rowe, “Preliminary Design of a Dedicated Synchrotron Radiation Facility”, IEEE Trans. Nucl. Sci NS-22, 1765 (1975).

[3] A Jackson, “A comparison of the Chasman-Green and triple bend achromat lattices”, LBNL Paper LBL-21279,1986.

[4] D. Einfeld and M. Plesko, “A modified QBA optics for low emittance storage rings”, Nuclear Instruments and Methods in Physics Research A, 335, 402 (1993).

[5] H. Tarawneh. M.Eriksson, L-J Lindgren and B. Anderberg, “MAX-IV lattice, the dynamic properties and magnet systems", Nuclear Instruments and Methods in Physics Research A, 508, 480 (2003).

[6] J. Murphy, “The Physics of Particle Accelerators”, AIP Conf. Proc. No. 249 ~AIP, 1939 (1992)

[7] S.Y. Lee, “Emittance optimization in three and multiple bend achromats”, Phys. Rev. E 54, 1940 (1996).

[8] Yi Jiao, et.al, “Modified theoretical minimum emittance lattice for an electron storage ring with extreme-low emittance”, Phys. Rev. Special Topics – Accelerators and Beams 14, 054002 (2011).

[9] D Angal-Kalinin, A Banerji, P R Hannurkar, M G Karmarkar, S Kotaiah, S P Mhaskar, P K Nema, S S Prabhu, M Pravin Kumar, S S Ramamurthi, S K Shukla, G Singh*, H C Soni and B J Vaidya, “ Synchrotron radiation source Indus-1”, Current Science 82(3), (2002).

[10] G Singh, G. K. Sahoo, D Angal, B Singh, A. D. Ghodke and Pradeep Kant, “Synchrotron Radiation Source INDUS-2”, Indian Journal of Pure and Applied Physics Vol.35, 183 (March 1997).

[11] B. Singh, G. Singh and S. S. Ramamurthi, “Injection into the synchrotron for Indus-1 and Indus-2”, Indian Journal Physics 65A (6) pp. 471-478 (1991).

[12] Ali Akbar Fakhri and Gurnam Singh, “Injection Optimization for Indus-2”, Asian Particle Accelerator Conference 2007, Indore, pp-146-148.

[13] A. D. Ghodke, Riyasat Husain, Pradeep Kumar, Surendra Yadav and T.A. Puntambekar, “Measurement of parameters in Indus-2 synchrotron radiation source”, Review of Scientific Instruments, 83, 10303(2012).

[14] P. Beloshitsky, E. Levichev, I. Meshkov and I. Tikova, “Effect of superconducting wiggler on the DELSY beam dynamics”, Nuclear Instruments and Methods in Physics Research A, 524 pp.13-26 (2004).

LIST OF FIGURES

LIST OF TABLES

CHAPTER-1

INTRODUCTION

Synchrotron radiation is the electromagnetic radiation emitted by highly relativistic charged particles, when they are radially accelerated under the influence of magnetic fields. Electron storage rings, which are designed specifically for the production of this radiation, are termed as synchrotron radiation sources. In an electron storage rings, an electron keeps revolving around a closed path at constant energy and this path is guided by the arrangement of magnets. Dipole magnets are used to bend the electron beam imparting above mentioned radial acceleration to electrons. In these storage rings, the radiation is produced using dipole magnets and insertion devices. A radio frequency (RF) cavity is used in the ring to provide energy to the electron beam during beam energy ramping as well as to compensate the loss of beam energy due to the radiation. Insertion devices are devices having periodic arrangements of dipole magnets, and are termed as wigglers and undulators. In the presence of these devices, an electron trajectory wiggles and on each wiggling, the radiation is emitted. In case of wiggler, the emitted radiation adds up incoherently, on the other hand in case of undulator, the emitted radiation adds up coherently. There is no sharp boundary between these two devices, they have similar structure and mainly have the difference in magnetic field strength.

In this chapter, an overview of synchrotron radiation sources is presented. The basic of accelerator physics of synchrotron radiation source for understanding the motion of an electron in the presence of magnetic elements is discussed. Topics such as radiation damping, beam emittance, chromaticity correction, longitudinal motion of an electron and transverse beam acceptance are explained. In next section, different types of magnetic lattices, suitable for synchrotron radiation sources, are discussed. Methods of the electron beam injection into synchrotron/storage ring are presented in subsequent section. In next section, effects of insertion devices on beam dynamical parameters are summarized. The objective and scope of thesis is to study beam injection, beam optics and insertion devices for synchrotron radiation sources. As a case study, these studies are presented for Indus-1 and Indus-2 storage ring. In the last section, a brief description of Indus-1 and Indus-2 synchrotron radiation sources at RRCAT, India is discussed.

1.1 Overview of synchrotron radiation sources

The spectrum of radiation, emitted from synchrotron storage rings has unique characteristics such as wide tuning range from infra-red to X-rays (broad band spectrum), high flux, high brightness, high polarization, pulsed time structure etc. For example brightness, which is defined as the number of photons per sec. per unit area, per unit solid angle, per 0.1% of bandwidth from a dipole magnet, is $\sim 10^{13}$, which is $\sim 10^{6}$ times higher as compared to the conventional rotating anode X-ray source. In the third generation synchrotron radiation sources, brightness from insertion devices is increased up to $\sim 10^{20}$.

The synchrotron radiation sources have emerged as a powerful tool to study material science, surface science, chemistry, biology, medicine and industrial applications due to above mentioned characteristics. Uninterrupted availability of the radiation for several hours from a synchrotron radiation source is very suitable for the study of materials requiring a long exposure time. The high flux and high brightness [1] are the figure of merit for the synchrotron radiation sources. These spectral characteristics are governed by the energy and current of the stored electrons, bending magnet field and configuration of insertion devices. The brightness of the radiation also depends on the electron beam transverse size and divergence, which are related to beam emittance. The brightness of this source can be increased by reducing the electron beam emittance.

The radiation from a dipole magnet is continuous. The critical energy of the emitted synchrotron radiation [2] (which is defined as an energy above and below which the power radiated is equal) from its

$$E_c(KeV) = 0.665E^2(GeV)B(T) \quad (1.1)$$

Here E and B represent beam energy and magnetic field of a dipole magnet respectively.

On the other hand, the radiation spectrum is continuous (broad band) and quasi monochromatic (narrow band) from a wiggler and an undulator, respectively. The energy of different harmonic component (E_n) of the radiation from an undulator and a wiggler magnet [2] is given by

$$E_n(KeV) = \frac{0.950nE^2(GeV)}{\lambda(cm)(1 + {K^2}/{2})} \quad (1.2)$$

Here K is deflection parameter, which is defined as K=0.934B_o(T)λ(cm), λ and B_o is the period length and peak magnetic field of insertion devices, for wiggler K>>1 and for undulator K<1, and n shows the nth harmonics of synchrotron radiation.

From the comparison of equation (1.1) and (1.2), it can be observed that the energy of the emitted synchrotron radiation from a dipole magnet as well as from an insertion device is proportional to the square of the stored beam energy. Thus to obtain hard X-ray from a dipole magnet or from an insertion device, it is preferable to keep stored beam at higher energy. The critical wavelength from a dipole magnet can be reduced with the help of a higher magnetic field, which can be obtained with the help of a wavelength shifter. This wavelength shifter is a special case of wiggler, which consists of one central dipole magnet with a higher magnetic field along with few side dipole magnets of reduced magnetic field. The critical energy of the emitted synchrotron radiation from the wavelength shifter is calculated in the same way as for dipole magnet. From equation (1.2), it can be seen that the radiation from insertion devices is inversely proportional to the period length of the insertion devices, thus shorter undulator period length is preferable for obtaining higher photon beam energy. The high flux (number of photons emitted per second per milli-radian in a given spectral bandwidth) is obtained with the help of insertion devices and higher stored beam current. The flux from wigglers and undulators is proportional to the number of periods and square of the number of periods, respectively.

Now we will give a brief description of a synchrotron radiation source. Typically a synchrotron source consists of an injector, a pre injector, a storage ring and the beamlines installed in the storage ring to tap the synchrotron radiation. An injector, either a linear accelerator or a synchrotron, is required for injecting an electron beam into the storage ring. The beam energy of the injector may be either equal or lower than the operating beam energy of the storage ring.

Historically, high energy synchrotrons designed for carrying out experimentation on particle physics [3], in which synchrotron radiation produced in dipole magnets was tapped are termed as first generation synchrotron radiation source. In the second generation synchrotron radiation sources, the storage rings were specially designed to produce the radiation from their dipole magnets. The modern synchrotron radiation sources, which are specially designed to produce the radiation from insertion devices, are termed as third generation synchrotron radiation sources. These sources have long straight sections to accommodate insertion devices. In these straight sections dispersion function is kept zero or very small to avoid any dilution of the beam emittance. For this, mostly double bend achromat or triple bend achromat lattice with a large number of unit cells are used. In last one or two decades, several third generation synchrotron radiation sources are operational in the world and they are in the process of up-gradation [4] to increase the brightness by reducing the beam emittance and increasing the length of insertion section for installation of longer insertion devices. The new facilities are also under consideration to get high brightness higher than 10^{18} in hard X-ray region (10-100

KeV) with the help of beam emittance in pm-rad range and stored beam energy above 4.5 GeV [5].

In the fourth generation synchrotron radiation sources [6], spectral brightness from insertion devices can be further increased by reducing the beam emittance closed to the diffraction limit i.e. a fraction of the photon beam ($\lambda/4\pi$). For this purpose, either energy recovery linear accelerator facility/ multi bend achromat magnetic lattice for storage ring has to be used.

In short in synchrotron radiation source, electron beam is injected from an injector into a storage ring and in the ring, a proper and optimized magnetic optics is arranged to obtain electron beam with a very small beam size and divergence and then to enhance the brightness of the emitted radiation, insertion devices are installed. In the thesis a case study of beam injection into the synchrotron, which is used as an injector for Indus-1 and Indus-2 storage ring, is discussed. A theoretical study of double bend achromat lattice and their application to Indus-2 lattice is presented and a scheme is also presented to reduce the beam emittance in Indus-2. To study the effect of insertion devices on the beam optics, a detailed theoretical study of a wavelength shifter in Indus-1 is done.

1.2 Brief description of accelerator physics of synchrotron radiation sources

To keep the electrons circulating in a storage ring/synchrotron, a series of dipole, quadrupole and sextupole magnets are arranged in a closed loop. The motion of an electron can be defined by using a local coordinate system (as shown in figure 1.1), which moves along the ideal orbit (design orbit) [7, 8]. The small deviation from the coordinates of an electron with respect to the ideal orbit is denoted by (x, y, s). Here x and y represent the motion along the radial (horizontal) and vertical direction, respectively and s denotes the motion along the beam direction.

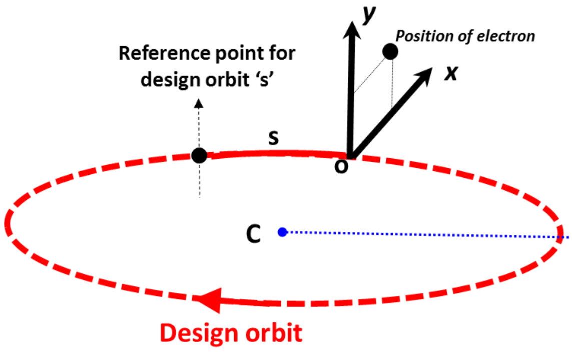

Figure 1. 1: Co-ordinate system for an electron motion in a circular accelerator

At a given point 's', (which is measured from an arbitrary reference point), the motion of electrons in horizontal plane is described by its position (x) and the angle (x'), x' is defined as a derivative of position with respect to longitudinal coordinates (s). Similarly in vertical plane, it is described by a position (y) and corresponding angle(y'). Now we will discuss the basic of beam dynamics [8-13].to study the motion of an electron.

1.2.1 Equation of motion

In the horizontal plane, the motion of an electron in a given magnetic element is governed by Hills equation [8-13], which is

$$\frac{d^2x(s)}{ds^2} + k(s)x(s) = 0 \tag{1.3}$$

Here $k(s)$ is the coefficient, which is related with the magnetic field strength of a given magnetic element.

The solution of Hill's equation is obtained using hard edge piece wise constant model, in which $k(s)$ is assumed to be a constant (k) over the length of the magnet. Under this condition, the solution in a given magnet is given by

$$x = A\exp(i\sqrt{k}s) + B\exp(-i\sqrt{k}s) \tag{1.4}$$

The angle (x') is obtained by differentiating equation (1.4) with respect to s,

$$x' = i\sqrt{k}\{A\exp(i\sqrt{k}s) - B\exp(-i\sqrt{k}s)\} \tag{1.5}$$

Here constants A and B are determined by initial values. Let at $s = 0$, $x = x_o$ and $x' = x_o'$. With these condition, above two equations yield

$$x = x_o\cos(\sqrt{k}s) + x_o'\frac{\sin(\sqrt{k}s)}{\sqrt{k}} \tag{1.6}$$

$$x' = -x_o\sqrt{k}\sin(\sqrt{k}s) + x_o'\cos(\sqrt{k}s) \tag{1.7}$$

The solutions of equation (1.6) and (1.7) can be represented using a transfer matrix, which relates coordinates at entry and exit of the element

$$\begin{bmatrix} x_1 \\ x_1' \end{bmatrix} = \widetilde{\boldsymbol{M}} \begin{bmatrix} x_o \\ x_o' \end{bmatrix} = \begin{bmatrix} M_{11} & M_{12} \\ M_{21} & M_{22} \end{bmatrix} \begin{bmatrix} x_o \\ x_o' \end{bmatrix} \tag{1.8}$$

Where $M_{11} = \cos\sqrt{k}s$, $M_{21} = -\sqrt{k}\sin\sqrt{k}s$, $M_{12} = \frac{\sin\sqrt{k}s}{\sqrt{k}}$, and $M_{22} = \cos\sqrt{k}s$

A similar matrix can be defined for the vertical plane, which is given by

$$\begin{bmatrix} y_1 \\ y_1' \end{bmatrix} = \widetilde{\boldsymbol{R}} \begin{bmatrix} y_o \\ y_o' \end{bmatrix} = \begin{bmatrix} R_{11} & R_{12} \\ R_{21} & R_{22} \end{bmatrix} \begin{bmatrix} y_o \\ y_o' \end{bmatrix} \tag{1.9}$$

These matrices ($\widetilde{\boldsymbol{M}}$ and $\widetilde{\boldsymbol{R}}$), which characterize magnetic elements, are knows as transfer matrices. Now we will write down the transfer matrix for drift space and different magnetic elements, explicitly.

i). Drift space

In this region $k(s)$ is zero thus an electron will not experience any field. In the horizontal plane, transfer matrix for drift space of length l is

$$\widetilde{\boldsymbol{M}} = \begin{bmatrix} 1 & l \\ 0 & 1 \end{bmatrix} \tag{1.10}$$

The same matrix is valid for the vertical plane also.

ii). Quadrupole magnet

Quadrupole magnet is used to focus the electron beam. A quadrupole magnet by virtue of its geometry and field direction is focusing in one plane, while it is defocusing in the other plane. The transfer matrix of a quadrupole magnet, which is focusing in the horizontal plane and defocusing in the vertical plane is obtained with the solution of Hill's equation

$$\widetilde{\boldsymbol{M}} = \begin{bmatrix} \cos\sqrt{|k|}l & \dfrac{\sin\sqrt{|k|}l}{\sqrt{|k|}} \\ -\sqrt{|k|}\sin\sqrt{|k|}l & \cos\sqrt{|k|}l \end{bmatrix} \tag{1.11}$$

Here, $k = \frac{1}{B\rho}\frac{\partial B_y}{\partial x}$, $B\rho$ is known as magnetic rigidity of an electron, which is given by $B\rho(Tm) = \frac{10}{3E(GeV)}$, and l is the length of quadrupole magnet.

In defocusing plane, matrix elements contain hyperbolic functions, which give an unbounded motion i.e. defocusing.

$$\widetilde{\boldsymbol{R}} = \begin{bmatrix} \cosh\sqrt{|k|}l & \dfrac{\sinh\sqrt{|k|}l}{\sqrt{|k|}} \\ \sqrt{|k|}\sinh\sqrt{|k|}l & \cosh\sqrt{|k|}l \end{bmatrix} \tag{1.12}$$

For defocusing quadrupole magnet, transfer matrix $\widetilde{\boldsymbol{M}}$ and $\widetilde{\boldsymbol{R}}$ are interchanged.

iii). Sector dipole magnet

In this magnet an electron enters and exits perpendicular to the edges of the magnet. Thus, a deviated orbit from the design trajectory traverses different path length inside the magnet, compared to the design orbit. This gives rise to a focusing phenomenon in the bending plane, known as "geometric focusing". Therefore, in the horizontal plane geometrical focusing ($^1/_{\rho^2}$) also took place along with bending action, where ρ is the radius of curvature for the design orbit inside the dipole magnet. In the horizontal plane, the transfer matrix is given by

$$\tilde{\boldsymbol{M}} = \begin{bmatrix} \cos\theta_b & \rho\sin\theta_b \\ -\frac{\sin\theta_b}{\rho} & \cos\theta_b \end{bmatrix} \tag{1.13}$$

Here θ_b is the bending angle. In the other plane, this dipole magnet acts as a drift space of length $l_b=\rho\theta_b$.

iv). Rectangular dipole magnet

In this magnet, the entry and exit edges are parallel, as a result an electron enters and exits at the half of bending angle. At the edges of the magnet, an electron will experience defocusing and focusing force in the horizontal and vertical planes respectively. In the horizontal plane, defocusing action is compensated by geometrical focusing ($k = {}^{1}/{}_{\rho^2}$). Thus the magnet acts like a drift space in the horizontal plane and acts as a focusing quadrupole in the vertical plane, commonly known as "edge focusing". In the horizontal and vertical planes, the matrices are given respectively by

$$\tilde{\boldsymbol{M}} = \begin{bmatrix} 1 & \rho\sin\theta_b \\ 0 & 1 \end{bmatrix} \tag{1.14}$$

$$\tilde{\boldsymbol{R}} = \begin{bmatrix} \cos\theta_b & \rho\sin\theta_b \\ -\frac{\sin\theta_b}{\rho} & \cos\theta_b \end{bmatrix} \tag{1.15}$$

1.2.2 Dispersion function

If an electron momentum is different (off-momentum) then in the dipole magnet magnetic force will be different in comparison to an on-momentum electron. In this case, equation of motion (1.3) [8-13] for the horizontal plane is given by

$$\frac{d^2x(s)}{ds^2} + k\,(s)x(s) = -\frac{1}{\rho}\frac{\Delta p}{p} \tag{1.16}$$

Here p is the design or on-momentum and Δp shows the off-momentum (deviation in momentum from p). The solution of above equation is written in terms of transfer matrix

$$\begin{bmatrix} x_1 \\ x_1' \\ \delta \end{bmatrix} = \begin{bmatrix} M_{11} & M_{12} & M_{13} \\ M_{21} & M_{22} & M_{23} \\ 0 & 0 & 1 \end{bmatrix} \begin{bmatrix} x_o \\ x_o' \\ \delta \end{bmatrix} \quad (1.17)$$

Here $\delta = {}^{\Delta p}/_{p}$

The trajectory of an off-momentum electron is defined as

$$x(s) = \eta(s)\delta \quad (1.18)$$

$$x'(s) = \eta'(s)\delta \quad (1.19)$$

Here, $\eta(s)$, $\eta'(s)$ is defined as dispersion function and derivative of dispersion function with respect to s respectively. The dispersion function relates deviation in a trajectory for the off-momentum electron with respect to the design trajectory due to a momentum offset (in first order of δ). Dispersion is mainly generated by dipole magnets. For sector dipole magnet $M_{13} = \rho(1 - \cos\theta_b)$ and $M_{23} = \sin\theta_b$ and for rectangular dipole magnet $M_{13} = \rho(1 - \cos\theta_b)$ and $M_{23} = 2\tan\frac{\theta_b}{2}$.

Similar to the dipole magnet, quadrupole magnet also has its effect depending on the momentum. In the quadrupole magnet k is changed for an off-momentum electron, which is

$$k = k\left(1 + \frac{\delta p}{p}\right)^{-1} \sim k\left(1 - \frac{\delta p}{p}\right) \quad (1.20)$$

Thus for an off-momentum electron, focussing forces in the horizontal and vertical planes are different as compared to an on-momentum electron.

1.2.3 Lattice parameters propagation along the ring

Instead of piece-wise constant model, which is discussed above, Hill's equation can also be solved, considering variation in k with s. These solutions give rise to some new parameters, known as twiss parameters [8-13]. The solution of Hill's equation (1.3), in terms of twiss parameters, for an on-momentum electron is discussed here. The general solution of Hill's equation in horizontal plane is

$$x(s) = A\xi(s)\cos(\mu_x(s) + \mu_o) \tag{1.21}$$

Here A and μ_o are constants, which are determined from the initial coordinates. The solution represents oscillatory motion and this oscillation is known as betatron oscillation. Due to dependence of k on 's', the amplitude of oscillations become 's' dependent, i.e. $A\xi(s)$, in which A is constant while $\xi(s)$ is a function of 's'. The function $\xi(s)$ and $\mu_x(s)$ are independent of μ_o, if following condition is satisfied.

$$\mu_x(s) = \int_0^s \frac{ds}{\xi^2(s)} \tag{1.22}$$

Differentiation of equation (1.22) with respect to s is given

$$\frac{d\mu_x(s)}{ds} = \frac{1}{\xi^2(s)} \tag{1.23}$$

With the help of equation (1.21), (1.22) and (1.23), equation for the $\xi(s)$ is given by

$$\frac{d^2\xi}{ds^2} + k(s)\xi(s) = \frac{1}{\xi^3} \tag{1.24}$$

Generally, $\xi(s)$ is written as $\sqrt{\beta_x(s)}$ and $\beta_x(s)$ is known as betatron function, which is governed according to the arrangement of different elements i.e. on $k(s)$. Equation (1.23) becomes

$$\mu_x(s) = \int_0^s \frac{ds}{\beta_x(s)} \tag{1.25}$$

$\mu_x(s)$ is betatron phase advance, which is obtained with the help of $k(s)$ and $\beta_x(s)$. We rewrite the equation (1.21) as

$$x(s) = C\sqrt{\beta_x(s)}\cos\mu_x(s) + D\sqrt{\beta_x(s)}\sin\mu_x(s) \tag{1.26}$$

Here C and D are constants, now $x'(s)$ (angle) is obtained after taking the derivative of equation (1.26) with respect to s

$$x'(s) = -\frac{C}{\sqrt{\beta_x(s)}}\{\alpha_x(s)\cos\mu_x(s) + \sin\mu_x(s)\}$$

$$+\frac{D}{\sqrt{\beta_x}(s)}\{\cos\mu_x(s) - \alpha_x(s)\sin(\mu_x(s)\ \} \tag{1.27}$$

Here

$$\alpha_x(s) = -\frac{1}{2}\frac{d\beta_x(s)}{ds} \tag{1.28}$$

The constants C and D are redefined in terms of initial coordinates

$$C = \frac{x(s)}{\sqrt{\beta_x(s)}},\ D = x'(s)\sqrt{\beta_x(s)} + \frac{x(s)\alpha_x(s)}{\sqrt{\beta_x(s)}}$$

By substituting the expressions of the constant into equations (1.26) and (1.27), one can obtain the matrix $\widetilde{\boldsymbol{M}}$ (S_2/S_1) from S_1 location to S_2 location

$$\begin{bmatrix} x_2 \\ x_2' \end{bmatrix} = \begin{bmatrix} \sqrt{\frac{\beta_{2,x}}{\beta_{1x}}}(\cos\Delta\mu_x + \alpha_1\sin\Delta\mu_x) & \sqrt{\beta_{1,x}\beta_{2,x}}\sin\Delta\mu_x \\ -\frac{1+\alpha_{1,x}\alpha_{2,x}}{\sqrt{\beta_{1,x}\beta_{2,x}}}\sin\Delta\mu_x + \frac{(\alpha_{1,x}-\alpha_{2,x})}{\sqrt{\beta_{1,x}\beta_{2,x}}}\cos\Delta\mu_x & \sqrt{\frac{\beta_{1,x}}{\beta_{2,x}}}(\cos\Delta\mu_x - \alpha_{2,x}\sin\Delta\mu_x) \end{bmatrix}\begin{bmatrix} x_1 \\ x_1' \end{bmatrix} \tag{1.29}$$

Here $\beta_{1,x}$ and $\alpha_{1,x}$, are horizontal twiss parameters at S_1 location and $\beta_{2,x}$ and $\alpha_{2,x}$, are horizontal twiss parameters at S_2 location, $\Delta\mu_x$ is the phase advance between S_1 and S_2 locations

Any synchrotron or storage ring is formed by repeating same structure of magnetic optics, i.e. ring is formed by periodic arrangement of some basic arrangement of a magnetic optics. The basic arrangement of magnetic optics is known as unit cell (also known as superperiod) and after repeating this unit call, complete lattice of the ring is constructed. The unit cell is constructed using different arrangement of magnetic elements. The twiss parameters at the start and at the end of the unit cell are periodic (same). If the length of unit cell is L then

$$\beta_x(s) = \beta_x(s+L)$$

$$\alpha_x(s) = \alpha_x(s+L)$$

Thus for one cell, transfer matrix after substituting above periodic condition of twiss parameters in equation (1.29) is given by

$$\widetilde{\boldsymbol{M}} = \begin{bmatrix} \cos\mu_x + \alpha_x(\mathrm{s})\sin\mu_x & \beta_x(\mathrm{s})\sin\mu_x \\ -\gamma_x(\mathrm{s})\sin\mu_x & \cos\mu_x - \alpha_x(\mathrm{s})\sin\mu_x \end{bmatrix} \tag{1.30}$$

Here μ_x represents phase advance over one unit cell. A new parameter, γ_x is also introduced, which is defined by

$$\gamma_x(s) = \frac{1+\alpha_x(s)^2}{\beta_x(s)} \tag{1.31}$$

By inspection, it can be seen that this form of the generalized matrix (1.30) can be split into two parts such that

$$\widetilde{\boldsymbol{M}} = \tilde{\boldsymbol{I}}\cos\mu_x + \widetilde{\boldsymbol{J}_x}\sin\mu_x \tag{1.32}$$

Here $\tilde{\boldsymbol{I}} = \begin{bmatrix} 1 & 0 \\ 0 & 1 \end{bmatrix}$ and $\widetilde{\boldsymbol{J}_x} = \begin{bmatrix} \alpha_x(s) & \beta_x(s) \\ -\gamma_x(s) & -\alpha_x(s) \end{bmatrix}$

It can be seen that $\widetilde{\boldsymbol{J}_x}^2 = -1$. Thus the algebra of $\widetilde{\boldsymbol{M}}$ is clearly the same as that of a complex number, so from De Moivre's formula after mth cell.

$$\widetilde{\boldsymbol{M}}^m = \tilde{\boldsymbol{I}}\cos(m\mu_x) + \widetilde{\boldsymbol{J}_x}\sin(m\mu_x) \tag{1.33}$$

$$\widetilde{\boldsymbol{M}}^{-m} = \tilde{\boldsymbol{I}}\cos(m\mu_x) - \widetilde{\boldsymbol{J}_x}\sin(m\mu_x) \tag{1.34}$$

If ring constitutes, *m* number of unit cell then matrix (1.30) for a ring is given by

$$\widetilde{\boldsymbol{M}} = \begin{bmatrix} \cos 2\pi\nu_x + \alpha_x(\mathrm{s})\sin 2\pi\nu_x & \beta_x(\mathrm{s})\sin 2\pi\nu_x \\ -\gamma_x(\mathrm{s})\sin 2\pi\nu_x & \cos 2\pi\nu_x - \alpha_x(\mathrm{s})\sin 2\pi\nu_x \end{bmatrix} \tag{1.35}$$

Here ν_x, represents horizontal tune, which is the phase advance of betatron oscillations, executed by of an electron in a one revolution. Physically, it shows number of betatron oscillations, executed by an electron in one complete revolution in the ring, which is given by

$$\nu_x = \frac{m\mu_x}{2\pi} = \frac{1}{2\pi}\oint \frac{ds}{\beta_x(s)} \tag{1.36}$$

In the vertical plane, similar transfer matrix can be written down

$$\widetilde{\boldsymbol{R}} = \begin{bmatrix} \cos 2\pi\nu_y + \alpha_y(\mathrm{s})\sin 2\pi\nu_y & \beta_y(\mathrm{s})\sin 2\pi\nu_y \\ -\gamma_y(\mathrm{s})\sin 2\pi\nu_y & \cos 2\pi\nu_y - \alpha_y(\mathrm{s})\sin 2\pi\nu_y \end{bmatrix} \quad (1.37)$$

Here ν_y, represents vertical tune

$$\nu_y = \frac{m\mu_y}{2\pi} = \frac{1}{2\pi}\oint \frac{ds}{\beta_y(s)} \quad (1.38)$$

The tune point of a ring is defined by (ν_x, ν_y)

i). Stability of betatron oscillations in a ring

The equation for the coordinate transformation through a unit cell with transfer matrix $\widetilde{\boldsymbol{M}}$ is given by

$$\widetilde{\boldsymbol{M}} \begin{bmatrix} x_1 \\ x_1' \end{bmatrix} = \lambda \begin{bmatrix} x_1 \\ x_1' \end{bmatrix} \quad (1.39)$$

Here λ and (x, x') is termed as Eigen value and Eigen vectors respectively

$$\lambda^2 - (M_{11} + M_{22})\lambda + (M_{11}M_{22} - M_{12}M_{21}) = 0 \quad (1.40)$$

The two roots of equation (1.40), for the transfer matrix, which have unit determinant is

$$\lambda_{a.b} = \frac{(M_{11} + M_{12}) \pm \sqrt{(M_{11} + M_{12})^2 - 4}}{2} \quad (1.41)$$

Let us choose $\cos\mu = (M_{11} + M_{12})/2$. In order that the motion is stable μ must be real.

$$\lambda_{a,b} = \cos\mu \pm j\sin\mu = e^{\pm j\mu} \quad (1.42)$$

It implies that

$$\frac{(M_{11} + M_{12})}{2} = \left|\frac{1}{2} Trace(M)\right| < 1 \quad (1.43)$$

In order to have the stable betatron oscillations (bounded motion) in both the planes, this condition has to be satisfied.

ii). Constant of motion

The constant A in equation (1.21) is evaluated with the help of equation (1.21) and (1.3). The constant is an invariant of the motion, which is given by

$$\gamma_x(s)x(s)^2 + 2\alpha_x(s)x(s)x'(s) + \beta_x(s)x'^2(s) = \ A \tag{1.44}$$

From equation (1.44) the maximum displacement (beam size) and maximum angle (beam divergence) of an electron at any location 's' are

$$x_{max}(s) = \sqrt{A\beta(s)} \tag{1.45}$$

$$x'_{max}(s) = \sqrt{A\gamma(s)} \tag{1.46}$$

From equation (1.45) and (1.46), it can be seen that twiss parameters β(s), γ(s) and α(s) provide an information of the beam size, beam divergence and a correlation between displacement and angle respectively at any location 's' in a ring. Here A, which is invariant of motion is known as beam emittance. Therefore, the beam emittance shows the area formed by the particle in *x-x'* plane (or in *y-y'* plane), i.e. beam emittance is the area in phase plane.

According to Louiville's theorem in the presence of conservative forces, emittance is a constant of motion. Thus phase space area (emittance) of an electron at exit and entry of a given magnetic element will remain unchanged. At entry and exit of a given magnetic element only shape and orientation of the phase space ellipse will be changed. The transfer matrix for twiss parameters is given by

$$\begin{bmatrix} \beta_{2,x} \\ \alpha_{2,x} \\ \gamma_{2,x} \end{bmatrix} = \begin{bmatrix} M_{11}^2 & -2M_{11}M_{12} & M_{12}^2 \\ -M_{11}M_{21} & M_{11}M_{22} + M_{12}M_{21} & -M_{21}M_{22} \\ M_{21}^2 & -2M_{21}M_{22} & M_{22}^2 \end{bmatrix} \begin{bmatrix} \beta_{1,x} \\ \alpha_{1,x} \\ \gamma_{1,x} \end{bmatrix} \tag{1.47}$$

Here $\beta_{1,x}$, $\alpha_{1,x}$ and $\gamma_{1,x}$ are horizontal twiss parameters at entry and $\beta_{2,x}$, $\alpha_{2,x}$ and $\gamma_{2,x}$ are horizontal twiss parameters exit of an element.

Similarly in the vertical plane, transformation of twiss parameters ($\alpha_y(s)$, $\beta_y(s)$ and $\gamma_y(s)$) can be obtained with the help of transfer matrix $\widetilde{\boldsymbol{R}}$.

iii). Dispersion function evaluation for the ring

The periodic solution of η-function (dispersion function) after one turn at a given location is given by

$$\begin{bmatrix}\eta_o\\ \eta'_o\\ \delta\end{bmatrix} = \begin{bmatrix}M_{11} & M_{12} & M_{13}\\ M_{21} & M_{22} & M_{23}\\ 0 & 0 & 1\end{bmatrix}\begin{bmatrix}\eta_o\\ \eta'_o\\ \delta\end{bmatrix} \qquad (1.48)$$

By solving above equation (1.48), η-function and its derivative at this location is given by

$$\eta'_o = \frac{M_{21}M_{13}+M_{23}(1-M_{11})}{2-M_{11}-M_{22}} \text{ and } \eta_o = \frac{M_{12}\eta'_o+M_{11}}{1-M_{11}} \qquad (1.49)$$

The solution of Hill's equation in terms of twiss parameters for an off-momentum electron is

$$x(s) = \sqrt{\varepsilon\beta_x(s)}\cos(\mu(s)+\mu_0) + \eta(s)\delta \qquad (1.50)$$

Similar expression in the vertical plane can be written, however, in general, in this plane η-function is zero, because bending of ideal orbit generally takes place in the horizontal plane (dispersion is generated by dipole magnet).

1.2.4 Radiation damping and equilibrium beam emittance

In the dipole magnet, the emission of synchrotron radiation from relativistic electron is a random and non-conservative process. In this process, energy loss per turn by an electron is given by

$$U = \frac{C_\gamma E^4}{2\pi}\int\frac{ds}{\rho^2} \qquad (1.51)$$

Here, integration is taken over the ring, C_γ is physical constant, for electron, which is given by $8.846*10^{-05}$ m/GeV^3, ρ is the bending radius of a dipole magnet and U is the energy of synchrotron radiation (loss from electron's energy E). This energy loss take place along the direction of beam, as a result transverse and longitudinal component of momentum are reduced. To replenish this lost energy of electrons, RF cavities are installed in the ring. The electric field in this cavity imparts the energy to the electron, when it passes through the cavity. The longitudinal component of momentum is compensated by an RF cavity, however, the transverse component of momentum cannot be compensated. In this process, transverse amplitude of betatron oscillations is reduced. This phenomenon is called radiation damping. In the dipole magnet, in the horizontal plane η-function (dispersion function) is nonzero. Thus during emission of synchrotron radiation, betatron oscillations are excited due to change in the orbit, which are governed by the off-momentum orbit. In this process, the amplitude of transverse oscillations increases, which is defined as quantum excitation. The equilibrium between radiation damping and quantum excitation will lead to equilibrium beam emittance, which can be obtained with the help of synchrotron radiation integrals and partation numbers. These radiation integrals are governed by the dipole magnets and properties of the lattice. First synchrotron radiation integral is not related to radiation effects, it relates the changes in the circumference for the off momentum electrons, which is given by

$$I_1 = \int \frac{\eta(s)}{\rho(s)} ds \tag{1.52}$$

Second synchrotron radiation integral is used to define the energy loss per turn from dipole magnets (equation 1.51) for an electron, which is defined as

$$I_2 = \int \frac{ds}{\rho^2(s)} \tag{1.53}$$

Third synchrotron radiation integral is used to define the effect of synchrotron radiation on longitudinal dynamics (longitudinal dynamics is discussed in section 1.2.6), it is given by

$$I_3 = \int \frac{ds}{\rho^3(s)} \tag{1.54}$$

The damping of horizontal betatron oscillations and longitudinal oscillations are proportional to the horizontal damping partition number j_x and longitudinal damping partition number j_z respectively. These partition number are given by

$$j_x = 1 - \frac{I_4}{I_2}, \qquad j_z = 2 + \frac{I_4}{I_2} \tag{1.55}$$

Here I_4 is fourth synchrotron radiation integral, which is governed by the bending radius of dipole magnet and dispersion function. This integral has to be modified, if the dipole magnet has a transverse gradient. Because in this case, magnetic field experienced by an electron, will also be governed by the horizontal position. The fourth synchrotron radiation integral is given by

$$I_4 = \int \frac{\eta(s)}{\rho(s)} \left\{ \frac{1}{\rho^2(s)} + 2k(s) \right\} ds \tag{1.56}$$

Here $k(s) = \frac{1}{B\rho}\frac{dB}{dx}$ is the quadrupole strength, which is arising due to gradient in the dipole magnet, for separated dipole magnet $k(s) = 0$.

The fifth synchrotron radiation integral, which is used to define quantum excitation, is given by

$$I_5 = \int \frac{H(s)ds}{\rho^3(s)} \tag{1.57}$$

Here $H(s) = \gamma_x(s)\eta^2 + 2\alpha_x(s)\eta(s)\eta^/(s) + \beta_x(s)\eta^{/2}(s)$, 's' is the longitudinal distance in a dipole magnet at which twiss parameters and dispersion functions in the horizontal plane are $\beta_x, \alpha_x, \gamma_x, \eta$ and $\eta^/$ respectively.

In an electron storage ring, equilibrium horizontal beam emittance is normally referred to the beam emittance [14-16], which is given by

$$\varepsilon = C_q \gamma_o^2 \frac{1}{j_x} \frac{I_5}{I_2} \tag{1.58}$$

Here γ_o is the reduced energy (ratio of total energy of electron to the rest mass energy) of the electrons and C_q is constant, which is given by 3.382*10^{-13} m and. For iso-magnet (ρ is constant) and for separated function dipole magnet $j_x = 1$, equation (1.58) can be written as

$$\varepsilon = C_q \gamma_0^2 \frac{\langle H \rangle}{j_x \rho} \tag{1.59}$$

Here $\langle H \rangle = \int \left(\gamma_x(s)\eta^2 + 2\alpha_x(s)\eta(s)\eta^/(s) + \beta_x(s)\eta^{/2}(s)\right) ds/2\pi\rho$

Neglecting weak focussing ($\propto {}^1/_{\rho^2}$) of the dipole magnet, the *H*-function is evaluated in the sector dipole magnet with following relation

$$\beta_x(s) = \beta_{o,x} - 2\alpha_{o,x}s + \gamma_{o,x}\, s^2 \tag{1.60}$$

$$\alpha(s) = \alpha_{o,x} - \gamma_{o,x}s \tag{1.61}$$

$$\gamma(s) = \gamma_{o,x} \tag{1.62}$$

$$\eta(s) = \eta_o + \eta_o^{/}\,(s)s + \rho(1 - \cos\theta_b) \tag{1.63}$$

$$\eta_o^{/}\,(s) = \eta_o^{/} + \sin\theta_b \tag{1.64}$$

Here ($\beta_{o,x},\ \alpha_{o,x},\ \gamma_{o,x}$) is twiss parameter at beginning of the dipole magnet and s is the distance from the dipole magnet.

In the vertical plane, beam emittance is mostly governed by the transverse coupling constant (κ) between the horizontal and vertical plane ($\kappa = \frac{\varepsilon_y}{\varepsilon_x}$). In this plane, dispersion function is zero, as a result there is no quantum excitation during emission of synchrotron radiation. However, due to finite opening angle of synchrotron radiation, the betatron oscillation are excited, with this excitation, the vertical beam emittance (ε_y), which is given by

$$\varepsilon_y = \frac{13}{55}\frac{C_q}{\rho j_y}\oint \beta_y(s)ds \tag{1.65}$$

Here j_y is the vertical partition function, which is equal to one.

From equation (1.51), it can be seen that for an off-momentum electron, energy loss per turn is dependent upon the electron energy. It means higher energy electrons will lose more energy as compared to the low energy electrons. This process leads to radiation damping in the longitudinal plane. In this plane, quantum excitation is also generated due to discrete emission of synchrotron radiation. The equilibrium between radiation damping and quantum excitation will lead to natural momentum spread.

i) Beam Size and beam divergence

In practice, we don't have a single electron, in the electron beam a large number of electrons are distributed in phase space. In which most electrons are close to the central orbit with small emittance and progressively fewer electrons at larger emittance. The electron beam emittance boundary is defined such that 68% Gaussian distribution of electrons are included in it. The maximum displacement and maximum angle of the electron beam at any location *s* are defined as beam size and beam divergence (as shown in figure 1.2).

These electrons are also distributed in momentum. In the vertical plane dispersion function is zero, thus center of the phase space is on the design orbit, however, in the horizontal plane, the center of phase space is modified for off-momentum electrons according to the dispersion function. Thus in the horizontal plane, electron beam size and divergence are modified according to dispersion function and energy spread, which are given by

$$\sigma_x = \sqrt{\beta_x(s)\varepsilon_x(s) + n^2(s)(^{\delta p}/_{p})^2} \tag{1.66}$$

$$\sigma_x^{/} = \sqrt{\beta_x(s)\gamma_x(s) + \eta'^2(s)\left(^{\delta p}/_{p}\right)^2} \tag{1.67}$$

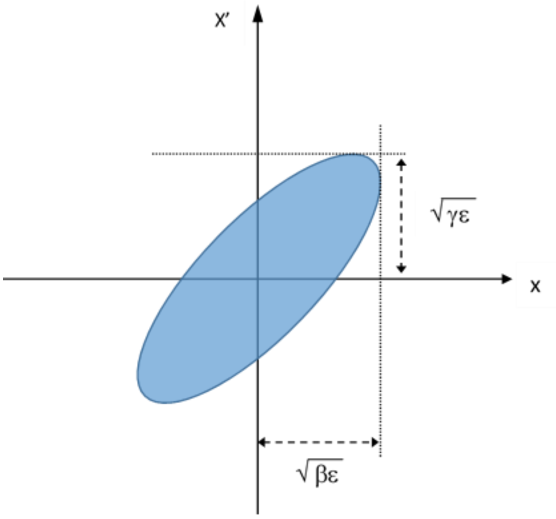

Figure 1. 2: Beam size and beam divergence of an electron beam in the phase space.

1.2.5 Chromaticity

For an off-momentum electron, the focusing effect of the quadrupole magnet is different as compared to on-momentum electron (equation 1.20) and therefore tune point in a ring for an off-momentum electron are different as compared to an on-momentum electron. In the ring, the ratio between fractional changes in betatron tune with fractional change in momentum is defined as chromaticity. In horizontal and vertical plane this is

$$\xi_x = -\frac{\frac{\delta\nu_x}{\nu_x}}{\delta} \tag{1.68}$$

$$\xi_y = -\frac{\frac{\delta\nu_y}{\nu_y}}{\delta} \tag{1.69}$$

In both horizontal and vertical planes, natural value of chromaticity is negative [17]. For the low emittance ring, due to strong focusing forces, natural value of chromaticity is very large. They may excite the head tail instability [11]. Chromaticity can be corrected using sextupole magnets which are placed at the non-zero dispersion region. The sextupole magnets provide extra focusing and defocusing forces for higher and lower off-momentum electrons. In thin lens approximation, electron which experience kick at the sextupole locations are given by

$$\theta_x = -\frac{m}{2}\left(x^2 - y^2\right) \tag{1.70}$$

$$\theta_y = mxy \tag{1.71}$$

Here θ_x and θ_y are the kick strength in horizontal and vertical plane respectively. m is the integrated normalized strength of the sextupole magnet, i.e. $m = \frac{1}{B\rho}\frac{\partial^2 B_y}{\partial x^2}$. The displacement of off-momentum electrons at the sextupole are

$$x = x_\beta + \eta\delta \tag{1.72}$$

$$y = y_\beta \tag{1.73}$$

Here x_β and y_β are displacements of an electron due to the betatron oscillation in horizontal and vertical plane respectively. Thus, for off-momentum electrons experience the kick due to sextupole is given by

$$\theta_x = -\frac{m}{2}\left(2x_\beta \eta\delta + x_\beta^2 + \eta^2\delta^2 - {y_\beta}^2\right) \tag{1.74}$$

$$\theta_y = m(\eta\delta + x_\beta)y_\beta \tag{1.75}$$

In these equations, first term is used to correct the chromaticity and remaining terms generate perturbations via nonlinear kicks, except for the $\eta^2\delta^2$ term. The non-linear kicks will generate the amplitude-dependent tune shifts [18]. The chromaticity correction term is proportional to dispersion function and amplitude of betatron oscillations. In order to reduce the strength of sextupole magnets, these are located in the lattice where beta and dispersion functions are high. Further in the both planes, beta functions should be well decoupled in such a way that at horizontal chromaticity correcting sextupole magnet β_x is high and β_y is low and at vertical chromaticity correcting sextupole magnet β_y is high and β_x is low.

1.2.6 Longitudinal motion of an electron

A radiofrequency (RF) cavity [8] is used to transfer energy to the beam along the beam direction for beam acceleration as well as for compensation of energy loss due to synchrotron radiation. This cavity has a special size and shape and normally made-up of metallic chamber, in which electromagnetic fields build up at a given frequency. This frequency is selected such that it should be an integer multiple of the revolution frequency of electrons. Longitudinal electric field component of electromagnetic field is used to transfer energy for the electron beam along the beam direction. Due to this field component, in the longitudinal direction, electron bunches are formed near the synchronous phase This synchronous phase is defined for a reference electron, which is moving with the design energy and synchronous time for this, energy gain from the RF cavity is equal to energy loss per turn (U). The synchronous phase is given by

$$\phi_s = \sin^{-1}\frac{U}{eV} \tag{1.76}$$

Here U is electron energy loss per turn and $\boldsymbol{V}$ is a peak value of Voltage.

The momentum offset and phase deviation for other electrons with respect to the reference electron at a given instant are given by.

$$\delta_f = \delta_i + \frac{eV}{Eo}\{\sin(\psi_i + \phi_s) - \sin(\phi_s)\} \tag{1.77}$$

$$\psi_f = \psi_i + 2\pi h \alpha_c \delta_f \tag{1.78}$$

Here an electron enters the cavity at a phase ψ_i with a momentum offset δ_i. The energy and phase of this electron at the time of exit from cavity is δ_f and ψ_f respectively. h and $\alpha_c = I_1/C$ are the harmonic number and momentum compaction factor respectively. Here I_1 is the first synchrotron radiation integral, which is given by equation (1.52) and C is the ring circumference.

Equations (1.75) and (1.76) show that if electrons, are deviated in momentum or in phase with respect to reference electron, they will oscillate around the synchronous phase. These oscillations are termed as synchrotron oscillation. The maximum number of bunches (RF bucket), which can be stored in the ring are governed by the harmonic number, which is the ratio of the RF frequency to the revolution frequency of the reference electron.

1.2.7 Acceptance of the ring

The parameter acceptance is defined as the maximum phase space area in which the injected and stored beam can be survived. This parameter plays an important role in deciding the beam injection [19] and beam lifetime. In a linear ring, the acceptance is defined with the help of physical aperture of vacuum chamber, in the presence of nonlinear magnetic components this is defined by dynamic acceptance. In horizontal plane, the physical acceptance is given by

$$A_x = \min\left(\frac{a_x(s) - |\eta_x(s)\delta p/p|}{\sqrt{\beta_x(s)}}\right)^2 \tag{1.79}$$

Here $a_x(s)$ is the half width of the horizontal vacuum chamber, $\beta_x(s)$ and η(s) are chosen at a point 's' in which horizontal acceptance is evaluated.

The acceptance can be increased by reducing the maximum beta function. In the ring, normally the injection septum magnet is kept close to the design orbit, thus the horizontal acceptance is limited at the location of septum magnet. The local projection of the acceptance gives the allowable minimum and maximum aperture, in which the electron beam survives.

$$x(s) = \pm\sqrt{A_x\beta_x}(s) + \eta(s)\delta p / p \tag{1.80}$$

During the beam injection, higher aperture is required at the point of beam injection, which can be obtained by increasing the beta function at the injection point. In vertical plane, vertical acceptance and aperture can be evaluated using the similar expression, in this plane η(s) is zero. Normally in an electron storage ring, the vertical acceptance is reduced due to smaller magnet pole gap of insertion devices.

In a real storage ring/synchrotron, there are always errors in the magnets and in the placement of these magnets, which affect the dynamics. In the ring, the design orbit is decided by the dipole magnets. Now any dipolar field errors will lead to deviation in the orbit, which is termed as closed orbit distortion (COD) [12]. From this distorted orbit, deviated electron will now exhibit betatron oscillations around this orbit. Similarly any quadrupolar field errors will change the pattern of the betatron oscillation and hence the beta function. This change in beta function with respect to design value is known as beta-beat (β-asymmetry). In presence of these errors, physical acceptance of the ring is also reduced.

In the presence of sextupole magnets and nonlinear imperfections of the ring magnets structural resonances ($P = S \times I$, where S is the periodicity of the machine, P and I is integer) and the random ($P = I$) resonances will be excited due to periodic or random field distribution of these forces respectively. The resonance condition is given by

$$l\nu_x + m\nu_z = P \tag{1.81}$$

$$|l| + |m| = n$$

Where l, m, n and P are the integers and n is the order of resonance. In an uncoupled motion, we can consider these cases separately for each plane. The n^{th} resonance is excited by the tune values $1/n$ for the 2n-pole field error. From equation (1.81), it can be seen that in the ring, resonances can be avoided by choosing the suitable tune point.

In the presence of linear and nonlinear forces, the acceptance is reduced due to excitation of nonlinear resonances. Thus in a real ring, the available acceptance, which is defined by dynamic acceptance may be smaller as compared to the physical acceptance. The dynamic acceptance is the maximum area in the phase space, in which motion of the electron remains stable. The projected area of horizontal and vertical dynamic acceptances on real space i.e. in a horizontal and a vertical plane, is known as 'dynamic aperture'. The dynamic aperture estimation is carried out on the basis of tracking simulations. In this, method different initial horizontal and vertical coordinates of electrons with on and off-momentum are tracked in a magnetic lattice of a storage ring for defined number of turns to check the stability of phase space. The tracking is performed by using the standard beam dynamic tracking code such as RACETRACK [20], MAD [21] etc. The dynamic aperture is mainly governed by the tune. Thus the tune point should be properly selected to obtain sufficient dynamic aperture.

As stated earlier, in this thesis, three different important and essential aspects of beam dynamics of synchrotron radiation sources are studied, i.e. beam injection in a synchrotron, double bend achromat lattice for achieving low emittance and effects of insertion devices on beam dynamics. Therefore, after having a basic review on elementary concepts of beam dynamics, basics of these three areas are discussed and presented in brief in the next sections. These aspects are studied using cases from Indus accelerator facility. Thus, a brief sketch of Indus accelerator facility is drawn. Subsequent chapter have details of beam injection with a case study of synchrotron, magnetic lattice for low emittance with a case study of Indus-2 and effects of a wavelength shifter with a case study of Indus-1.

1.3 Magnetic lattices for synchrotron radiation sources

The smaller beam emittance (higher brightness) can be achieved by adopting a suitable magnetic lattice which defines the arrangement of magnetic elements namely dipole, quadrupole and sextupole magnets in the synchrotron radiation source. In a third generation synchrotron radiation source, the magnetic lattice is designed such that besides providing a small beam emittance, long straight sections preferably dispersion free are also made available for installation of insertion devices.. The dispersion free region can be obtained with the help of specially designed and optimized configuration of magnetic structure known as achromat section. The achromat section is formed with at least two dipole magnet and a suitable arrangement of focussing and defocusing magnets in between the dipole magnets. The brightens from an insertion devices is given by [1]

$$\text{Brightness} = \frac{\text{Flux}}{4\pi^2 \sqrt{\sigma_x^2 + \sigma_\lambda^2}\ \sqrt{\sigma_x'^2 + \sigma_\lambda'^2}\ \sqrt{\sigma_y^2 + \sigma_\lambda^2}\ \sqrt{\sigma_y'^2 + \sigma_\lambda'^2}} \tag{1.82}$$

Here $\sigma_{x,y}$ and $\sigma'_{x,y}$ are the rms beam size and rms beam divergence of the electron beam, σ_λ and σ'_λ are the sizes and angle for the particular wavelength (λ) of the photon beam, subscript x and y denotes horizontal and vertical plane respectively. The equation shows that up to certain limit by reducing the electron beam size and divergence, the brightness from insertion devices can be increased.

The beam emittance for a given lattice is governed by following relation [11]

$$\varepsilon = F_{lattice} C_q \gamma_o^2 \theta_b^3 \tag{1.83}$$

Here $F_{lattice}$ is a form factor, which is the intrinsic property of a given lattice. C_q is the compton wavelength of the electron, γ_o is the reduced energy (ratio of total energy of electron to the rest energy) of the electrons and θ_b is the bending angle of a dipole magnet.

The equation (1.83) shows that in a lattice, beam emittance is proportional to the third power of bending angle (θ_b), therefore smaller beam emittance is achieved by reducing the bending angle. In this case, for storage ring more number of unit cells are required. The smaller beam emittance (higher brightness) is also achieved by adopting a suitable magnetic lattice ($F_{lattice}$), which defines the arrangement of magnetic elements namely dipole, quadrupole and sextupole magnets. The commonly used magnetic lattices [22-33] are FODO lattice, double bend achromats (DBA), triple bend achromats (TBA) and multiple bend achromats (MBA). Here we give a brief description of different choices of lattices.

1.3.1 FODO lattice

In FODO lattice, dipole magnet is located between QF and QD magnet. This structure is more compact [28], thus in a given ring more number of unit cells of this structure can be accommodated. In the unit cell, dispersion function is non zero at the location of insertion section, which is used for insertion devices. The zero dispersion function can be obtained with the help of missing dipole scheme. However, in this case, twiss parameters are not symmetric with respect to center of insertion section. For this lattice, minimum value of $F_{lattice}$ is equal to 1.2 thus beam emittance for such structure can be defined as

$$\varepsilon = 1.2 C_q \gamma_o^2 \theta_b^3 \tag{1. 84}$$

1.3.2 Double bend achromat lattice

In the double bend achromat lattice, a double bend achromat is accompanied by sections having zero dispersion function on both sides for installation of insertion section (as shown in figure 1.3). In the double bend achromat, the dispersion function and its derivative for an electron beam entering the first dipole magnet and of the beam coming out of second dipole magnet are zero. In this lattice, the horizontal beam emittance [8] is given by

$$\varepsilon = C_q \gamma_o^2 \theta_b^3 \frac{1}{j_x}\left(\frac{1}{3}\frac{\beta_{o,x}}{l_b} - \frac{1}{4}\alpha_{o,x} + \frac{1}{20}\gamma_{o,x} l_b \right) \tag{1.85}$$

Here $\alpha_{o,x}, \beta_{o,x}$ & $\gamma_{o,x}$ are the horizontal twiss parameters at the beginning of the dipole magnet.

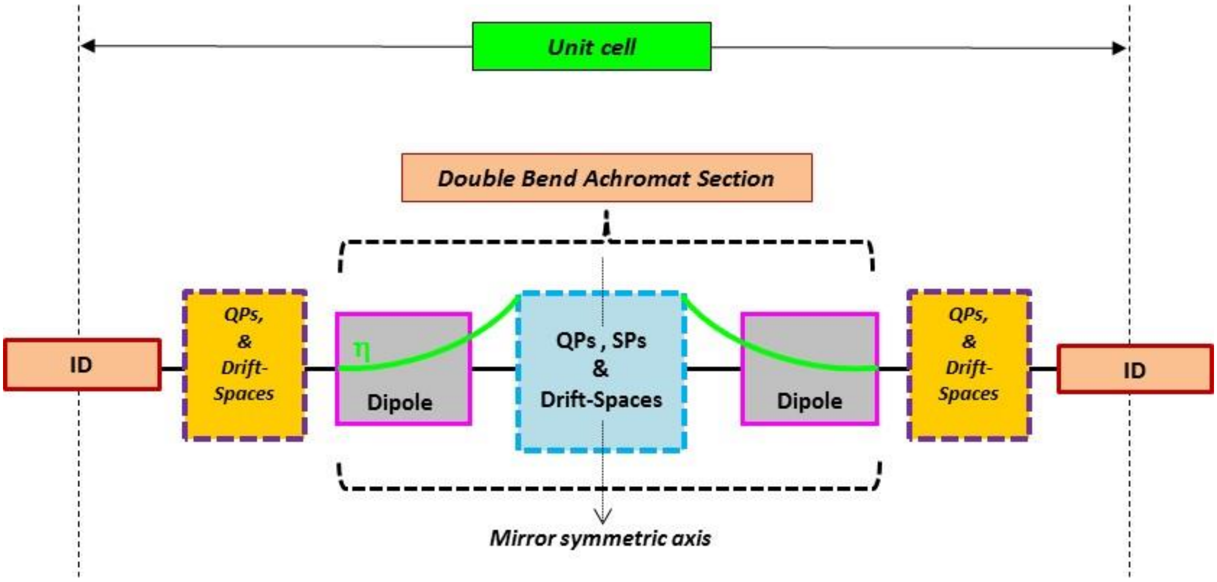

Figure 1. 3 A schematic diagram of double bend achromat lattice, in which along with a double bend achromat section, long straight sections for installation of insertion devices are shown. The symbol QP, SP and ID denote quadrupole magnet, sextupole magnet and insertion device respectively.

In the lattice, a variation of beta (β) and dispersion (η) functions within the dipole magnet are shown in the figure 1.4. The minimum beam emittance [29] is searched by finding the optimum values of $\beta_{o,x}$ and $\alpha_{o,x}$. At optimum values of $\beta_{o,x}^*$ and $\alpha_{o,x}^*$, minimum beam emittance is

$$\varepsilon_{min} = C_q \gamma_0^2 \theta_b^3 \frac{1}{4\sqrt{15}} \tag{1.86}$$

With $\alpha_{o,x}^* = \sqrt{15}$ and $\beta_{o,x}^* = \sqrt{\frac{12}{5}}\, l_b$, $\beta_{min,x}^* = \sqrt{\frac{3}{320}}\, l_b$ at $3/8 l_b$ of the dipole magnet

Here β_{min} is the minimum horizontal beta function in the dipole magnet and an asterisked quantity means the quantity is evaluated when the minimum beam emittance condition is fulfilled. In this lattice the beam emittance is smaller than the FODO lattice by a factor of 5.0.

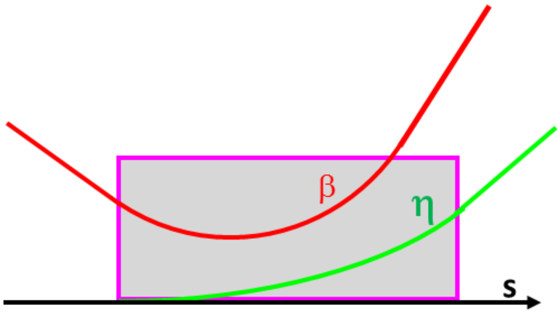

Figure 1. 4 A schematic diagram showing variation of beta and dispersion functions in a dipole magnet of a double bend achromat lattice.

1.3.3 Theoretical minimum beam emittance lattice

In the double bend achromat lattice, beam emittance is further reduced with the help of optimizing dispersion function in the dipole magnet, this lattice is termed as theoretical minimum beam emittance lattice. In the lattice achromatic condition is broken as a result outside the achromat dispersion function is finite. A variation of beta and dispersion function within the dipole magnet of the lattice is shown in the figure 1.5. In this case, for minimum beam emittance $\langle H \rangle$ function, where H defined in equation (1.59), is optimised with respect to twiss parameters $(\beta_{o,x}, \alpha_{o,x})$ and dispersion function. The minimum beam emittance [30] by considering equal bending angle of all dipole magnets is given by

$$\varepsilon_{min} = C_q \gamma_0^2 \theta_b^3 \frac{1}{12\sqrt{15}} \tag{1.87}$$

For this, in the center of the dipole magnet $\beta_{min,x} = {l_b}/{\sqrt{15}}$ and $\eta_{min} = {l_b}^2/{24\rho}$.

And at the start of dipole magnet $\alpha_{o,x}^* = \sqrt{15}$, $\beta_{o,x}^* = \frac{8}{\sqrt{15}} l_b$, $\eta_o^* = {L\theta_b}/{6}$ and $\eta_o'^* = {-\theta_b}/{2}$.

In this case, $F_{lattice}$ is equal to $\frac{1}{12\sqrt{15}}$. In this lattice, the beam emittance is smaller than the double bend achromat lattice by a factor of three and from the FODO lattice by a factor of 15.5. At the insertion section, dispersion function is non-zero, which will increase the beam emittance due to emission of synchrotron radiation from insertion devices. Thus in most of the synchrotron radiation sources [34], the beam emittance is optimized with slight leakage of the dispersion function in the insertion section. With this condition, beam emittance is reduced by a factor of two in comparison to the design value of beam emittance in achromatic condition.

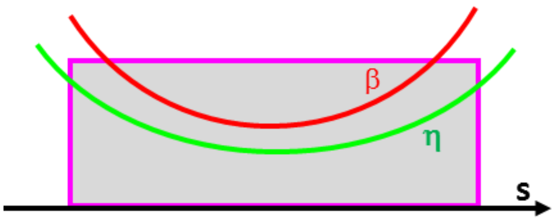

Figure 1. 5 A schematic diagram showing variation of beta and dispersion functions in a dipole magnet of a theoretical minimum beam emittance lattice.

1.3.4 Triple or multiple bend achromat lattice

For theoretical minimum emittance lattice, the minimum beam emittance is one third of double bend achromat lattice. For this lattice, in the insertion straight section dispersion function is non zero, this drawback is overcome with triple bend achromat lattice. A triple bend achromat lattice, is a combination of the double bend achromat and theoretically minimum beam emittance lattice. In triple bend achromat section, in the middle of double bend achromat at the mirror symmetry point one dipole is placed (as shown in figure 1.6). With this additional dipole, bending angle is reduced. For example by considering equal bending angle for all dipole magnets, beam emittance is reduced by one third. Further at the dipole, variations of beta and dispersion functions have to be optimized according to the theoretical minimum beam emittance lattice with the adjustment of length of dipole magnet, quadrupole strengths and drift space between the magnetic elements. In this condition horizontal beta and dispersion functions are to be kept small between the dipoles, which results strong strength of chromaticity correcting sextupoles to correct the natural chromaticity resulting in the reduction of dynamic aperture. In the lattice, the minimum beam emittance [31, 33] is

$$\varepsilon_{min} = C_q \gamma_0^2 \theta_b^3 \frac{7}{9} \frac{1}{4\sqrt{15}} \tag{1.88}$$

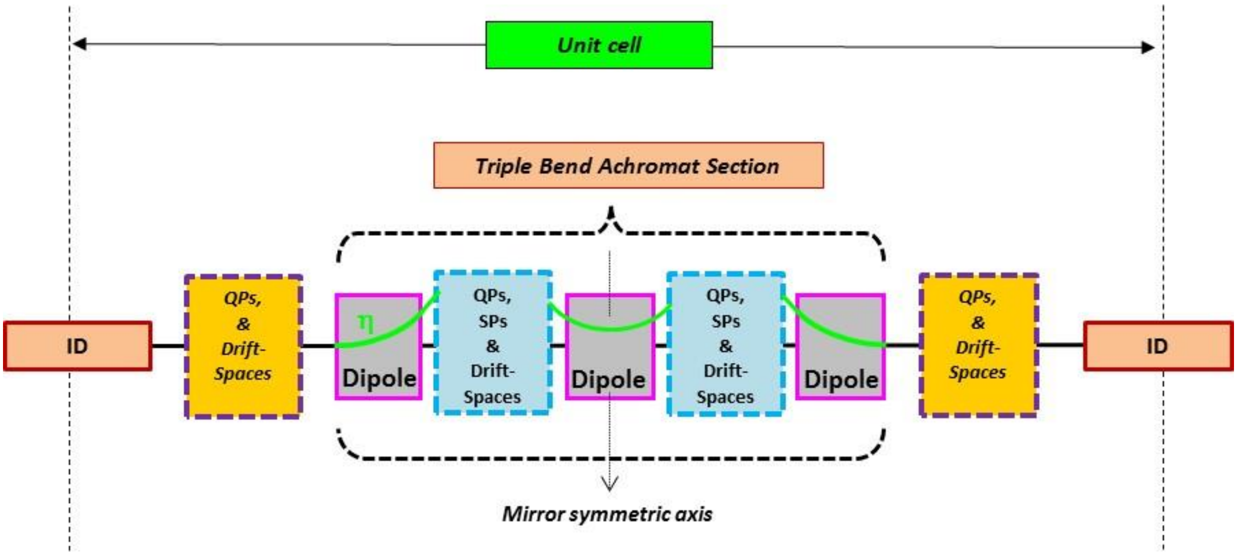

Figure 1. 6 A schematic diagram of triple bend achromat lattice, in which along with a triple bend achromat section, long straight sections for installation of insertion devices are shown The symbol QP, SP and ID indicate quadrupole magnet, sextupole magnet and insertion device respectively.

The beam emittance can be further reduced if bending angle of the centre dipole is kept 1.5 times higher in comparison to the bending angle of side dipole magnet. Generally in this configuration, the strong strength of chromaticity correcting sextupoles may reduce the dynamic aperture. Keeping this into mind, in Indus-2 double bend lattice is preferred over the triple bend achromat lattice.

In the triple bend achromat lattice by using more than one dipole (multiple bend achromat) in between the two dipole magnet, beam emittance can be further reduced. This type of lattice is termed as multiple bend achromat lattice. In this lattice minimum beam emittance [33] is

$$\varepsilon_{min} = C_q \gamma_o^2 \theta_b^3 \left(\frac{M+1}{M-1}\right) \frac{1}{12\sqrt{15}} \qquad (1.89)$$

Here M is the number of dipole magnet.

Recently, multi-bend achromat lattices have been chosen in various synchrotron radiation sources [4.5] to reduce the beam emittance in pm-rad range.

1.4 Injection scheme

The objective of the injection scheme is to trap injected beam in the synchrotron/storage ring vacuum chamber with minimum residual betatron oscillations [19, 35-37]. Here, we will discuss in brief about beam injection.

The beam is transported with the help of transfer line from exit of one accelerator to entry of another accelerator and afterwards the beam is injected into the ring with the help of the injection septum magnet. The transport line is used to manipulate the beam twiss parameters and dispersion function to satisfy the requirements of beam injection. The twiss parameters and dispersion function of the injection septum magnet are matched with those of the ring then it is called matched beam injection otherwise it is called mismatch beam injection. Similarly in the longitudinal plane, timing of injected beam and its momentum spread should be such that injected beam should be trapped inside the RF bucket with minimum synchrotron oscillations. The injection septum magnet is located inside the ring, which provides deflection to the incoming beam with minimum disturbances to the stored beam. At exit of the magnet, the beam executes betatron oscillation around the design orbit due to finite displacement of the injected beam with respect to this orbit. In this process, the beam may be lost at the magnet within a few turns. For example, for $\nu_x = 2.25$, after 4^{th} revolution the beam hits to the septum magnet as its displacement at the magnet is same as that of before injection. This loss can be avoided with the help of single turn and multi-turn injection schemes. The single turn and multi-turn injection schemes are classified depending upon the pulse duration of injection kicker magnet (T_k from start of injection), in which its magnetic field is reduced to zero.

1.4.1 Single turn injection scheme:

In this scheme, injection kicker pulse amplitude as well as its timing are to be adjusted such that in the next turn after beam injection the beam does not experience any deflection from the kicker magnet, otherwise the beam will be deflected out of the ring acceptance. In the scheme, pulse of injected beam is shorter as compared to the revolution period of the ring. Generally, this scheme is applicable to the synchrotron when there is no stored beam.

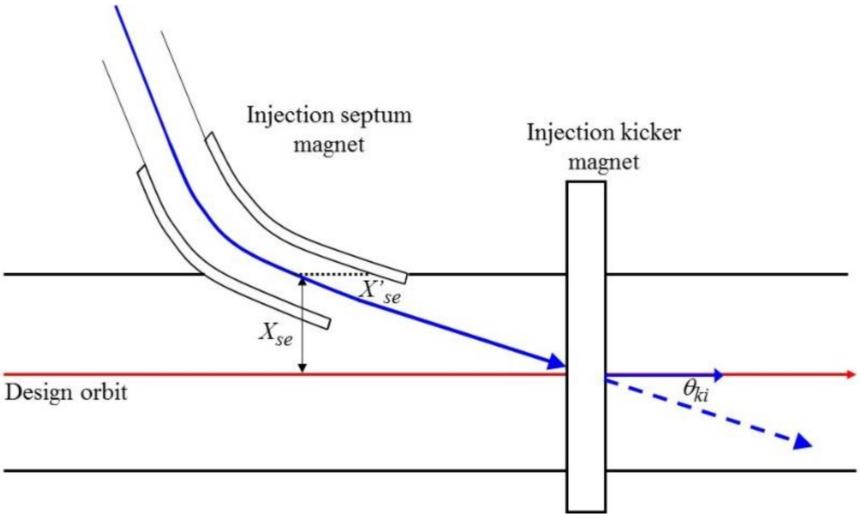

Figure 1. 7 A schematic diagram of single turn injection scheme

A schematic diagram of the scheme is shown in the figure 1.7. The beam is injected into the ring with the help of the injection septum magnet. The transfer matrix from the injection septum magnet (se) to injection kicker magnet location (ki) is written as

$$\begin{bmatrix} x_{ki} \\ \theta_{ki} \end{bmatrix}$$

$$= \begin{bmatrix} \sqrt{\frac{\beta_{ki,x}}{\beta_{1x}}}(\cos\Delta\mu_x + \alpha_{se,x}\sin\Delta\mu_x) & \sqrt{\beta_{se,x}\beta_{ki,x}}\sin\Delta\mu_x \\ -\frac{(1+\alpha_{se,x}\alpha_{ki,x})\sin\Delta\mu_x + (\alpha_{se,x}-\alpha_{ki,x})\cos\Delta\mu_x}{\sqrt{\beta_{si,x}\beta_{ki,x}}} & \sqrt{\frac{\beta_{se,x}}{\beta_{ki,x}}}(\cos\Delta\mu_x - \alpha_{ki,x}\sin\Delta\mu_x) \end{bmatrix} \begin{bmatrix} x_{se} \\ x'_{se} \end{bmatrix} \tag{1.90}$$

With $\Delta\mu_x = \mu_{ki,x} - \mu_{se,x}$

The beam position at the kicker magnet location is

$$x_{ki} = x_{se}\sqrt{\frac{\beta_{ki,x}}{\beta_{se,x}}}(\cos\Delta\mu_x + \alpha_{se,x}\sin\Delta\mu_x) + \mathrm{x'}_{se}\sqrt{\beta_{se,x}\beta_{ki,x}}\sin\Delta\mu \tag{1. 91}$$

In the single injection kicker scheme, it is necessary that at the injection kicker magnet location, the injected beam displacement should be zero.

$$x_{ki} = 0.0 \tag{1.92}$$

The required strength of injection kicker magnet (θ_{ki}) and injected beam angle at the septum magnet ($\mathrm{x'}_{se}$) to bring the injected beam on the orbit are estimated with following relations

$$x'_{se} = -x_{se}\frac{(\alpha_{se,x} + \cot\Delta\mu_x)}{\beta_{se,x}} \tag{1.93}$$

$$\theta_{ki} = -\frac{x_{se}}{\sqrt{\beta_{se,x}\beta_{ki,x}}\sin\Delta\mu_x} \tag{1.94}$$

To minimize the strength of θ_{ki}, the injection septum and injection kicker magnet should be kept at high value of beta-function and simultaneously the phase advance between them should be 90^o.

1.4.2 Multi- turn injection scheme:

This scheme is generally used for beam injection into the synchrotron and storage ring. In the scheme, injected beam pulse length acceptance may be higher as compared to the revolution period the ring. This can be achieved with the help of the fractional horizontal tune around 0.25

and a small bump reduction rate. To capture the injected beam, ring acceptance is moved towards the septum magnet with the help of time dependent orbit bump, which is created for few turns. This bump is generated, either, with the help of single kicker magnet (globally) or locally with the help of two, three or four kicker magnets.

The bump and its reduction rate are optimized such that in consecutive turn the injected beam can be accepted and the beam which is already stored should not hit to the any part of the ring. In this process, early beam occupies near to the center of the acceptance and later beam at the periphery of the ring acceptance.

The amplitude of bump (B) and the location of the septum magnet from the designed orbit (L_s) can be approximately calculated from the following relation.

$$B = 4\sigma_{xi} + 2S_c + S_t \tag{1.95}$$

$$L_s = B + 4\sigma_{xs} + S_c \tag{1.96}$$

Here σ_{xi} and σ_{xs} denotes beam size of the injected and stored beam respectively, S_c and S_t denotes clearance and thickness of the injection septum magnet.

In synchrotron, Indus-1 and Indus-2, three, single and four injection kicker schemes are adopted respectively to carry multi-turn beam injection. The detail of multi-turn injection scheme is discussed for single kicker, three kicker and four kickers in Chapter-5, 2 and 4, respectively.

1.5 Effect of insertion devices on beam dynamics

The insertion device is a periodic arrangement of magnetic field either in vertical plane (planner) or in both transverse planes (horizontal and vertical). This can be classified on the basis of deflection parameter (*K*), which is defined as K=0.934B_o(T)λ(cm), here λ and *Bo* is the period length and peak magnetic field of insertion devices respectively. Generally, the deflection parameter for undulator is less than 1 and for wiggler this is greater than 1. The magnetic field [38-41] of a planner insertion device is given as;

$$
\begin{aligned}
B_x &= (k_x / k_y) B_o \sinh(k_x x)\sinh(k_y y)\cos(kz) \\
B_y &= B_o \cosh(k_x x)\cosh(k_y y)\cos(kz) \\
B_z &= -(k / k_y) B_o \cosh(k_x x)\sinh(k_y y)\sin(kz) \\
k_x^2 + k_y^2 &= k^2 = (2\pi / \lambda)^2
\end{aligned}
\tag{1.97}
$$

Here, x, y and z are horizontal, vertical and longitudinal directions respectively.

The parameter k_x measures the transverse variation of the field and if $k_x \neq 0$ then B_y increases with x and hence provide the horizontal focusing. If k_x is imaginary then B_y will fall with x and provide horizontal defocusing. The above expressions are valid if deviation of the electron beam trajectory from the central axis is small.

Ideally, the insertion device should be designed such that effect of this device on the beam dynamical parameters is negligible. In reality, this device has significant linear and nonlinear effects [38-41] on the dynamics of the beam. These are arises due to its intrinsic magnetic field configuration and residual field errors which are attributing due to in-homogeneities of the magnetization within the magnet block, assembly and machining tolerances etc.

The first condition is to match the orbit at entry and exit of insertion devices (sinusoidal trajectory of electron beam inside the device) with the ring orbit. These conditions are satisfied with

$$I_1 = \int_{-L}^{L} B_{x,y} ds = 0 \tag{1.98}$$

$$I_2 = \int_{-L}^{L} \int_{-L}^{s} B_{x,y} ds' ds = 0 \tag{1.99}$$

The linear and nonlinear effects on the beam dynamics due to its intrinsic magnetic field configuration can be studied with the help of Hamiltonian.

1.5.1 Hamiltonian in presence of insertion devices

The Hamiltonian of an electron [39] under above magnetic field (equation (1.97) can be written as,

$$H = \frac{1}{2}\left(p_z^2 + [p_x - A_x \sin(kz)]^2 + [p_y - A_y \sin(kz)]^2\right) \tag{1.100}$$

Here

$$A_x = \frac{1}{k\rho}\cosh(k_x x)\cosh(k_y y) \tag{1.101}$$
$$A_y = -\frac{k_x}{k_y}\frac{\sinh(k_x x)\sinh(k_y y)}{k\rho}$$

Here $\rho = \frac{3.33E(\text{GeV})}{B_o(\text{T})}$, which is the radius of curvature corresponding to the field B_o

In equation (1.100), after a canonical transformation to change the betatron variables with the oscillating trajectory of electron beam and hyperbolic function of cosine and sine are expanded up to fourth order in x and y. Afterwards H is given by

$$H = \frac{1}{2}\left(p_x^2 + p_y^2\right) + \frac{1}{4k^2\rho^2}\left(k_x^2 x^2 + k_y^2 y^2\right) + \frac{1}{12k^2\rho^2}\left(k_x^4 x^4 + k_y^4 y^4 + 3k_x^2 k^2 x^2 y^2\right) \tag{1.102}$$
$$-\frac{\sin(ks)}{2k\rho}\left[p_x\left(k_x^2 x^2 + k_y^2 y^2\right) - 2k_x^2 p_x xy\right]$$

The equations of motion are given by Hamiltonian's equations.

$$x' = \frac{\partial H}{\partial p_x},\ p_x' = -\frac{\partial H}{\partial x},\ y' = \frac{\partial H}{\partial p_y} \text{ and } \quad p_y' = -\frac{\partial H}{\partial y} \tag{1.103}$$

The equations of motion are same as betatron equations of motion in the storage ring. They are given as:

$$x'' = -\frac{k_x^2}{2k^2\rho^2}\left[x + \frac{1}{6}k_x^2 x^3 + \frac{1}{2}k_y^2 xy^2\right] \tag{1.104}$$
$$-\frac{\cos(ks)}{\rho}\left[\frac{1}{2}\left(k_x^2 x^2 + k_y^2 y^2\right) + \frac{1}{4}k_x^2 k_y^2 x^2 y^2 + \frac{1}{24}\left(k_x^4 x^4 + k_y^4 y^4\right)\right]$$
$$-\frac{\sin(ks)}{\rho}kyy'\left[1 + \frac{1}{2}k_x^2 x^2 + \frac{1}{6}k_y^2 y^2\right]$$

$$y'' = -\frac{k_y^2}{2k^2\rho^2}\left[y + \frac{1}{6}k_y^2 y^3 + \frac{1}{2}k_x^2 x^2 y\right] + \frac{\cos(ks)}{\rho}\left[k_x^2 xy + \frac{1}{6}k_x^2 k_y^2 xy^3 + \frac{1}{6}k_x^4 x^3 y\right] \tag{1.105}$$
$$+\frac{\sin(ks)}{\rho}kyx'\left[1 + \frac{1}{2}k_x^2 x^2 + \frac{1}{6}k_y^2 y^2\right]$$

In equation (1.104) and (1.105), oscillating terms contain normal and skew sextupole, octupole like non-linarites and are equal to zero after averaging over the period length. After averaging over the period length equation of motions are

$$x'' = -\frac{k_x^2}{2k^2\rho^2}\left[x + \frac{1}{6}k_x^2 x^3 + \frac{1}{2}k_y^2 x y^2\right] \tag{1.106}$$

$$y'' = -\frac{k_y^2}{2k^2\rho^2}\left[y + \frac{1}{6}k_y^2 y^3 + \frac{1}{2}k_x^2 x^2 y\right] \tag{1.107}$$

1.5.2 Linear and nonlinear effect of insertion devices

The first term in equation (1.106) and (1.107) represents quadrupole field, second and third terms represent octupole like fields. Due to quadrupole components periodicity of the lattice will be broken due to distortions of betatron functions. These will cause a change in beam sizes that can affect the users, reduce beam lifetime and break the symmetry of chromaticity correcting sextupoles. The break in symmetry can excite additional linear and nonlinear resonances. In thin lens approximation, tune shift and maximum β-asymmetry (beta-beat) [11] due to quadrupole component for the sinusoidal planner insertion device are

$$\Delta\nu_y = \frac{1}{4\pi}\int \frac{\beta_y k_y^2 ds}{2k^2\rho^2} \tag{1.108}$$

$$\left[\frac{\Delta\beta_y}{\beta_y}\right]_{\max} = \frac{\beta_y k_y^2 L}{4k^2\rho^2 \sin(2\pi\nu_y)} \tag{1.109}$$

$$\Delta\nu_x = \frac{1}{4\pi}\int \frac{\beta_x k_x^2 ds}{2k^2\rho^2} \tag{1.110}$$

$$\left[\frac{\Delta\beta_x}{\beta_x}\right]_{\max} = \frac{\beta_x k_x^2 L}{4k^2\rho^2 \sin(2\pi\nu_x)} \tag{1.111}$$

Here L denotes the length of insertion devices.

The octupole like components will produce the amplitude-dependent tune-shifts and can excite the following 4th order resonances.

$$4\nu_x = m \text{ , } 4\nu_y = m \text{, } 2\nu_x \pm 2\nu_y = m \tag{1.112}$$

Where m is any integer

Since the effect of quadrupole and octupole components depends upon the horizontal and vertical beta function. Thus it is preferable to keep small value of these functions at insertion devices. It can be also shown that at lower energy, the linear and nonlinear effects of insertion devices will be more significant.

Now we will present a brief description of Indus-1 and Indus-2 storage ring

1.6. Indus synchrotron radiation source

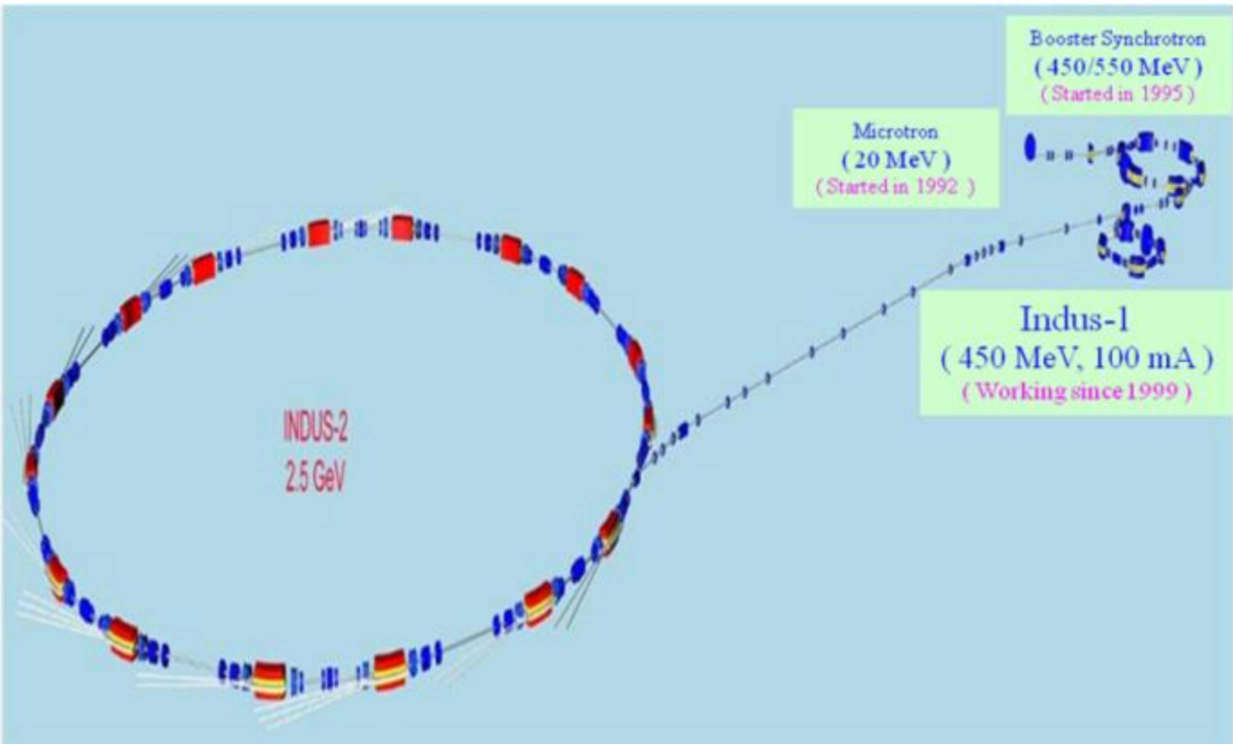

Figure 1. 8 A schematic view of Indus-1 and Indus-2 ring along with synchrotron and microtron.

Raja Ramanna Centre for Advanced Technology (RRCAT) in Indore (India) houses two synchrotron radiation sources, namely Indus-1 [42, 43] and Indus-2 [44-46]. Indus-1 is a 450 MeV, small storage ring, which is designed to produce radiation in vacuum ultraviolet (VUV) region. On the other hand, Indus-2 is a 2.5 GeV, moderate third generation X-ray synchrotron radiation source. Both the storage rings share common pre-injector microtron and injector synchrotron. Microtron raises the electron beam energy to 20 MeV and this electron beam is sent to the synchrotron via Transfer Line-1 (TL-1). Electrons are extracted from the synchrotron at 450/550 MeV, transported and injected to the Indus-1 or Indus-2. In Indus-1, electrons are injected at the peak energy of the ring i.e. at 450 MeV whereas in Indus-2 they are injected at 550MeV. The above process is repeated every second until the desired current is achieved. In Indus-2 after storage of required beam current, electrons are accelerated to 2.5 GeV. A schematic layout showing these sources is displayed in figure 1.8. A brief description of these rings is discussed below.

1.6.1 Synchrotron

A synchrotron is used for accelerating the electron beam energy from 20 MeV to 450/550 MeV, its schematic layout is given in figure 1.9. It is a separated function accelerator, which has a six super-periods and each super-period consists of one sector dipole, one horizontal focussing (QF) and one defocusing (QD) quadrupole magnet. S1 to S6 are six straight sections. The section S1 accommodates the injection septum and injection kicker magnet (K2). The injection kicker (K3) and extraction kicker magnet are located in section S2. In S4 section extraction septum magnet is located from which beam is extracted and S6 section is used to accommodate the RF cavity and injection kicker (K1) magnet.

A 20 MeV, 500 ns long electron beam pulse from the microtron is injected into it with the help of a multi-turn injection scheme [47, 48]. The energy of the injected electrons is increased with the help of the RF cavity and the beam orbit kept constant by synchronously increasing the magnetic fields in dipole, quadrupole and steering magnets. A capacitive loaded re-entrant structure [43] was chosen for the RF cavity. For orbit correction, six horizontal corrector magnets (secondary coil on each dipole) and five vertical corrector magnets are used, which are located almost uniformly around the ring.

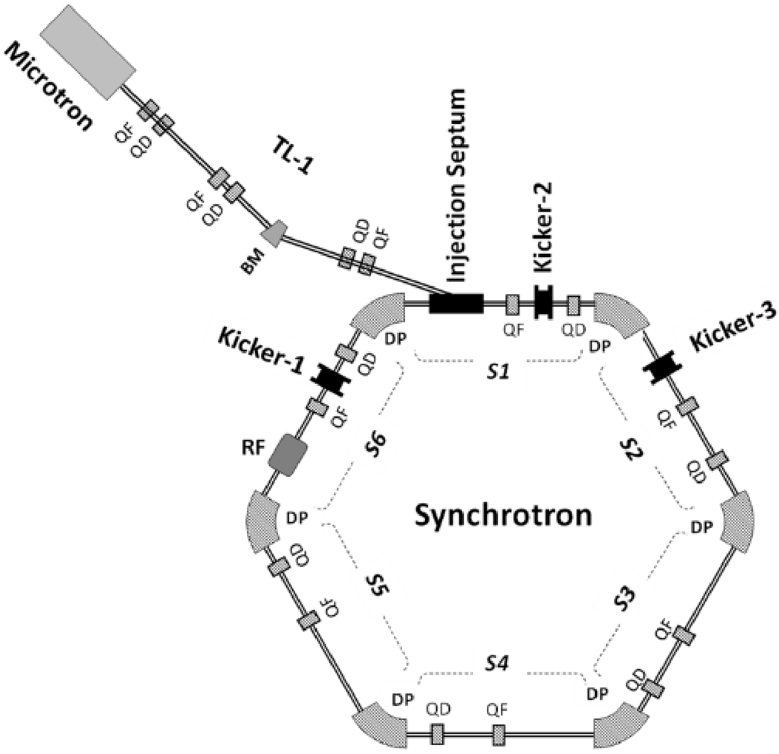

Figure 1. 9 A schematic layout of synchrotron

Table 1. 1: Parameters of the synchrotron

Final beam energy	450/550 MeV*
Current	~3-4 mA
Circumference	28.45 m
Super-periods	6
Tune point	2.11,1.44
Harmonic number	3
RF frequency	31.619 MHz

* 450 MeV for injecting into Indus-1 and 550 MeV for injecting into Indus-2

After acceleration to 450 /550 MeV, the electrons are extracted from the synchrotron [47] and then transported with the help of transfer lines (TL-2/TL-3) to the Indus-1/Indus-2 storage ring. In the synchrotron three electron bunches are formed, as its RF frequency is three times the revolution frequency. These bunches are extracted with the help of the fast extraction kicker and extraction septum magnet. At present, the rise time of the magnetic field of fast extraction kicker is 45 ns and separation between two bunches is 30 ns thus two bunches out of three bunches are extracted and one bunch is lost during the extraction process. The main parameters of the synchrotron are shown in table 1.1

1.6.2 Indus-1

Indus-1 is a 450 MeV storage ring, which generates synchrotron radiation in the range 30 - 2000 Å, mainly from the dipole magnet. This magnetic lattice consists of 4 superperiods, each having one dipole magnet with a field index of 0.5, two doublets of quadrupoles (QF and QD) and a 1.3 m long straight section.

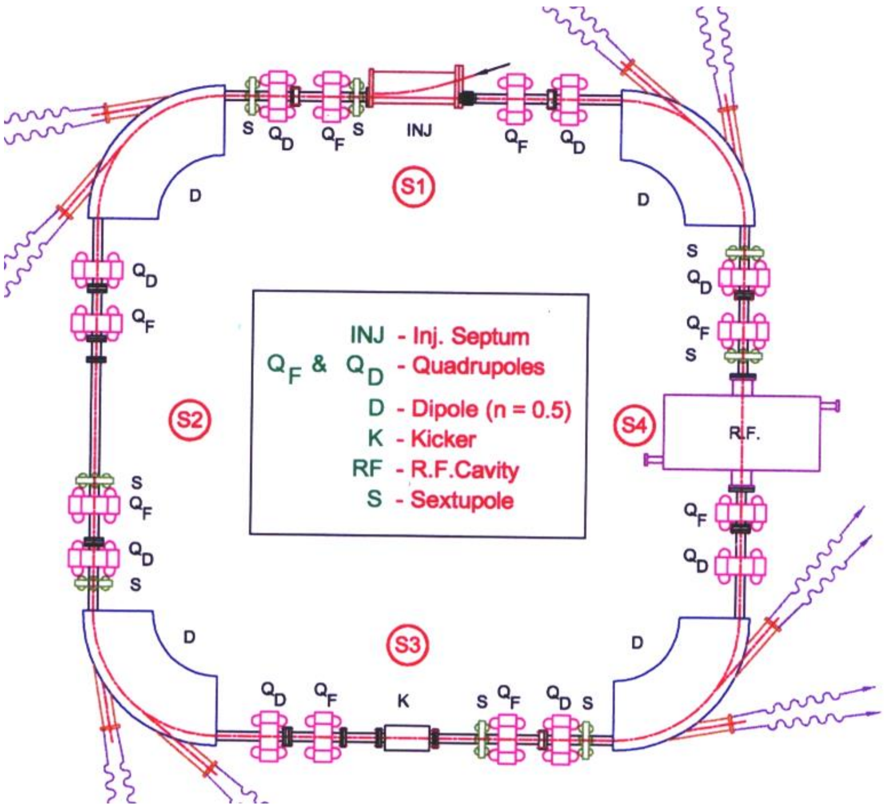

Figure 1. 10 A schematic layout of Indus-1 ring, here QF, and QD, represent focusing and defocusing quadrupole magnet respectively.

The ring has four straight sections S1 to S4, out of these two sections namely S1 and S3 are used for beam injection. The injection septum and kicker magnets are placed in the sections S1 and S3 respectively. Of the remaining two sections (S2 and S4), S2 section is kept to accommodate a 3 Tesla wavelength shifter and S4 section is used to accommodate an RF cavity. The layout and the main parameters of Indus-1 are given in figure-1.10 and table-1.2 respectively. The structure of the RF cavity is similar to the RF cavity of synchrotron i.e. capacitive loaded re-entrant structure. This wavelength shifter is considered to shift its critical wavelength from 61 A^o to 31 A^o. A comparison of spectral flux variation with energy for the bending magnet and the wavelength shifter is shown in figure-1.11. The wavelength shifter will be a superconducting device with total length of 0.54 m. The device will have three dipoles magnets. The peak magnetic field of the central dipole and side dipole will be 3.0 T and 1.5 T respectively.

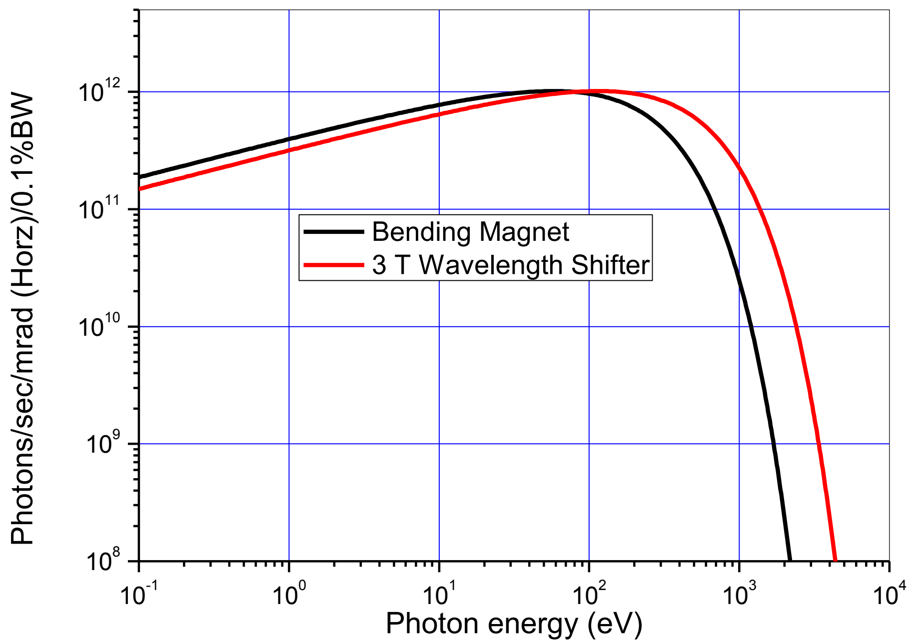

Figure 1. 11 In Indus-1, spectral flux of bending magnet and wavelength shifter with respect to photon energy.

1.6.3 Indus-2

Indus-2 is a 2.5 GeV a moderate third generation synchrotron radiation source, in which critical wavelength of the radiation from dipole magnets is 2 Å. A double bend achromat lattice having 8 unit cells is adopted for this source. One of its unit cell along with ring is shown in figure

1.12. Each unit cell has a 4.6 m long straight section, two 22.5° rectangular bending magnets, a triplet of quadrupoles (QF-QD-QF) to control the dispersion in the achromat section, two quadrupole triplets (QD-QF-QD) for the adjustment of beam sizes in the 4.6 m long straight sections and four sextupoles in the achromat section for the correction of natural chromaticity. In the ring for orbit correction, 48 horizontal correctors, 40 vertical correctors and 56 beam position indicators are located around the ring. Out of eight 4.6 m straight sections, one is used for the beam injection, two for the RF cavities and the remaining five for insertion devices. The structure of RF cavities are bell shaped. The main parameters of the ring are tabulated in table-1.2.

Table 1. 2: Main parameters of Indus-1 and Indus-2

Parameters	**Indus-1**	**Indus-2**
Beam energy at injection	450 MeV	550 MeV
Final stored beam energy	450 MeV	2.5 GeV
Circumference	18.966 m	172.474 m
Operating beam current	125 mA	175 mA
Critical wavelength	61 Å	1.98 Å
Beam emittance($\varepsilon_{x}/\ \varepsilon_{y}$)	$7.0\times10^{-8}/7.0\times10^{-9}$ m-rad	$5.8\times10^{-8}/5.8\times10^{-10}$ m-rad
Periodicity	4	8
No. of dipole, quadrupole and sextupole magnets	4,16,8	16,72,32
Harmonic number	2	291
RF frequency	31.619 MHz	505.812MHz
Energy loss per turn from dipole magnets	3.6 keV	623 keV
RF voltage	22 kV	1.27 MV
Number of cavities	1	4

In the ring, a multi turn injection scheme, employing a compensated bump generated by four kickers is used, which are located in first long straight section. The electron beam is injected, from the synchrotron at a peak energy of 550 MeV with a repetition rate of 1 Hz. In the ring, injection is carried out to store up to 200 mA beam current with the help of multi bunch filling scheme [50, 51]. After accumulation of the desired beam current, the stored beam is accelerated to 2.5 GeV by slowly increasing magnetic field of the all the magnets of the storage ring in a synchronous manner.

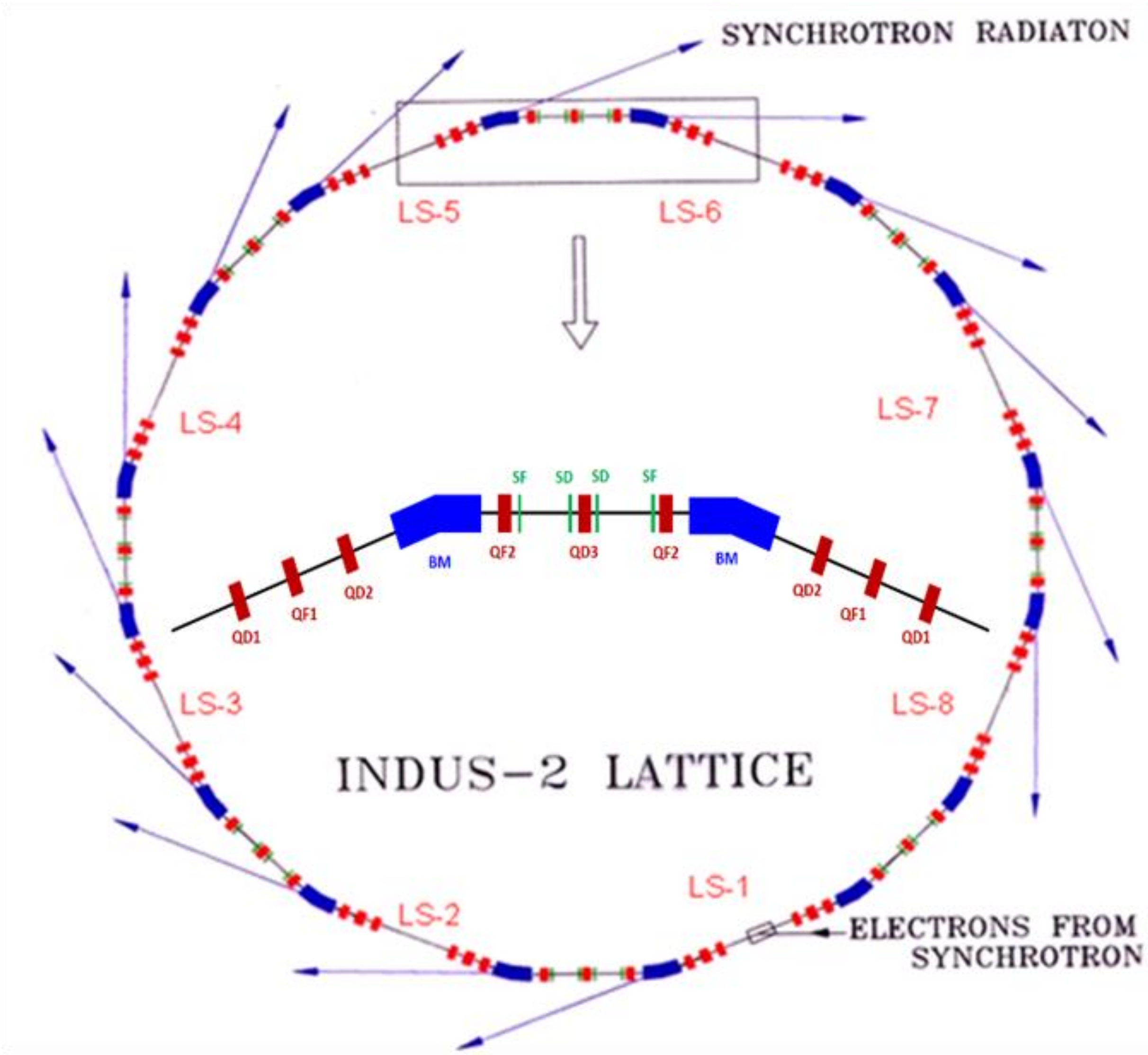

Figure 1. 12 A schematic diagram of Indus-2 ring

CHAPTER 2

BEAM INJECTION INTO SYNCHROTRON

In this chapter, the mechanism of beam injection into the synchrotron is studied. As discussed in Chapter-1, the synchrotron is a common injector for Indus-1 and Indus-2 synchrotron radiation sources. Electron beam is injected into it in the horizontal (radial) plane through an injection septum magnet, employing a three-kicker multi-turn injection scheme [47]. The injection septum magnet is kept close to the focusing quadrupole magnet, where twiss parameters (β and α) have large values. The high value of horizontal beta function helps in maximizing horizontal beam acceptance of the synchrotron, which is desirable for beam injection. The large α-function (alpha function) plays an important role in deciding beam displacement and residual betatron oscillations during beam injection.

In the synchrotron, the injected beam oscillations after beam injection do not die during first few milliseconds and during this time a major part of the beam loss takes place, since the damping time of betatron oscillation at 20 MeV, the energy at which electrons are injected into the synchrotron is 14 minutes. The loss of electron beam is mainly attributed to the un-bunched electron beam pulse injection, a small dynamic aperture, variation of tune point during beam energy ramping, absence of chromaticity correction etc.

In the injection plane, when the beam acceptance is small, it is better to inject few turns (pulse length equal to few revolution periods of the synchrotron) with small residual betatron oscillations, so that injected turns are lodged within the real physical acceptance/dynamic acceptance. With this in view, beam injection is performed in the compensated and uncompensated orbit bump schemes [48] at present operating tune point ($\nu_x = 2.11, \nu_y = 1.44$) of the injection energy. It is noticed that accelerated beam current in the uncompensated bump scheme (keeping the strengths of the kickers magnets equal) is higher as compared to the compensated bump scheme.

Theoretical as well as experimental studies are carried out to explain why the performance of the synchrotron is better in the uncompensated bump scheme as compared to the compensated bump scheme. Normally in an electron storage ring, beam injection is carried out in such a way that the entire injected beam pulse undergoes the same deflection in passing through the septum magnet. This is achieved by injecting the beam at the top of the injection septum magnet pulse. Here, we have also extended studies in both injection schemes to the case in which the angle of the injected beam is varied from turn to turn, which is done by injecting the beam on rising part of the injection septum magnet.

2.1 Injection scheme

In the synchrotron, the compensated or uncompensated bump during beam injection is produced by using three kicker magnets or kickers, which are located inside vacuum chamber in S6 (first kicker), S1 (second kicker) and S2 (third kicker) straight sections as shown in figure 1.9 of Chapter-1. The parameters of the microtron [52] are tabulated in table 2.1.

Table 2. 1: Parameters of the Microtron

Parameters	**Value**
Output	20 MeV
Output current	15 mA
Pulse length	0.5 μs
Pulse	1 Hz
Energy spread	±0.1%
Emittance	1π mm mrad horizontally, 3π mm mrad vertically

At the time of beam injection, the center of injected beam is separated from the injection septum magnet at a radial distance (x_c) of 38 mm from the design beam orbit as shown in figure 2.1. The injection septum magnet is azimuthally located between first and second kicker, having thickness (S_t) of 3 mm and its inner edge is at 32 mm from the design orbit.

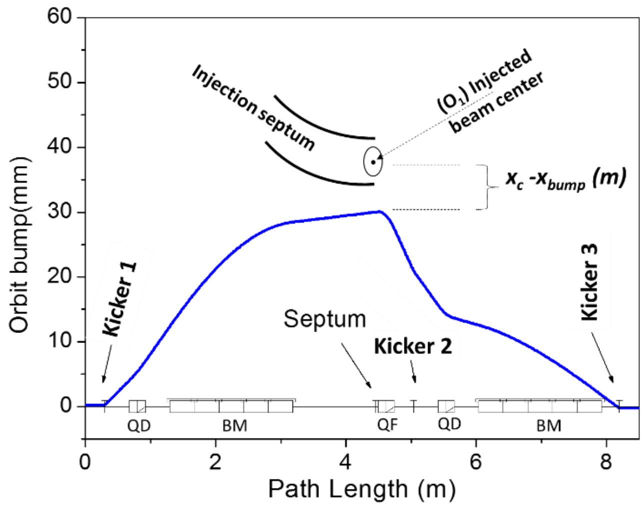

Figure 2. 1 Compensated orbit bump of 30 mm, generated by kicker-1, 2 and 3.

The kicker magnetic field pulses are half sinusoids. The electron beam is injected during the last 1 μs of the falling part of the pulse to achieve nearly linear rate of fall of the orbit bump. During this period, the injection kicker strengths are changed with time according to the relation

$$\delta_i(n) = \frac{\theta_i \cos\pi\{(n-1)T_r + T_d\}/T_k}{\cos(T_d\pi/T_k)} \qquad (2.1)$$

Where *i* (*i* =1-3) denotes kicker -1,2 and 3 respectively, θ_i is maximum deflection imparted by the kicker *i*, n corresponds to number of turns of the injected electrons in the synchrotron, (*n* = 1 represents the initial injection time), T_r is revolution period in the synchrotron (~94 ns), T_k is the duration of kicker pulse, which is 14.2 μs and T_d is additional delay in the pulse length from peak of the injection kicker pulse to the injection point (6.1 μs).

A theoretical study of the injection dynamics is presented assuming the length of the incoming electron beam pulse to be 1 μs with constant beam current. The initial part of incoming beam enters the synchrotron 1 μs before, the kickers are switched off. The injected beam pulse is divided into 11 equal parts (slices). The pulse length of each slice is equal to one synchrotron revolution period (~T_r). The kicker strengths are reduced linearly during injection, as a result the starting part of a slice and its last part appearing after 94 ns experiences different injection bump depending upon the bump reduction rate. The first slice corresponds to the initial part of the incoming beam and the 11th represents the last part of the 1 μs beam pulse. The last slice length is ~64 ns, which is shorter in comparison to 94 ns. The beam is injected in the ramp mode, in which current of synchrotron magnets (dipole, quadrupole and steering) are raised synchronously. In this mode, during beam injection beam energy ramp rate is ~1 keV/μs, which is negligible.

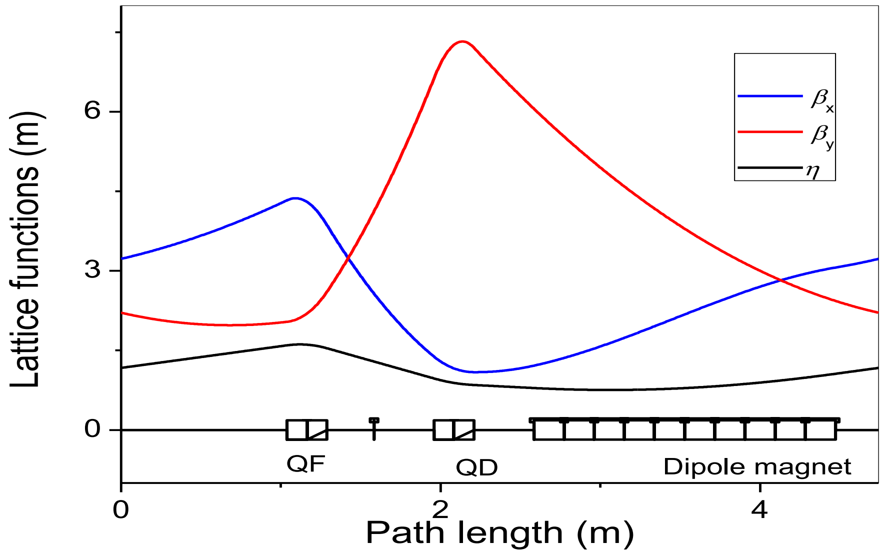

Figure 2. 2 For one superperiod of synchrotron lattice functions at the operating tune point (ν_x=2.11, ν_y=1.44)

The lattice functions (twiss parameters) of the synchrotron at the tune point (2.11, 1.44) are shown in figure 2.2. The maximum beta function at the focussing quadrupole location (4.33 m) is slightly higher as compared to the beta function at the septum magnet location (4.28 m). The maximum of the orbit bump occurs near the septum magnet. The inner edge of the septum magnet is at 32 mm, whereas all over the ring physical aperture is ±45 mm. Therefore if the beam does not hit the septum magnet it will not hit the vacuum chamber anywhere else. In these studies, we have, therefore, tracked the position of the slices at the septum magnet location.

The slices, which have injected beam displacement (in the presence of injection bump) and residual betatron oscillation amplitude (after beam injection) less than 31.5 mm (by considering septum magnet clearance (S_i) as 0.5 mm) are considered to be accepted. The amplitude of the residual betatron oscillation is the amplitude of coherent betatron oscillation after beam injection. To carry out the injection simulations, the computer program RACETRACK [20] is modified as per the requirement.

2.1.1 Compensated orbit bump scheme

i) Theory

The synchrotron acceptance at the septum magnet location is shifted with the help of the orbit bump to trap the injected beam (which is away from the synchrotron). In three kicker injection scheme, the compensated orbit bump and its slope for first turn at the septum magnet location [8 -12] are given by

$$x_{bump}(1) = \theta_1 \sqrt{\beta_{1,x}\beta_{s,x}}\,\sin(\mu_{s,x} - \mu_{1,x}) \tag{2.2}$$

$$x'_{bump}(1) = \theta_1 \sqrt{\frac{\beta_{1,x}}{\beta_{s,x}}}\left[\cos(\mu_{s,x} - \mu_{1,x}) - \alpha_{s,x}\sin(\mu_{s,x} - \mu_{,1,x})\right] \tag{2.3}$$

To generate the bump, the strengths of the kickers are calculated using the following relation.

$$\theta_1 = \frac{x_{bump}(1)}{\sqrt{\beta_{1,x}\beta_{s,x}}\,\sin(\mu_{1,x}-\mu_{s,x})}\,,\quad \theta_2 = -\theta_1\sqrt{\frac{\beta_{1,x}}{\beta_{2,x}}}\,\frac{\sin(\mu_{3,x}-\mu_{1,x})}{\sin(\mu_{3,x}-\mu_{2,x})}\quad \text{and} \tag{2.4}$$

$$\theta_3 = \theta_1\sqrt{\frac{\beta_1}{\beta_3}}\,\frac{\sin(\mu_{2,x}-\mu_{1,x})}{\sin(\mu_{3,x}-\mu_{2,x})}$$

Here, $\beta_{s,x}, \beta_{1,x}, \beta_{2,x}, \beta_{3,x}$ and $\mu_{s,x}, \mu_{1,x}, \mu_{2,x}, \mu_{3,x}$ are the beta functions and phase advance at the septum magnet and at the kicker-1, 2 and 3 location respectively. In this case, phase advances at the septum and at the kickers-1,2 and 3 are taken with respect to an arbitrary fixed point in the synchrotron, $\alpha_{s,x}$ denotes the α-function at the septum magnet location, For different turns (n), $x_{bump}(n)$ is calculated with $\delta_i(n)$, $\delta_i(n)$ is calculated via equations (2.1) and (2.4). In figure 2.1, the compensated three-magnet orbit bump of ~30 mm is shown.

The bump is gradually reduced as the beam is injected. The displacement of the injected beam, during and after beam injection depends on initial injected beam coordinates (displacement and angle) with respect to the bumped orbit. In order to find out the feasibility of injected turns, it is necessary to know its displacement from the design orbit. (Undistorted orbit). Here we present a mathematical formulation [35-37] to get an idea of displacement of the injected beam during beam injection and maximum residual betatron oscillation amplitude after beam injection. The phase space of the injected beam in the normalized coordinates is shown in figure 2.3 with reference to position of the bump at the injection septum (point O). The twiss parameters of the incoming beam are assumed to be matched with those of the synchrotron. The point O_1 represents the center of the injected beam and O_2 is the point where the injected beam touches the circle with radius OO_2 (equal to ρ) in which the injected beam executes betatron oscillations. This circle with radius ρ defines the maximum residual betatron oscillation amplitude after beam injection. The center of injected beam coordinates $(x_e, x_e^{/})$ for m^{th} slice (number of turn (n) starts from m), with respect to bumped orbit are defined by

$$x_e = x_c - x_{bump}(m) \tag{2.5}$$

$$x_e^{/} = \theta - x_{bump}^{/}(m) \tag{2.6}$$

Here x_c and θ are the center of injected beam position and angle coordinates with respect to design orbit.

The equation of injected beam circle is given by

$$(X - X_e)^2 + (X^{/} - X_e^{/})^2 = \beta_{s,x}\varepsilon \tag{2.7}$$

Here $X_e = x_e$, $X_e^{/} = \alpha_{s,x}x_e + \beta_{s,x}x_e^{/}$ and $X = x$, $X^{/} = \alpha_{s,x}x + \beta_{s,x}x^{/}$, x and $x^{/}$ are the displacement and angle of an electron beam with respect to the center of injected beam.

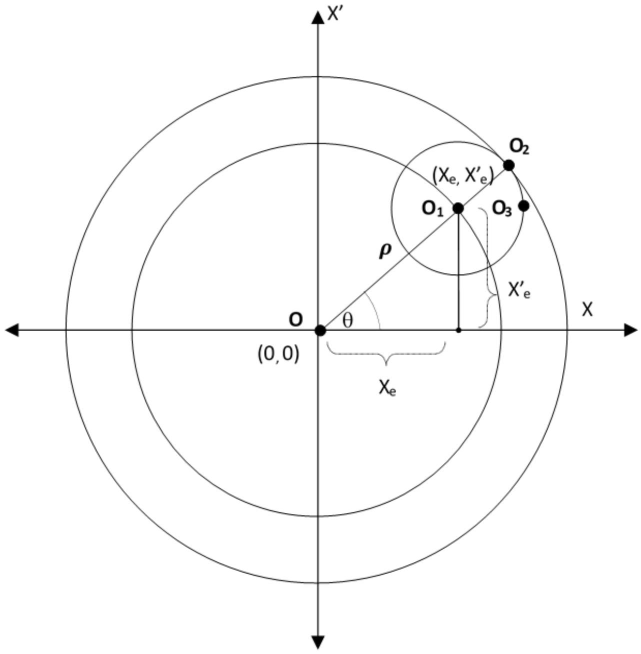

Figure 2. 3 A normalized phase space circles of injected beam and for residual oscillation.

The equation of the circle, in which injected beam executes betatron oscillations having radius ρ and center at O (0, 0) is

$$X^2 + X^{/2} = \rho^2 \tag{2.8}$$

The radius ρ and angle Θ as shown in figure 2.3 are

$$\Theta = \tan^{-1}\left(\frac{\alpha_{s,x}x_e + \beta_{s,x}x_e^{/}}{x_e}\right) \tag{2.9}$$

$$\rho = \sqrt{(\alpha_{s,x}x_e + \beta_{s,x}x_e^{/})^2 + x_e^2} + \sqrt{\varepsilon\beta_{s,x}} \tag{2.10}$$

The equation (2.9) shows that ρ is minimum, when $x_e^{/} = -\frac{\alpha_{s,x}x_e}{\beta_{s,x}}$, which leads Θ equals to zero degree.Coherent betatron oscillation amplitude (ρ_m) for mth slice is calculated after substituting $(x_e, x_e^{/})$ from equation (2.5) and (2.6) into equation (2.10) leading to,

$$\rho_m = \sqrt{\left[\left\{\alpha_{s,x}(x_c - x_{bump}(m)\right\} + \beta_{s,x}\left\{\theta - x_{bump}^{/}(m)\right\}\right]^2 + \left\{x_c - x_{bump}(m)\right\}^2} + \sqrt{\varepsilon\beta_{s,x}} \tag{2.11}$$

The minimum of ρ_m can be obtained with the help of following condition

$$\theta - x_{bump}^{/}(m) = -\frac{\alpha_{s,x}\left\{x_c - x_{bump}(m)\right\}}{\beta_{s,x}} \tag{2.12}$$

This equation shows that for a finite $\alpha_{s,x}$, as the bump reduces the difference between the injection angle and bump slope increases. In order to constrain the amplitude of residual betatron oscillation, either injection angle or bump slope or both of them need to be adjusted so that the condition of equation (2.12) is satisfied. In three kicker compensated bump scheme, it is not possible to adjust the bump slope for different slices, in the absence of this the only possibilities is to adjust the injection angle with the help of injection septum magnet for different slices.

While it is desirable to have minimum betatron oscillation of the injected beam slices, it is essential to first trap the injected beam slices in the synchrotron. It is therefore important to study the beam motion during the process of injection. During beam injection, the radius OO_1 is varying according to Θ and horizontal tune. The displacement of the extreme particle (point O_3 of figure 2.3) for m^{th} slice, in n^{th} turn from the design orbit depends upon the orbit bump and OO_1. This is given by the following relation.

$$x_m(n) = x_{bump}(n) + B_m \cos\{2(n-m)\pi\nu_x + \Theta(m)\} \pm \sqrt{\varepsilon\beta_{s,x}} \tag{2.13}$$

$$\Theta(m) = \tan^{-1}\left[\frac{\alpha_{s,x}\{x_c - x_{bump}(m)\} + \beta_{s,x}\{\theta - x'_{bump}(m)\}}{\{x_c - x_{bump}(m)\}}\right] \tag{2.14}$$

$$B_m = \sqrt{\left[\{\alpha_{s,x}(x_c - x_{bump}(m)\} + \beta_{s,x}\{\theta - x'_{bump}(m)\}\right]^2 + \{x_c - x_{bump}(m)\}^2} \tag{2.15}$$

In equation (2.13), a sign of last term (beam size $\sqrt{\varepsilon\beta_{s,x}}$) depends upon the sign of cosine function (of second term). If cosine function is positive, last term is positive otherwise it is negative. From equation (2.13), it can be shown, that in the presence of the bump after one turn, the injected beam reaches the septum magnet. This value will depend upon the bump reduction rate, horizontal tune as well as on Θ . To keep the injected beam far away from the septum magnet for a given horizontal tune, the bump reduction rate has to be properly adjusted. With a proper choice of Θ (which is adjusted with the injected beam coordinates), after one turn injected beam is kept away from the septum magnet, however, in this case residual betatron oscillations after beam injection is increased due to non-zero value of Θ .

In an ideal condition, for initial slice amplitude of residual betatron oscillation is equal to the injected beam size. For this bump reduction rate that is the rate at which bump is reduced, should be nearly equal to

$$\text{Bump reduction rate} = 2\,\sigma_{s,x} + S_c + S_t + S_i \tag{2.16}$$

Here $\sigma_{s,x}$ ($\sqrt{\beta_{s,x}\varepsilon}$) denotes the horizontal beam size, S_t septum magnet thickness, S_c septum magnet clearance for injected beam (inside the septum) and S_i septum magnet clearance for the stored beam.

Since in the three kicker injection scheme, an arbitrary bump slope is not possible at the injection point. Thus for different slices, θ have to be adjusted. In this case, first slice is on the design orbit and for consecutive slices residual betatron oscillations are increased according to bump reduction rate. If bump reduction rate is large, few slices will be accepted In the case of lower bump reduction rate, injected beam can be kept away from the septum magnet by slightly increasing the residual betatron oscillations of a first slice and properly choosing the horizontal tune. The horizontal tune needs to be kept away from an integer so that after one turn, the injected beam oscillations can be kept away from the septum magnet. In this aspect, fractional horizontal tune around 0.25 is more suitable choice. In this case, many slices can be accepted in the synchrotron and for consecutive slices, the residual betatron oscillations will be increased by a small value. In nutshell, in the process of injection optimization, the injection bump, bump reduction rate as well as injection angle (θ) for a given horizontal tune has to optimized such that maximum slices are accepted and for these slices residual betatron oscillations remain small.

ii) Injection simulations

In the synchrotron, at the septum magnet location σ_S is 2.1 mm, S_t is 3 mm and by choosing S_c and S_i 1 mm. With these parameters, the bump reduction rate required for the beam at the present horizontal tune (ν_x=2.11) to clear the septum magnet and circulation using equation (2.16) should be 8.7 mm/turn. With this bump reduction rate, first slice is on the orbit and for consecutive slices, residual betatron oscillations are increased by large value. Thus, it is required to find a moderate solution.

In the present configuration, an orbit bump of 38 mm is generated by operating the kickers $\delta_1(1)$, $\delta_2(1)$ and $\delta_3(1)$ at the strengths which correspond to beam deflection of 12.9 mrad, 9.8 mrad and 9.4 mrad respectively. The slope of the bump at the injection point with respect to the design orbit is 1.6 mrad. The bump reduction rate per turn is 3.5 mm. At the injection point on the present operating tune point, $\alpha_{s,x} / \beta_{s,x} = -0.16\,\mathrm{m}^{-1}$, where $\beta_{s,x}$ =4.3 m and $\alpha_{s,x}$ = -0.7 rad. With these parameters, from equation (2.12), in every turn, either injection angle of the injected beam should be increased or bump slope should be decreased in a step of 0.57 mrad to obtain the minimum residual betatron oscillation for all slices. In the present setup for 38 mm bump, the initial slope of the bump is 1.6 mrad and the bump is reduced in 11 turns, rate of the change of bump slope per turn is ~0.15 mrad. With this rate of change of bump slope, it is not possible to satisfy the condition (2.12) for all slices.

While it is desirable to have minimum betatron oscillation of the injected beam slices, it is essential to first trap the injected beam slices in the synchrotron. For the first slice, $x_{bump}(1)$ =38 mm, $x^1_{bump}(1)$ =1.6 mrad, the injected beam may hit the inner part of the injection septum magnet, after one turn of injection due to the lower bump reduction rate. This can be avoided by allowing higher residual betatron oscillation amplitude, which is obtained either by lowering the bump or by changing the injection angle of injected beam. For a fixed value of the bump and length of incoming beam pulse, the bump reduction rate is fixed. In order to optimize the injection process, in following studies, the position of the slices has been tracked at the septum magnet location for different injection angles.

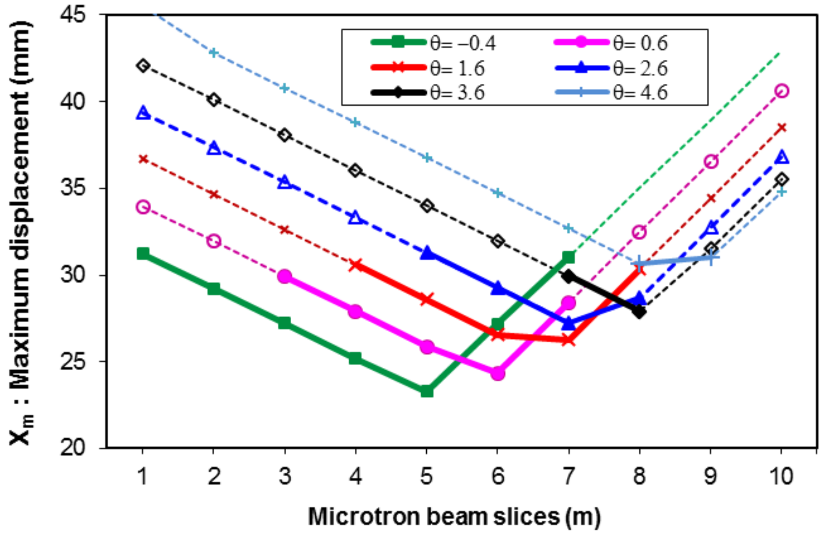

Figure 2. 4 In the compensated bump scheme, effect of injection angle (θ) on maximum beam displacement for different slices. The solid and dotted line indicates accepted and unaccepted part of the beam slices respectively. The calculations have been carried out by equation (2.13).

The effect of injected beam angle on the position of a slice during injection is calculated using equation (2.13). Figure 2.4 gives the displacement of injected slices during injection i.e. when the bump is being lowered. The displacement shown is the maximum value of the displacement in first 12 turns after the injection of a slice considering the bump at the start of beam injection to be 38 mm. Figure 2.5 gives the amplitude of the residual betatron oscillation ρ_m calculated using equation (2.11).

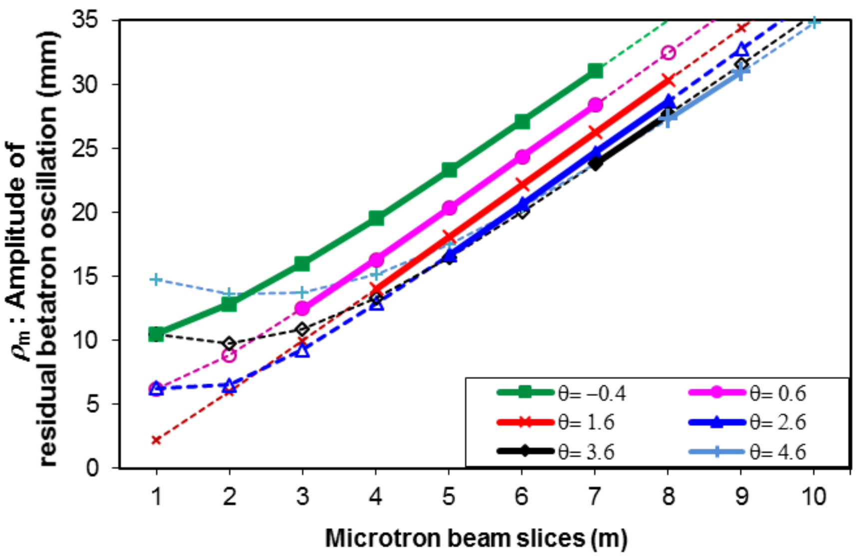

Figure 2. 5 In the compensated bump scheme, effect of injection angle (θ) on amplitude of residual betatron oscillation for different slices. The solid and dotted line indicates accepted and unaccepted part of the slices respectively. The calculations have been carried out by equation (2.11).

These figures 2.4 and 2.5 indicate that for the initial 5 slices, if the injection angle is reduced, displacement of an injected slice from the design orbit decreases but the amplitude of residual betatron oscillation is minimum for a certain injection angle as also indicated by equation (2.12). For the injection angle of 1.6 mrad, the first slice is injected on the bumped orbit and the amplitude of its residual betatron oscillation resulting from its beam size is minimum, other slices have higher residual betatron oscillation amplitude due to their finite displacement from the bumped orbit and also due to their non-optimum injection angle. The slices, which have injected beam oscillation less than 31.5 mm are considered. The figure 2.4 and 2.5 shows that at injection angle of -0.4 mrad, the number of slices accepted is maximum and their residual betatron oscillations after beam injection remains within the limit. This angle is – 2.0 mrad less as compared to the bump slope (1.6 mrad), which provides optimum angle of injection for the first slice. The amplitude of residual betatron oscillations for -0.4 mrad injection angle is much higher because the mismatch from the optimum angle is substantially increased. For the first slice, the amplitude of residual betatron oscillation is 10.5 mm and for other slices it increases progressively. In this case six slices are accepted and their residual betatron oscillation amplitudes are 10.5, 12.8, 15.9, 19.5, 23.2 and 27.0 mm. To look into the more details, the phase space plots for first to sixth slices are shown in the figure 2.6. The phase space plots also show a similar behaviour.

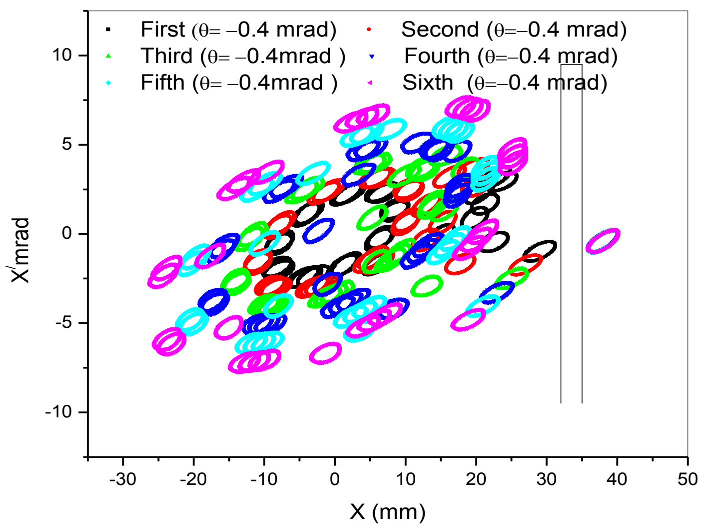

Figure 2. 6 In the compensated bump scheme, for the bump of 38 mm the injected beam phase space of first to six slices at the septum magnet for the injection angle (θ) of -0.4 mrad. The phase space is plotted by using computer code RACETRACK.

At higher bump reduction rate, the amplitudes of residual betatron oscillation are higher for all slices except that of one slice, which is on the bumped orbit. Presently, with the existing power supplies bump can be increased by 15%. In this case, for one accepted slice amplitude of residual betatron oscillation after beam injection can be reduced to 8.8 mm and for other slices, their amplitudes are 12.7, 17.1, 21.6 and 26.2 mm. which are significantly higher.

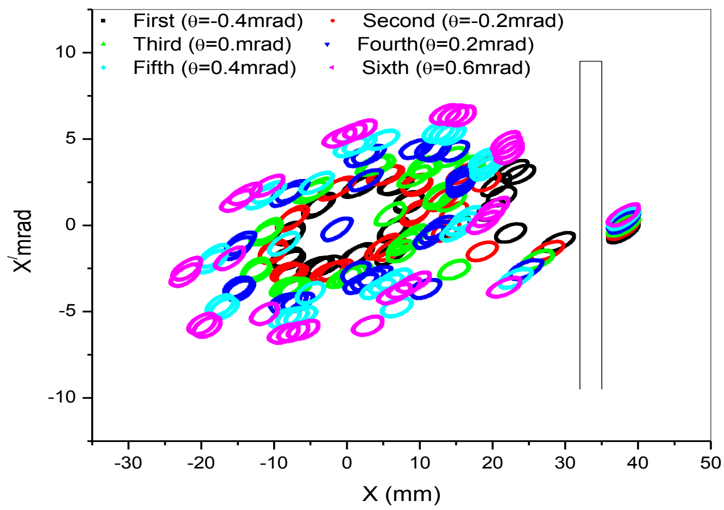

Figure 2. 7 In the compensated bump scheme, phase space of first to six slices of the injected beam when the beam injection angle (θ) is varied from -0.4 mrad to 0.8 mrad in step of 0.2 mrad during injection. The phase space is plotted by using computer code RACETRACK.

The above injection simulation (figure 2.4 and figure 2.5) indicate if injection angle is changed, the displacement of the injected beam as well as residual beam oscillation amplitude is changed. So the possibility to change the injection angle during beam injection is explored. When beam injection is performed on the rising part of the injection septum magnet pulse, different slices of the injected beam will also experience different injection angle. Due to limitation of injection septum magnet power supply, the injection angle for each slice can be increased up to 0.2 mrad only. In the compensated bump (38 mm) injection scheme, if injection angle (-0.4 mrad) is increased by 0.2 mrad for each slice, the residual betatron oscillation for different slices will be reduced in 0.0-2.7 mm range. The amplitudes of residual betatron oscillation, for 1st to 6th slices are 10.5, 12.0, 14.5, 17.5, 20.9 and 24.3 mm respectively. Their phase space plots are shown in the figure 2.7.

2.1.2 Uncompensated orbit bump scheme

At the injection septum magnet, orbit bump and its slope reduction rate can be adjusted by allowing closed orbit distortion all over the synchrotron. The orbit bump is not localized in the injection region thus this method of injection is called as uncompensated injection scheme. Here, bump, bump slope and their reduction rate are additional parameters for optimization. In this scheme, it is possible to reduce the residual betatron oscillations for at least few slices as compared to the compensated bump scheme. However, due to uncompensated bump for initial few turns, injected beam oscillation amplitude all over the synchrotron remains higher.

The bumped orbit $x_o(n)$ and its slope $x_o^{/}(n)$, at an observation point in the synchrotron for an arbitrary strength of three injection kickers are given by the following equations [11].

$$x_o(n) = \frac{\sqrt{\beta_{o,x}}}{2\sin\pi\nu_x}\sum_{i=1}^{3}\delta_i(n)\sqrt{\beta_{i,x}}\cos(\pi\nu_x - |\mu_{o,x} - \mu_{i,x}|) \tag{2.17}$$

$$x_o^{/}(n) = \frac{\sqrt{\beta_{i,x}}}{2\sqrt{\beta_{o,x}}\sin\pi\nu_x}\sum_{i=1}^{3}\delta_i(n)\left[\pm\sin(\pi\nu_x - |\mu_{i,x} - \mu_{o,x}|) - \alpha_{i,x}\cos(\pi\nu_x - |\mu_{i,x} - \mu_{o,x}|)\right] \tag{2.18}$$

Where $\beta_{o,x}$ and $\mu_{o,x}$ are the beta function and betatron phase advances at the observation point. The sign of the sine term in the second expression is positive if $\mu_{o,x} > \mu_{i,x}$ and negative if $\mu_{o,x} < \mu_{i,x}$.

The present operating condition, in which all injection kickers are operated at the strength of 14.6 mrad is discussed. This generates 60 mm orbit bump with bump slope of 8.2 mrad at the injection septum magnet location. The bumped orbit over the synchrotron is shown in figure 2.8 by using equation (2.17).

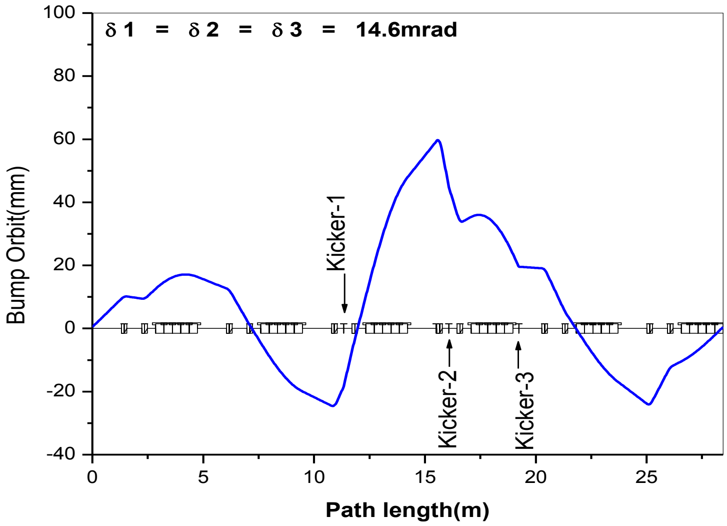

Figure 2. 8 The bumped orbit in the uncompensated orbit bump scheme with all injection kicker magnets set at 14.6 mrad. The bumped orbit is calculated by equation (2.17).

The injected beam angle sensitivity during and after beam injection are plotted for this scheme in figure 2.9 and 2.10. Figure 2.9 gives the displacement of injected slices, during injection i.e. when the bump is being lowered. The displacement shown is the maximum displacement in first 12 turns after the injection of a slice considering the bump at the start of beam injection to be 60 mm. Since the starting bump is much higher than the distance of the septum magnet from the design orbit, initial few slices are not accepted. Accordingly, in figure 2.9, initial three slices are not considered. The advantage of the higher bump gives a higher bump reduction rate and higher bump slope rate i.e. 5.5 mm per turn and 0.7 mrad per turn respectively, which helps in accepting some slices into the synchrotron. Figure 2.10 gives the amplitude of the residual betatron oscillation obtained by tracking the slices for forty turns. The amplitude of residual betatron oscillation for the 6^{th} slice is minimum for the injection angle of 5.6 mrad. This slice is not accepted as during injection this slice hits the septum magnet.

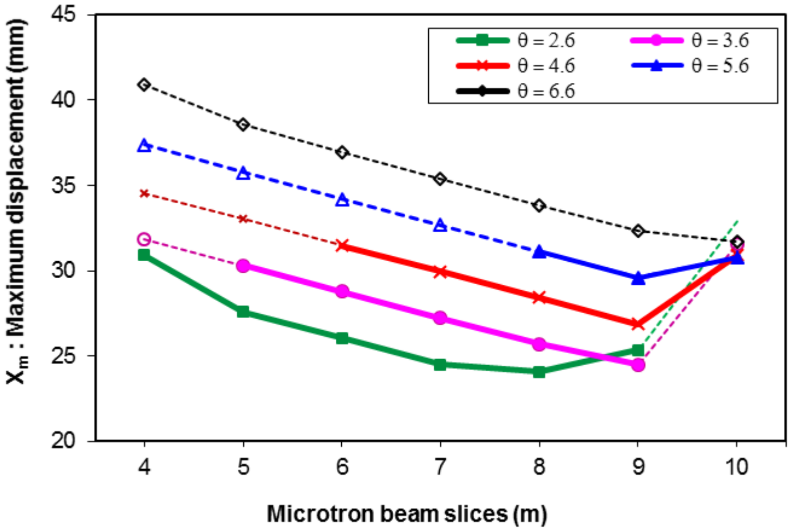

Figure 2. 9 In the uncompensated bump scheme, variation of maximum beam displacement with injection angle (θ) for different slices. The solid and dotted line indicates accepted and unaccepted part of the beam slices respectively. The simulations are carried out by using computer code RACETRACK.

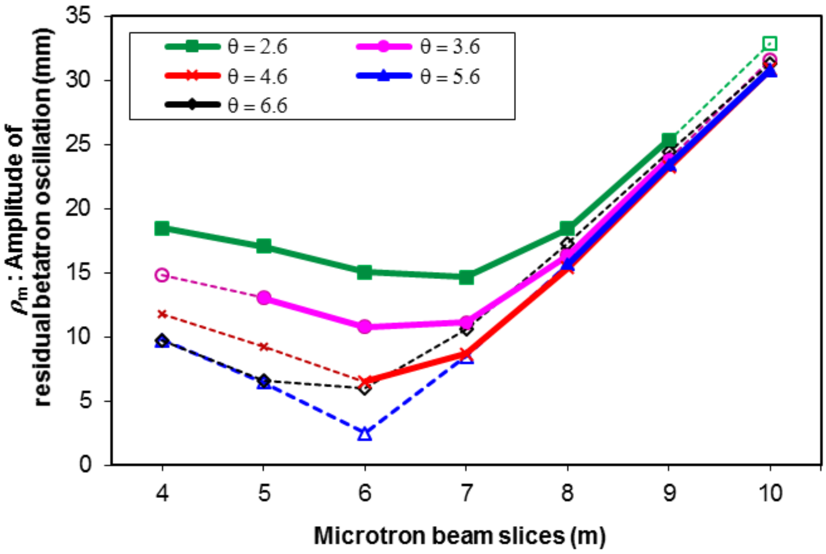

Figure 2. 10. In the uncompensated bump scheme, effect of injection angle (θ) on amplitude of residual betatron oscillation for different slices. The solid and dotted line indicates accepted and unaccepted part of the slices respectively. The simulations are carried out by using computer code RACETRACK.

At an injection angle of 4.6 mrad, four (6^{th} to 9^{th}) slices having an injected beam pulse length ~380 ns are fully accepted. For the 5^{th} slice, injected beam displacement at the septum magnet goes up to 33 mm, as a result a part of this slice hits the septum magnet and remaining part is accepted. The phase space for 5^{th} -9^{th} slices at the septum magnet is plotted in figure 2.11. For these slices, the amplitudes of residual betatron oscillation are 9.2, 6.5, 8.6, 15.3 and 23.1 mm. The results show that for consecutive 5^{th}, 6^{th} and 7^{th} slices residual betatron oscillations is increased by amounts which are much smaller than the bump reduction rate of 5.5 mm per turn. This is attributed to the nature of the bump and bump slope. This is the main benefit available, when the kickers are operated at equal currents.

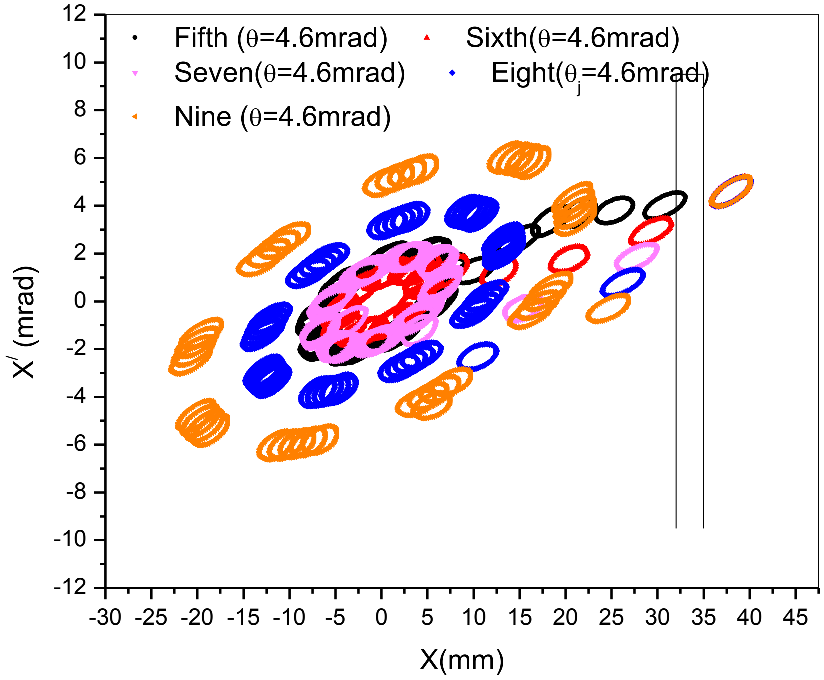

Figure 2. 11 At the septum magnet location, movement of the injected beam in phase space of fifth to nine slice at the injection angle (θ) of 4.6 mrad for the uncompensated bump scheme. The simulations are carried out by using computer code RACETRACK.

As mentioned earlier, it is possible to change the injection angle up to 0.2 mrad per slice or turn during injection by injecting the electron beam on the rising part of the septum magnet pulse. Beam injection dynamics is also studied for this case. Taking the variation of injection angle per turn as 0.2 mrad, the phase space during and after injection is plotted in figure 2.12 for the starting injection angle of 4.4 mrad. This figure shows that the part of the 5^{th} slice, which is hitting the septum magnet, is considerably reduced and the acceptance of this slice is accordingly increased. The amplitudes of residual betatron oscillation of 5^{th} to 9^{th} slice are 10.0, 6.5, 8.4, 15.3 and 23.2 mm. These are nearly the same as those obtained when the injection angle is fixed during injection.

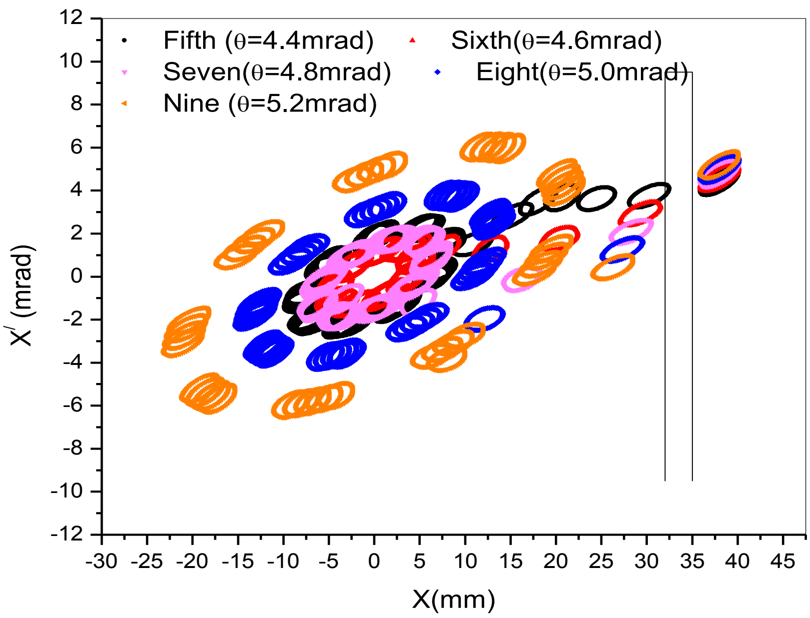

Figure 2. 12 At the septum magnet location, injected beam movement in phase space of fifth to nine slice, when the beam injection angle (θ) is varied from 4.4 mrad to 5.2 mrad in step of 0.2 mrad in the uncompensated bump scheme. The simulations are carried out by using computer code RACETRACK.

2.2. Performance of the synchrotron in different injection schemes

The results of two experiments performed to compare the performance of the synchrotron in the two injection schemes are discussed. In the first experiment, a 500 ns pulse from the microtron is injected into the synchrotron. In this experiment, the injection kickers current and timings are adjusted in such a way that in the compensated bump scheme, incoming beam experiences kicker magnetic field corresponding to 1st to 5th slices and in the uncompensated bump scheme (by keeping all kicker current at the same value) it corresponds to 5th to 9th slices. In the compensated and uncompensated bump scheme, ~1.3 mA (figure 2.13) and ~3.2 mA (figure 2.14) accelerated beam current is observed respectively. The results reported here correspond to acceleration of the beam to 550 MeV. There is no change in the performance of the synchrotron when electrons are accelerated to 450 MeV.

The beam injection is also performed by injecting the beam on the rising part (figure 2.15) of the septum magnet. The resultant increase in the injection angle of consecutive slices is 0.2 mrad /turn. In the compensated bump scheme, hardly any improvement in accelerated beam current is observed. In the uncompensated bump injection scheme accelerated beam current increases from ~3.2 mA to ~3.6 mA (figure 2.16).

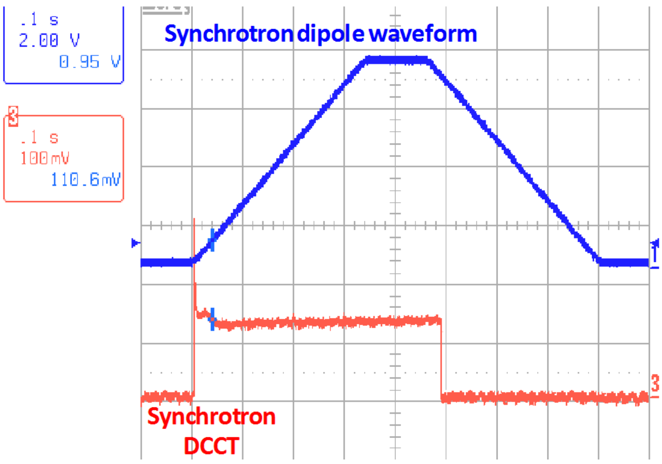

Figure 2. 13 Beam current in the compensated bump scheme, the dipole ramp profile and accelerated current (DCCT signal, 100 mV/mA) are label in the figure.

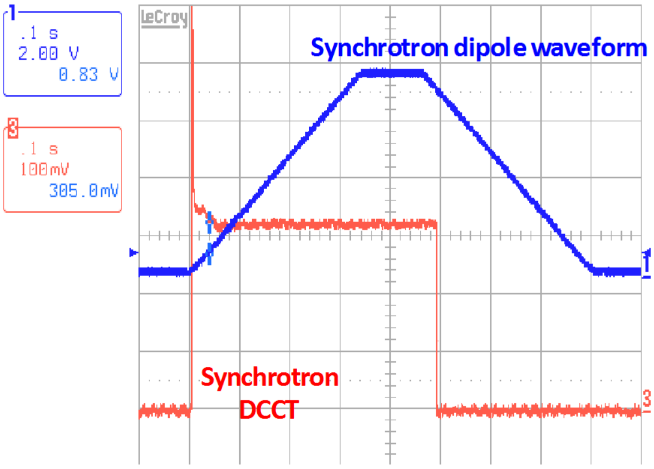

Figure 2. 14. Synchrotron DCCT in uncompensated bump scheme. All injection kicker current are set at 14.6 mrad kick.

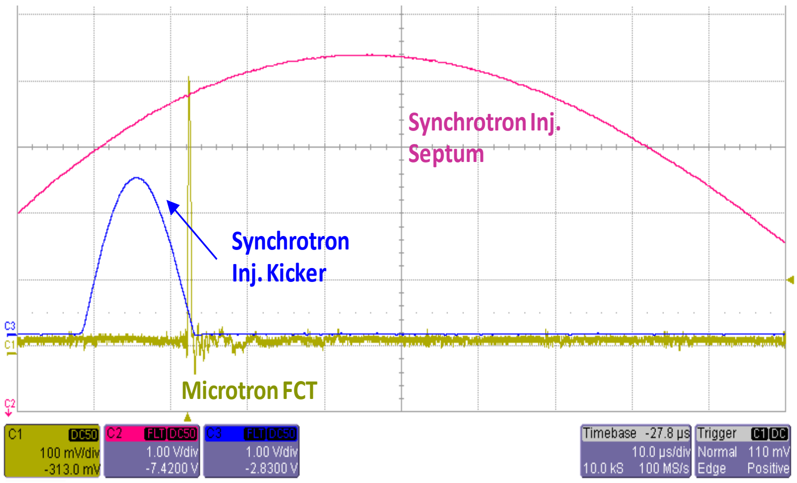

Figure 2. 15 Beam injection on the rising part of the septum magnet pulse (Injected beam pulse, synchrotron injection septum, injection kicker are label in the figure).

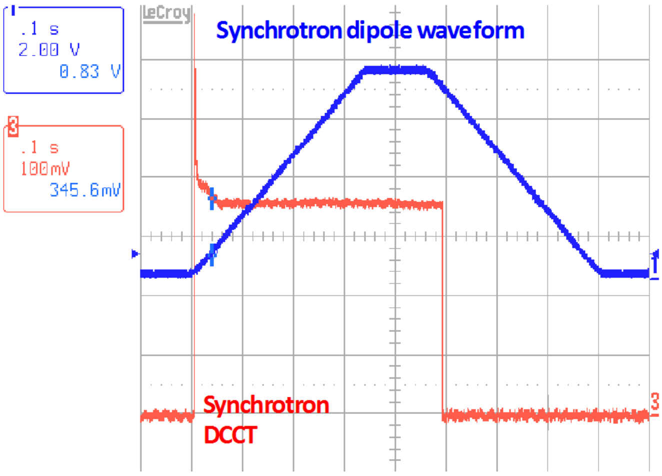

Figure 2. 16 Synchrotron DCCT in uncompensated bump scheme (Beam injection is performed on the rising part of the injection septum magnet pulse)

In the second experiment, a 60 ns pulse (~6 mA) is extracted from the microtron and injected into the synchrotron to find out the length of the entering electron beam, which can be accepted in the synchrotron. Here, all three kickers are set according to the compensated and uncompensated bump injection schemes. The incoming pulse is moved on time scale with respect to the kicker pulses. The accelerated currents for different slices are shown in figure 2.17. It is observed that in the compensated bump injection scheme, two slices are accepted whereas in the uncompensated bump injection scheme three slices are accepted. In the both schemes, when beam injection is performed on the rising part of the injection septum magnet pulse, the same slices are accepted. In the uncompensated bump scheme, the acceptance of the first slice representing the 5th slice is much higher, when the injection is done on the rising part of the septum magnet pulse than when the injection angle is held fixed during injection.

The relation between theoretical simulations and the experimental results are summarized in table 2.2. In the theoretical simulations for each slice, the calculation of displacement and residual betatron oscillations are done assuming the start of the slice. Since the actual slice length is 94 ns long. The residual betatron oscillations mentioned in this table are for the start and end of the slice. The table indicates that in both the schemes, injected beam pulse length acceptance is smaller as compared to the theoretical prediction. In the compensated bump scheme, injected beam pulse length acceptance should be 560 ns containing 1st to 6th slices, whereas practically the acceptance is 190 ns, which include 1st and 2nd slices. Similarly in the uncompensated bump scheme, the pulse acceptance should be 380 ns containing 6th to 9th slices, whereas practically it is 280 ns, which includes 5th to 7th slices. In the uncompensated bump scheme, increase in pulse length of the accepted beam and improvement in the beam current is attributed to smaller residual betatron oscillation amplitudes of the accepted slices. In the uncompensated scheme by varying the injection angle, 5th slice acceptance is improved. As per injection simulations, acceptance of this slice can be improved by changing the injection angle from 4.6 mrad to 4.4 mrad (figure 2.11 and 2.12). In the compensated bump scheme by varying the injection angle hardly any improvement is noticed. It may be due to the fact that the amplitudes of residual betatron oscillations of accepted slices are the same in the both cases.

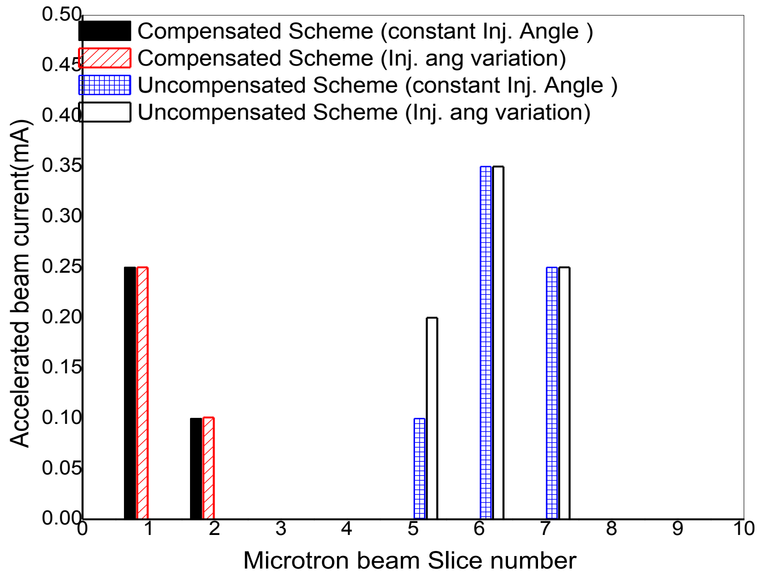

Figure 2. 17 Accelerated beam current with 60 ns injected beam pulse in the compensated and uncompensated bump schemes.

Table 2. 2: Comparison between experiments and theoretical simulations of compensated and uncompensated injection schemes in terms pulse length acceptance of injected beam (T_{pul}), accelerated beam current (I_{acc}) and residual betatron oscillation amplitude (ρ_m) in a slice (pulse length 94 ns). Brackets in the columns of the two schemes denote the sequence number of the accepted slices.

<table>
<tr><th rowspan="3">Mode of beam acceptance</th><th colspan="6">Resultant data at different mode of beam acceptance</th></tr>
<tr><th colspan="3">Compensated bump scheme</th><th colspan="3">Uncompensated bump scheme</th></tr>
<tr><th>Θ</th><th>Experimental I_{acc} (mA)</th><th>Theoretical ρ_m(mm)</th><th>Θ</th><th>Experimental I_{acc} (mA)</th><th>Theoretical ρ_m (mm)</th></tr>
<tr><td>T_{pulse} = 500 ns (Nominal)</td><td rowspan="5">-0.4 (mrad)</td><td>1.3 mA</td><td>----</td><td rowspan="5">4.6 (mrad)</td><td>3.2 mA</td><td>----</td></tr>
<tr><td rowspan="3">T_{pulse} = ~60 ns (Slice wise acceptance)</td><td>0.25 mA$_{(1)}$</td><td>10.5-12.8 mm$_{(1)}$</td><td>0.1 mA$_{(5)}$</td><td>9.2-6.5 mm$_{(5)}$</td></tr>
<tr><td>0.1 mA$_{(2)}$</td><td>12.8-15.9 mm$_{(2)}$</td><td>0.35 mA$_{(6)}$</td><td>6.5-8.6 mm$_{(6)}$</td></tr>
<tr><td>----</td><td>----</td><td>0.25 mA$_{(7)}$</td><td>8.6-15.3 mm$_{(7)}$</td></tr>
<tr><td>T_{pulse} of accepted total slices</td><td>Pulse length <190 ns$_{(1 \text{ to } 2)}$</td><td>Pulse length 560 ns$_{(1 \text{ to } 6)}$</td><td>Pulse length <280 ns$_{(5 \text{ to } 7)}$</td><td>Pulse length 380 ns$_{(6 \text{ to } 9)}$</td></tr>
<tr><td>T_{pulse} = 500 ns (Nominal)</td><td rowspan="5">-0.4 to 0.6 (mrad)</td><td>1.3 mA</td><td>----</td><td rowspan="5">4.4 to 5.2 (mrad)</td><td>3.6 mA</td><td>----</td></tr>
<tr><td rowspan="3">T_{pulse} = ~60 ns (Slice wise acceptance)</td><td>0.25 mA$_{(1)}$</td><td>10.5-12.0 mm$_{(1)}$</td><td>0.2 mA$_{(5)}$</td><td>10.2-6.5 mm$_{(5)}$</td></tr>
<tr><td>0.1 mA$_{(2)}$</td><td>12.0-14.5 mm$_{(2)}$</td><td>0.35 mA$_{(6)}$</td><td>6.5-8.4 mm$_{(6)}$</td></tr>
<tr><td>----</td><td>----</td><td>0.25 mA$_{(7)}$</td><td>8.4-15.3 mm$_{(7)}$</td></tr>
<tr><td>T_{pulse} of accepted total slices</td><td>Pulse length <190 ns$_{(1 \text{ to } 2)}$</td><td>Pulse length 560 ns$_{(1 \text{ to } 6)}$</td><td>Pulse length <280 ns$_{(5 \text{ to } 7)}$</td><td>Pulse length 470 ns$_{(5 \text{ to } 9)}$</td></tr>
</table>

The table 2.2 indicates that for experimentally accepted slices transverse acceptance is ~15 mm, whereas as per the theoretical simulations it should be ~ 30 mm. In both the cases, the acceptance of one slice is higher in comparison to other slices, indicating that the slice with smaller amplitude of residual betatron oscillation contributes more to the final beam current. Within this allowable aperture, in the uncompensated bump scheme more slices contribute to beam current compared to the compensated bump scheme. The above results suggest that uncompensated bump scheme can thus be applied to the synchrotron, which have a smaller beam acceptance.

2.3. Conclusions

In the compensated injection scheme, twiss parameters (β and α) at the injection septum magnet have large values in order to constrain the amplitude of residual betatron oscillation of different slices during injection, bump slope or injection angle has to be adjusted.

In the synchrotron beam acceptance is small. Its performance is improved with the adjustment of bump, bump slope and optimization of injection angle in such a way that after injection residual betatron oscillations increases by small values. It is possible to do so by employing an uncompensated bump scheme in which the strengths of the kickers are not co-related to one another unlike the compensated bump. In this scheme shorter injected beam pulse is accepted and the amplitudes of residual betatron oscillations of the few slices are smaller as compared to the compensated bump injection scheme. For example in the synchrotron in uncompensated bump scheme three slices have residual betatron oscillations less than 10 mm. Such a condition cannot be obtained in the compensated bump scheme. Thus performance of the synchrotron is better in uncompensated scheme as electrons with smaller residual betatron oscillations have higher probability to be accepted in it. In this scheme, increase in the beam current is also achieved when the injection beam angle is regulated during beam injection by injecting the beam on the rising part of the septum magnet pulse. In view of the possibility of having smaller residual betatron oscillations of the injected slices, the uncompensated bump scheme thus may be applied to ring, which have smaller acceptance in the injection plane.

CHAPTER 3

STUDY OF DOUBLE BEND ACHROMAT LATTICE

In this chapter, beam optics of the double bend achromat lattice has been studied. The double bend achromat lattice, consists of a double bend achromat (DBA structure) accompanied by sections having zero dispersion on both sides for accommodating insertion devices. In third generation synchrotron radiation source, the double bend achromat lattices have been widely used. The double bend achromat structure contains two dipole magnets and the drift space between two dipole magnets contains either a single focusing quadrupole magnet or combination of focusing and defocusing quadrupole magnets to form the achromat. In the structure, dispersion (η) function which is generated by the first dipole magnet is adjusted at the entry of the second dipole magnet in such a way that at the exit of the second dipole magnet dispersion function is zero. The zero dispersion function is helpful to avoid the beam emittance growth due to insertion devices.

The achromat structure plays an important role in deciding the beam emittance and dynamic aperture. The beam emittance in a lattice is proportional to the cube of bending angle of its dipole magnet. The beam emittance thus can be reduced significantly by reducing the bending angle of the dipole magnet. Condition of achromaticity requires strong quadrupoles thus the chromaticity of the ring is high in such lattice In this case, dynamic aperture is reduced due to higher strengths of sextupole magnets, needed for chromaticity correction, which is a consequence of smaller dispersion function. In a storage ring with a smaller number of unit cells, bending angle is relatively large as compared to the rings with a higher number of unit cells. In the latter case, beam emittance is higher, and consequently sextupole strengths are lower. The beam emittance in a given lattice can also be optimized with a proper choice of the achromat structure.

In table-3.1 [53], double bend achromat structures for different synchrotron radiation sources are shown. In these structures, a symmetrical distribution of twiss parameters and dispersion function about the center of the achromat are achieved by using a single QF (focusing quadrupole magnet) or with combination of QF and QD (defocusing quadrupole magnet). The table-3.1 also shows that in Elettra and Indus-2 storage ring QF-QD-QF structure has been adopted, and this gives lower ratio of the design beam emittance (ε_{des}) to the theoretical minimum beam emittance (ε_{min}) as compared to other combinations used in different storage rings. In Elettra storage ring, the emittance is further minimized by using a gradient in dipole magnets.

Table 3. 1: DBA structure at different synchrotron radiation sources

Ring	**Energy (GeV)**	ε_{min} **(nmrad)**	ε_{des} **(nmrad)**	**Dipole Magnet**	$\varepsilon_{des}/\varepsilon_{min}$	**DBA structure**
CAMD	1.5	104.1	342	8	3.29	QF
Indus-2	2.5	36.1	54	16	1.5	QF-QD-QF
ANKA	2.5	36.1	72.8	16	2.01	QF
ELETTRA	2.5	6.9	7	24	1.02	QF-QD-QF
APS	7	2.3	8.22	80	3.63	QD-QF-QF-QD
Spring-8	8	1.7	5.57	96	3.25	QD-QF-QF-QD

Here ε_{des} is the design beam emittance.

In the literature, no analytical approach is available for providing guidance on how to choose quadrupole magnets in the achromat part of a double bend achromat to obtain theoretical minimum beam emittance. In a double bend achromat, Chasman-Green lattice [24] represents the basic structure for low emittance synchrotron radiation sources. In this lattice, single focussing quadrupole magnet (QF) is used to form an achromat. In this chapter, we carry out study of this structure assuming quadrupole magnets to be a thin lenses and derive an analytical expression, showing the limitation of this lattice in providing the theoretical minimum beam emittance. From the point of view of achieving the theoretical minimum emittance, analytical expressions are derived for the achromats having two, three and four quadrupole magnets. In a two quadrupole magnet structure, two focusing quadrupole magnets are used. The three and four-quadrupole magnet structures consist of three and four quadrupole magnets respectively. Indus-2 has a double bend achromat lattice in which its achromat part has QF-QD-QF structure. This analytical study is extended for Indus-2 addressing the issue of achromat length chosen for it.

3.1 Beam emittance in a double bend achromat

The horizontal beam emittance in a storage ring is determined by equilibrium between the rate of quantum excitation and the rate of damping of betatron oscillations in horizontal plane. For a double bend achromat (separated function, j_x =1) structure, it is given by [8, 10, 54]

$$\varepsilon \approx C_q \gamma_o^2 \theta_b^3 \left(\frac{1}{3} \frac{\beta_{o,x}}{l_b} - \frac{1}{4} \alpha_{o,x} + \frac{1}{20} \gamma_{o,x} l_b \right) \tag{3.1}$$

Where C_q :Compton wavelength of the electron, γ_o : reduced energy of the electrons, θ_b :bending angle, l_b : length of the dipole magnet and ρ: bending radius . $\alpha_{o,x}, \beta_{o,x}$ and $\gamma_{o,x}$ are the horizontal twiss parameters at the beginning of the dipole magnet.

The theoretically minimum emittance is searched by finding the optimum $\beta_{o,x}$ and $\alpha_{o,x}$. With these optimum values, theoretically minimum beam emittance [29] is given by

$$\varepsilon_{min} = C_q \gamma_o^2 \theta_b^3 \frac{1}{4\sqrt{15}} \tag{3.2}$$

Here $\alpha_{o,x}^* = \sqrt{15}$, $\beta_{o,x}^* = \sqrt{\frac{12}{5}} l_b$, $\beta_{min,x}^* = \sqrt{\frac{3}{320}} l_b$ at $3/8 l_b$ of the dipole magnet, $\beta_{min,x}$ is the minimum horizontal beta function inside the dipole magnet.

Neglecting 1/ρ[2] focusing, accordingly the horizontal phase advance ($\mu_{BM,x}$) [11] in a dipole magnet is given by

$$\mu_{BM,x} = \int_0^{l_b} \frac{ds}{(\beta_{o,x} - 2\alpha_{o,x}s + \gamma_{o,x}s^2)} \tag{3.3}$$

The twiss parameter ($\beta_{1,x}, \alpha_{1,x}$) at the exit of the dipole magnet for the minimum beta function, which is located at $3/8 l_b$ of the dipole magnet, can be obtained from

$$\beta_{1,x} = \beta_{min,x} + \frac{s^2}{\beta_{\ min,x}} \tag{3.4}$$

$$\alpha_{1,x} = -\frac{1}{2}\frac{d\beta_{1,x}}{ds} = \ -\frac{s}{\beta_{min,x}} \tag{3.5}$$

Here s is the distance of the exit of the dipole magnet from the point where β_x is $\beta_{min,x}$.

From equation (3.4 and 3.5), ratio between $\beta_{1,x}$ and $\alpha_{1,x}$is

$$\frac{\beta_{1,x}}{\alpha_{1,x}} = -\left(\frac{\beta_{min,x}^2}{s} + s\right) = \sim - s \tag{3.6}$$

The dispersion-function generated by a dipole magnet [11] at its exit is given by

$$\eta_1 = \rho(1 - \cos\theta) \tag{3.7}$$

$$\eta_1^{/} = \sin\theta \tag{3.8}$$

A transfer matrix to transform dispersion function of the electron beam from one location (say 1) to another location (say 2) with the help of twiss parameters and betatron phase [11] advance is given by

$$\begin{bmatrix}\eta_2 \\ \eta_2^{/}\end{bmatrix} = \begin{bmatrix} \sqrt{\frac{\beta_{2,x}}{\beta_{1,,x}}}(\cos\Delta\mu + \alpha_{1.x}\sin\Delta\mu) & \sqrt{\beta_{1,x}\beta_{2,x}}\sin\Delta\mu \\ -\frac{1+\alpha_{1,x}\alpha_{2,x}}{\sqrt{\beta_{1,x}\beta_{2,x}}}\sin\Delta\mu + \frac{(\alpha_{1,x} - \alpha_{2,x})}{\sqrt{\beta_{1,x}\beta_{2,x}}}\cos\Delta\mu & \sqrt{\frac{\beta_{1,x}}{\beta_{2,x}}}(\cos\Delta\mu - \alpha_{2,x}\sin\Delta\mu) \end{bmatrix} \begin{bmatrix}\eta_1 \\ \eta_1^{/}\end{bmatrix} \tag{3.9}$$

Here $(\beta_{1,x}, \alpha_{1,x})$ and $(\beta_{2,x}, \alpha_{2,x})$ are twiss parameters at location 1 and 2 respectively and $\Delta\mu$ is the phase advance between 1 and 2.

The achromatic condition can be obtained by matching the twiss parameters at the exit of first dipole magnet $(\beta_{1,x}, \alpha_{1,x})$ with those at the entry of second dipole magnet $(\beta_{1,x}, -\alpha_{1,x})$, in this case transfer matrix equation (3.9) can be rewritten as

$$\begin{bmatrix} \eta_1 \\ -\eta_1^{/} \end{bmatrix}_2 = \begin{bmatrix} \cos\mu_{stru,x} + \alpha_{1,x}\sin\mu_{stru,x} & \beta_{1,x}\sin\mu_{stru,x} \\ -\frac{(1-\alpha_{1,x}^2)\sin\mu_{stru,x} - 2\alpha_{1,x}\cos\mu_{stru,x}}{\beta_{1,x}} & \cos\mu_{stru,x} + \alpha_{1,x}\sin\mu_{stru,x} \end{bmatrix} \begin{bmatrix} \eta_1 \\ \eta_1^{/} \end{bmatrix}_1 \tag{3.10}$$

Here, $\mu_{stru,x}$ is phase advance between the two dipole magnets.

The phase advance $(\mu_{stru,x})$ between the two dipole magnet is estimated from solving equation (3.10), which is estimated by following equations

$$\cos\mu_{stru,x} = \frac{\left(\frac{\eta_1}{\eta_1^{/}}\right)^2 - \left(\alpha_{1,x}\frac{\eta_1}{\eta_1^{/}} + \beta_{1,x}\right)^2}{\left(\frac{\eta_1}{\eta_1^{/}}\right)^2 + \left(\alpha_{1,x}\frac{\eta_1}{\eta_1^{/}} + \beta_{1,x}\right)^2} \tag{3.11}$$

$$\sin\mu_{stru,x} = \frac{2\eta_1\left(\alpha_{1,x}\eta_1 + \beta_{1,x}\eta_1^{/}\right)}{{\eta_1}^2 + \left(\alpha_{1,x}\eta_1 + \beta_{1,x}\eta_1^{/}\right)^2} \tag{3.12}$$

$$\tan\left(\frac{\mu_{stru,x}}{2}\right) = \left|\alpha_{1,x} + \beta_{1,x}\frac{\eta_1^{/}}{\eta_1}\right| \tag{3.13}$$

$\mu_{stru,x}$ is obtained by solving equation (3.11) and (3.12) or with equation (3.13), those solutions of $\mu_{stru,x}$ will be preferred for which $\mu_{stru,x}$ is less than 180°. The total phase advance $(\mu_{cell,x})$ in the achromat cell (from the starting point of the first dipole magnet to the exit point of the second dipole magnet) is given by

$$\mu_{cell,x} = 2\mu_{BM,x} + \mu_{stru,x} \tag{3.14}$$

For a given beam emittance, initial twiss parameters of the achromat is selected from equation (3.1). From these parameters, phase advance requirement within a dipole magnet is obtained by equation (3.3) and between the two dipole magnets, it is decided by equations

(3.11) and (3.12). For the theoretical minimum beam emittance, horizontal phase advance between the two dipole magnets ($\mu^*_{stru,x}$) and within a dipole magnet ($\mu^*_{BM,x}$) are ~122° and 156.7° respectively. Accordingly from equation (3.14), horizontal phase advance in the achromat for the theoretical minimum beam emittance is ~435°.

In figure 3.1, horizontal phase advance requirement between two dipole magnets for different values of beam emittance (which is obtained from equation 3.1, with the variation of initial twiss parameters), is plotted by considering a dipole magnet having θ_b = 22.5°, l_b= 2.18 m, beam energy (E) 2.5 GeV (parameters of Indus-2).

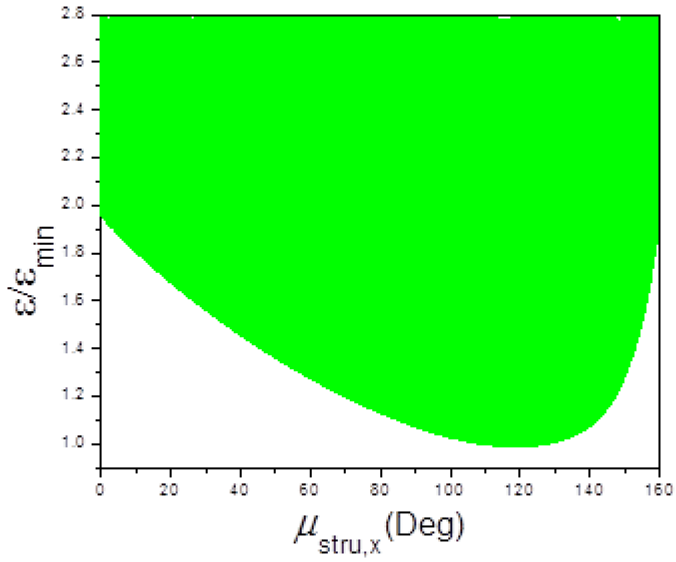

Figure 3. 1 A requirement of phase advance ($\mu_{stru,x}$) between two dipole magnets (from the exit of first dipole magnet to entry of second dipole magnet) of a double bend achromat structure, versus beam emittance by considering parameters of Indus-2 (θ_b = 22.5°,l_b = 2.18 m, E(beam energy) = 2.5 GeV).

3.2. Double bend achromat structure

For a given beam emittance, the achromatic condition is satisfied with a proper relationship between dispersion function and twiss parameters, which is obtained with the help of quadrupole magnets. In the achromat section, an electron beam coming out from the first dipole magnet passes through a drift space and then enters the quadrupole magnet. In thin lens approximation phase advance within a quadrupole magnet ($\Delta\mu$) is negligible. With this approximation, with the help of equation (3.9), the dispersion function (η_3) and its derivative ($\eta_3^{/}$) at the exit of the first quadrupole magnet are related to those at its entrance $\eta_2, \eta_2^{/}$ are given by

$$\begin{bmatrix} \eta_3 \\ \eta_3^{/} \end{bmatrix} = \begin{bmatrix} 1 & 0 \\ -\dfrac{(\alpha_{3,x} - \alpha_{2,x})}{\beta_{2,x}} & 1 \end{bmatrix} \begin{bmatrix} \eta_2 \\ \eta_2^{/} \end{bmatrix} \tag{3.15}$$

Here $\alpha_{2,x}$ and $\alpha_{3,x}$ are α-functions at the entrance and at the exit of the quadrupole magnet respectively. In thin lens approximation $\beta_{3,x} = \beta_{2,x}$and $\eta_3 = \eta_2$ are assumed.

From equation (3.15), integrated strength of quadrupole magnet (k_{QP}) is

$$k_{QP} = -\frac{(\alpha_{3,x} - \alpha_{2,x})}{\beta_{2,x}} = \frac{(\eta_3^{/} - \eta_2^{/})}{\eta_2} \tag{3.16}$$

$$\eta_3^{/} = \eta_2 \left\{ -\frac{(\alpha_{3,x} - \alpha_{2,x})}{\beta_{2,x}} + \frac{\eta_2^{/}}{\eta_2} \right\} \tag{3.17}$$

In the horizontal plane, focusing and defocusing action of the quadrupole magnet will be decided by $\alpha_{3,x}$. For $\alpha_{3,x} > \alpha_{2,x}$, quadrupole magnet is QF and for $\alpha_{3,x} < \alpha_{2,x}$, quadrupole magnet is QD. Thus strength of QF is negative and strength of QD is positive.

Now the feasibility of achieving the required phase advance in achromats of double bend achromat having (1) one QF (2) two QFs (3) a combination of three quadrupole magnets (consisting different combination of QFs and QD) and (4) a combination of four quadrupole magnets consisting of QFs and QDs are discussed.

3.2.1 With single quadrupole magnet (Basic Chasman-Green structure)

In this structure, one quadrupole magnet is placed at the center of the drift space between the two dipole magnets (figure 3.2). The length of drift space, from exit of the first dipole magnet to center of quadrupole magnet is l_1. The strength of quadrupole magnet is adjusted such that an electron entering the first dipole magnet with zero dispersion (η_o) and derivative of η_o ($\eta_o^{/}$) comes out second dipole magnet with zero η_o and $\eta_o^{/}$. This condition is satisfied with the help of focusing quadrupole magnet (QF) with defocusing quadrupole magnet (QD) above condition cannot be satisfied. The η-function and its derivative after the drift space of length l_1, at which QF is located is given by

$$\eta_2 = \rho(1-\cos\theta) + l_1\sin\theta \tag{3.18}$$

$$\eta_2^{/} = \sin\theta \tag{3.19}$$

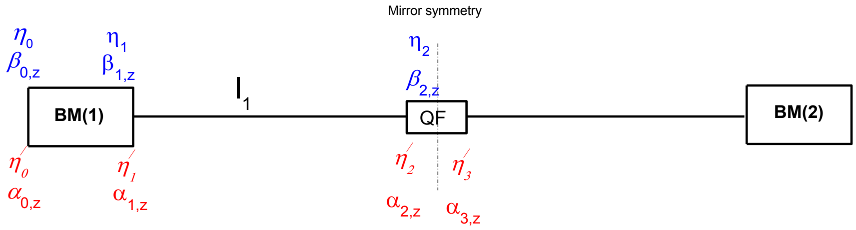

Figure 3. 2. Layout of double bend achromat with single QF. At i^th location β, α, η and $\eta^{/}$ function is denoted by $\beta_{i,z}$ $\alpha_{i,z}$, η_i and $\eta_i^{/}$ respectively, here i=0 and 1 entrance and exit of dipole magnet(BM), similarly i=2 and 3 entrance and exit of the QF. Here z=x or y for horizontal or vertical planes respectively.

To satisfy achromatic condition and to have a mirror symmetrical distribution of beta - functions about the center of QF, at the QF, $\alpha_{3,x} = -\alpha_{2,x}$ ($\eta_3^{/} = -\eta_2^{/}$), so from equation (3.16), integrated strength of QF is given by

$$k_{QF} = \frac{2\alpha_{2,x}}{\beta_{2,x}} = -\frac{2\eta_2^{/}}{\eta_2} \tag{3.20}$$

For a small bending angle, $\frac{\eta_2}{\eta_2^{/}}$ from equation (3.18 and 3.19) is equal to $\sim l_1 + \frac{l_b}{2}$. The ratio $\frac{\beta_{2,x}}{\alpha_{2,x}}$ from equation (3.20) is

$$\frac{\beta_{2,x}}{\alpha_{2,x}} \sim -\left(l_1 + \frac{1}{2} l_b\right) \tag{3.21}$$

From equation (3.6), $\frac{\beta_{2,x}^*}{\alpha_{2,x}^*}$ for the theoretical minimum beam emittance is written as

$$\frac{\beta_{2,x}^*}{\alpha_{2,x}^*} \sim -\ \left(l_1 + \frac{5}{8} l_b\right) \tag{3.22}$$

The difference between $\frac{\beta_{2,x}^*}{\alpha_{2,x}^*}$ and $\frac{\beta_{2,x}}{\alpha_{2,x}}$ of the minimum beam emittance and of Chasman-Green structure is obtained from equation (3.22) and (3.21), which is given by

$$\frac{\beta_{2,x}^*}{\alpha_{2,x}^*} - \frac{\beta_{2,x}}{\alpha_{2,x}} \sim -\frac{l_b}{8} \tag{3.23}$$

The equation (3.23) shows that due to this difference, in a basic Chasman-Green structure, minimum beam emittance cannot be achieved. The optimum twiss parameters for minimum beam emittance in the case of basic Chasman-Green structure ($\varepsilon_{CG,min}$)has to be redefined. The $\frac{\beta_{2x}}{\alpha_{2x}}$ (equation (3.21)) in terms of initial twiss parameters is written as

$$\frac{\beta_{2,x}}{\alpha_{2,x}} = \frac{\beta_{o,x} - 2\alpha_{o,x}(l_1 + l_b) + \ \gamma_{o,x}(l_1 + l_b)^2}{\alpha_{o,x} - \gamma_{o,x}(l_1 + l_b)} = \ -\left(l_1 + \frac{1}{2} l_b\right) \tag{3.24}$$

From equation (3.24), γ_o is written as

$$\gamma_{o,x} = \frac{1 + \alpha_{o,x}^2}{\beta_{o,x}} = \frac{\alpha_{o,x}(2l_1 + 3l_b) - 2\beta_{0,x}}{(x + l_b)l_b} \tag{3.25}$$

The relation between $\beta_{o,x}$ and $\alpha_{o,x}$ is obtained with the help of equation (3.25),

$$\frac{\partial\alpha_{o,x}}{\partial\beta_{o,x}} = \frac{\alpha_{o,x}(2l_1 + 3l_b) - 4\beta_{o,x}}{2l_b(l_1 + l_b)\alpha_{o,x} - (2l_1 + 3l_b)\beta_{o,x}} \tag{3.26}$$

For the basic Chasman-Green structure, initial value of twiss parameters at the start of achromat should follow the relation (3.26). Here, the optimum values of twiss parameters are obtained by solving equation (3.1), (3.25) and (3.26). After solving the above equations, the value of $\beta_{o,x}$ in terms of $\alpha_{o,x}$ is

$$\beta_{o,x} = \alpha_{o,x} l_b \left\{ \frac{29 l_1 l_b + 22 {l_1}^2 + 10 l_b^2}{52 l_1 l_b + 18 l_b^2 + 40 {l_1}^2} \right\} = C_1 \alpha_{o,x} l_b \tag{3.27}$$

Where

$$C_1 = Const = \frac{29 l_1 l_b + 22 {l_1}^2 + 10 l_b^2}{52 l_1 l_b + 18 l_b^2 + 40 {l_1}^2} \tag{3.28}$$

$\alpha_{o,x}$ is estimated by equation (3.24), after substituting $\beta_{o,x}$ from equation (3.27)

$$\alpha_{o,x} = \pm \sqrt{\frac{(l_1 + l_b)}{C_1\{(2l_1 + 3l_b) - 2C_1 l_b\} - (l_1 + l_b)}} \tag{3.29}$$

The equation (3.29) gives two roots of $\alpha_{o,x}$, with positive root beta function reduces in the dipole magnet, this is required to obtain the minimum beam emittance. Thus positive root of $\alpha_{o,x}$ is selected to obtain minimum beam emittance.

The expression for the beam emittance (ε_{CG}) in the basic Chasman-Green structure with the help of equation (3.1), (3.27) and (3.29) is

$$\varepsilon_{CG} = C_q \gamma_o^2 \theta_b^3 \frac{1}{j_x} \left[\frac{(20C_1 l_1 + 14C_1 l_b - 9l_1 - 6l_b)}{60(l_1 + l_b)^{3/2} \sqrt{(2C_1 l_1 + 3C_1 l_b - 2C_1^2 l_b - l_1 - l_b)}} \right] \tag{3.30}$$

The horizontal phase advance in the achromat ($\mu_{cell,x}$)is given by integrating the equation (3.3) over the length of achromat from the start of achromat up to the end of the achromat $2(l_1 + \mathrm{l_b})$. The expression for $\mu_{cell,x}$ can be written as

$$\mu_{cell,x} = 2\left[\tan^{-1}\{\gamma_{o,x}(l_1 + l_b) - \alpha_{o,x}\} - \tan^{-1}(-\alpha_{o,x})\right] \tag{3.31}$$

For minimum beam emittance in Chasman-Green structure, $l_1 \gg l_b$, for this $C_1 \sim 0.55$, $\alpha_{o,x} \sim 3.16$, $\beta_{o,x} \sim 1.74 l_b$, and $\varepsilon_{CG,min}$ is

$$\varepsilon_{CG,min} \cong C_q \gamma_o^2 \theta_b^3 \frac{1}{2.45\sqrt{15}} \tag{3.32}$$

By using equation (3.2) and (3.32), ratio between minimum beam emittance in Chasman-Green structure to theoretical minimum beam emittance is given by

$$\frac{\varepsilon_{CG,min}}{\varepsilon_{min}} \sim 1.63 \tag{3.33}$$

This indicates here that the minimum beam emittance in the Chasman-Green structure is 63 % higher as compared to theoretical minimum beam emittance.

In this structure $\beta_{2,x}$ at QF is given by

$$\beta_{2,x} = \beta_{o,x}\left\{1 + \frac{(l_1 + l_b)}{C_1 l_b}\right\}^2 + \frac{(l_1 + l_b)^2}{\beta_{xo}} \tag{3.34}$$

In vertical plane twiss parameters $\alpha_{2,y}$ at QF location are determined by defocusing action of QF. To obtain symmetrical solution $\beta_{2,y}$ is a free parameter, which should be kept at minimum value. $\alpha_{2,y}$ is estimated on the basis of QF strength, which is given by

$$\alpha_{2,y} = -\frac{k_{QF}\beta_{2,y}}{2} = +\frac{\beta_{2,y}}{\left(l_1 + \frac{1}{2} l_b\right)} \tag{3.35}$$

From this relation initial vertical beta ($\beta_{o,y}$) at the start of the achromat is back calculated for a given length of $-(l_1 + l_b)$. Its relation is

$$\beta_{o,y} = \frac{\left\{\beta_{2,y} + \alpha_{2,y}(l_1 + l_b)\right)\}^2 + (l_1 + l_b)^2}{\beta_{2,y}} \tag{3.36}$$

By using the relation of $\alpha_{2,y}$, the equation (3.36) can be rewritten in the following form.

$$\beta_{o,y} = \beta_{2,y}\left\{1 + \frac{(l_1 + l_b)}{(l_1 + \frac{1}{2} l_b)}\right\}^2 + \frac{(l_1 + l_b)^2}{\beta_{2,y}} \tag{3.37}$$

Now we will see the variation of $\mu_{cell,x}$, $\varepsilon_{CG}/\varepsilon_{min}$, $\beta_{2,x}$, $\beta_{o,y}$ versus l_1 by using equation (3.31), (3.30), (3.34) and (3.37) respectively for Indus-2 conditions for $\beta_{2,y} = 4\ m$. The figure-3.3 shows that initially $\varepsilon_{CG}/\varepsilon_{min}$ reduces on increasing the gap between the dipole magnet and focusing quadrupole magnet (l_1). After certain l_1, this reduction becomes negligible. The phase advance in the achromat cell ($\mu_{cell,x}$) increases slowly due to a high value of horizontal beta function. The maximum value of $\mu_{\text{cell,x}}$ is~320^{o}, in which contribution of dipole magnet ($\mu_{\text{BM,x}}$) is~290^{o} and structure ($\mu_{\text{stru,x}}$) is~30^{o}.

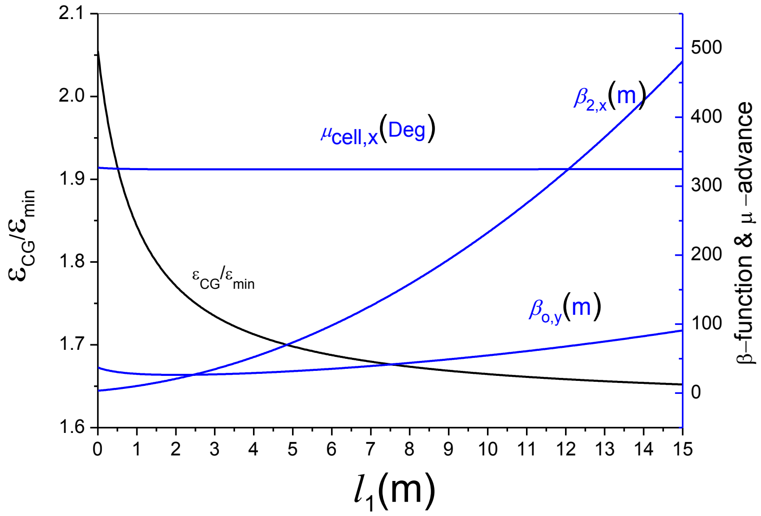

Figure 3. 3For the basic Chasman-Green structure $\varepsilon_{CG}/\varepsilon_{min}$,$\beta_{2,x}$(m),$\beta_{o,y}$(m) and $\mu_{cell,x}$(deg.) versus l_1 (length between from the exit of dipole magnet to the center of the achromat) for Indus-2 parameters (θ_b=22.5^{o}, l_b=2.18 m,$\beta_{2,y}$=4 m and E=2.5 GeV). The calculations have been carried out by using equation (3.31), (3.30), (3.34) and (3.37).

In the structure, preferred location for horizontal chromaticity correcting sextuple magnet (SF) and vertical chromaticity correcting sextuple magnet (SD) is near QF and dipole magnet respectively. Strength of SF is inversely proportional to $\beta_{2,x}$ and η_2[17]. As a result, as l_1 increases, strength of SF and SD will be reduced due to a higher value of $\beta_{2,x}$ *and* η_2 near QF and higher value of vertical beta function ($\beta_{1,y}$) near dipole magnet location respectively. However, due to a large value of beta function ($\beta_{2,x}$ and $\beta_{o,y}$), physical acceptance will be reduced as well as sensitivity towards linear and nonlinear imperfections will be increased, and this imposes a practical limitation to the keep a higher value of maximum horizontal and vertical beta function.

3.2.2. With two quadrupole magnets (QF-QF structure)

We have shown above that with one QF, phase advance requirement for the theoretical minimum beam emittance is not feasible. To study this, two focusing quadrupole magnet structure is discussed. Here the strength of focusing quadrupole magnet and gap between the two focusing quadrupole magnets (l_2) are available for optimization. In this case, it is possible to make α-function positive, as a result higher value of phase advance can be generated due to small value of β_x. In order to obtain the mirror symmetry about the center of the achromat, two focusing quadrupole magnets are placed symmetrically about the center of the achromat (as shown in figure 3.4).

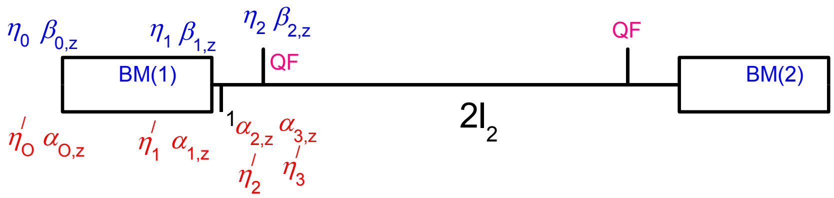

Figure 3. 4 Layout of a double bend achromat with two QFs. At i^th location β, α, η and $\eta^{/}$ function is denoted by $\beta_{i,z}$ $\alpha_{i,z}$, η_i and $\eta_i^{/}$ respectively, here i=0 and 1 at entrance and exit of dipole magnet, i=2 and 3 at entrance and exit of QF. Here z=x or y for horizontal or vertical planes respectively.

The phase advance$(\Delta\mu_{QF})$ between the two QFs can be obtained by equating the elements of the transfer matrix used in equation (3.9, 3.10) with transfer matrix of drift space of length $2l_2$ and is given by

$$\begin{pmatrix} cos\Delta\mu_{QF} + \alpha_{3,x} sin\Delta\mu_{QF} & \beta_{2,x} sin\Delta\mu_{QF} \\ -\frac{(1-\alpha_{3,x}{}^2) sin\Delta\mu_{QF} - 2\alpha_{3,x} cos\Delta\mu_{QF}}{\beta_{2,x}} & cos\Delta\mu_{QF} + \alpha_{3,x} sin\Delta\mu_{QF} \end{pmatrix} = \begin{pmatrix} 1 & 2l_2 \\ 0 & 1 \end{pmatrix} \tag{3.38}$$

$$\Delta\mu_{QF} = sin^{-1}\frac{2l_2}{\beta_{2,x}} \tag{3.39}$$

From equation (3.39), it can be seen that the phase advance for minimum beam emittance can be obtained, for which a suitable $\alpha_{3,x}$ is required, which is always positive. $\alpha_{3,x}$ is governed by the achromatic condition, according to which, the derivative of dispersion function has to be zero between the two QFs. From equation (3.17)

$$-\frac{(\alpha_{3,x} - \alpha_{2,x})}{\beta_{2,x}} + \frac{\eta_2'}{\eta_2} = 0 \tag{3.40}$$

Thus required strength of each QF by using equation (3.16) will be given by

$$k_{QF} = -\frac{(\alpha_{3,x} - \alpha_{2,x})}{\beta_{2,x}} = -\frac{\eta_2'}{\eta_2} = -\frac{1}{l_1 + \frac{l_b}{2}} \tag{3.41}$$

Accordingly

$$\alpha_{3,x} = \alpha_{2,x} + \frac{\beta_{2,x}}{l_1 + \frac{l_b}{2}} \tag{3.42}$$

$\alpha_{3,x}$ is required as per equation (3.42) and is generated by choosing a suitable strength of QF. For the theoretical minimum beam emittance, $\alpha_{3,x}$ can be estimated on the basis of initial twiss parameter of dipole magnet after substituting $\alpha_{2,x} = \alpha_{2,x}^*$, $\beta_{3,x} = \beta_{2,x} = \beta_{2,x}^*$ term in equation (3.42).

$$\alpha_{3,x} = \frac{1}{(l_1 + \frac{l_b}{2})\beta_{min,x}.}\left\{\beta_{min,x}^2 + \frac{l_b}{8}(\frac{5l_b}{8} + l_1)\right\} \tag{3.43}$$

When $l_1 = 0$, $\alpha_{2,x}^* \sim -6.45$, $\beta_{2,x}^* = 4.13 l_b$ and from (3.43) $\alpha_{3,x}$ is 1.81

The point in the drift space, where α becomes zero is called the center of the achromat. At the center of achromat, α is zero, with this condition, l_2 can be estimated and is given by equation (3.44). Variation of l_2 with $l_1$is plotted in figure 3.5.

$$l_2 = \frac{\alpha_{3,x}\beta_{2,x}}{1+\alpha_{3,x}^2} \tag{3.44}$$

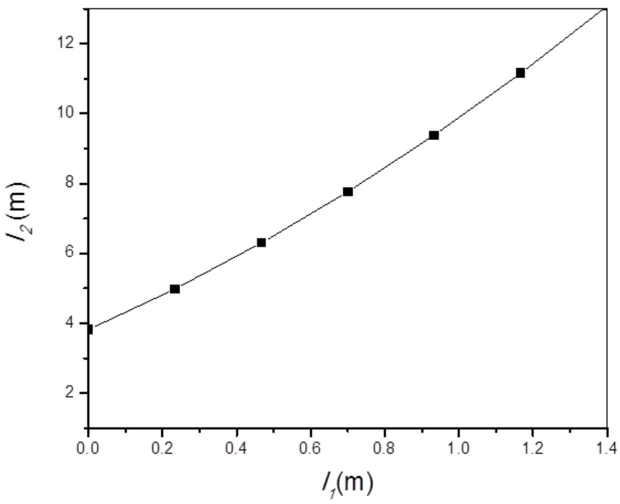

Figure 3. 5 In QF-QF structure of a double bend achromat, for theoretical minimum beam emittance l_2 (gap from exit of QF to center of achromat) versus l_1 (gap from exit of dipole magnet to QF) is plotted for l_b= 2.18 m. The calculation has been performed by using equation (3.44) and (3.43).

The figure 3.5 shows that for a shorter l_2, QF should be close to dipole magnet (small l_1). Normally the separation between the dipole magnet and QF is more than 0.5 m, keeping in view the finite length of the quadrupole magnet and space requirement of other elements such as beam position monitors, steering magnet etc. For example in the case of Indus-2, the length of dipole magnet is 2.18 m and the gap between dipole magnet and QF is ~0.75 m for this gap the gap between the two QFs ($2l_2$) should be around 18 m to achieve the condition of theoretical minimum beam emittance.

At QF location, twiss parameters will be decided on the basis of initial twiss parameters at the start of achromat. In this way, l_2 is related to the beam emittance (the initial twiss parameters at the start of achromat). The variation of allowable minimum beam emittance with different choices of l_2 for Indus-2 is plotted in figure 3.6, which also shows that for theoretically minimum beam emittance gap between two QFs is 18m. The figure-3.6 also shows that by increasing the gap between the two focusing quadrupole magnet beam emittance reduces with a higher value as compared to single focusing quadrupole magnet.

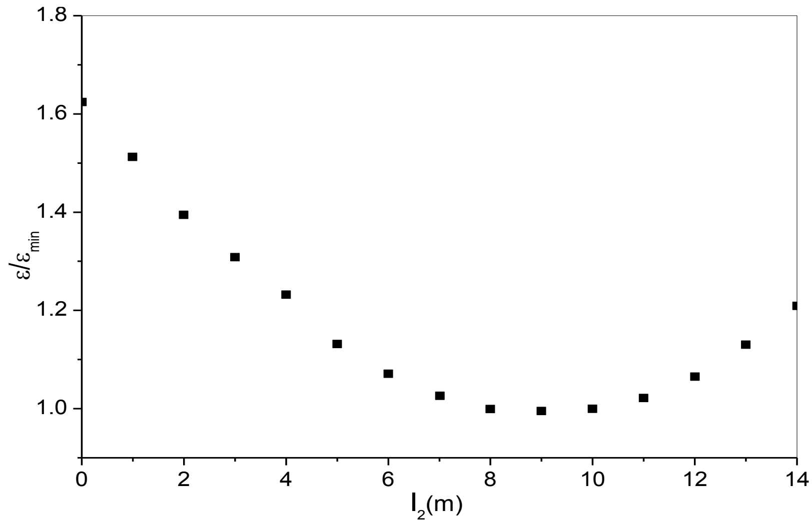

Figure 3. 6 In QF-QF structure of a double bend achromat, variation of l_2 (gap from exit of QF to center of achromat) versus the allowable ratio of achievable minimum beam emittance ($\varepsilon/\varepsilon_{min}$) is plotted for Indus-2 parameters (θ_b=22.5º, l_b= 2.18 m, l_1=0.75 m and E=2.5 GeV). The calculation has been performed by using equation (3.1), (3.4), (3.41) and (3.44).).

In the vertical plane, to get a symmetric solution $\alpha_{4,y}$ is zero, twiss parameters $\beta_{3,y}$ $(\beta_{2,y})$ and $\alpha_{3,y}$ at QF location is

$$\beta_{2,y} = \beta_{4,y} + \frac{{l_2}^2}{\beta_{4,y}} \tag{3.45}$$

$$\alpha_{3,y} = \frac{l_2}{\beta_{4,y}} \tag{3.46}$$

The defocusing action of QF will change, $\alpha_{3,y}$in following way

$$\alpha_{2,y} = \alpha_{3,y} + \frac{\beta_{2,y}}{\left(l_1 + \frac{1}{2} l_b\right)} \tag{3.47}$$

The above equation shows that at QF location $\beta_{2,y}$ will be higher as compared to that at the center of achromat. The twiss parameters $\beta_{2,y}$ and $\alpha_{2,y}$ depend up on l_2. The initial $\beta_{o,y}$ can be obtained from equation (3.36) after using twiss parameters at QF location ($\beta_{2,y}$ and $\alpha_{2,y}$). Thus $\beta_{o,y}$ is increased for higher length of l_2.

In the QF-QF structure preferred location of SF and SD is close to QF and dipole magnet respectively. Due to small gap between QF and BM (l_1) beta function are not well decoupled in horizontal and vertical plane. Thus higher strength of chromaticity correcting sextupole magnets are required, which will degrade the dynamic aperture.

3.2.3. With three quadrupole magnets

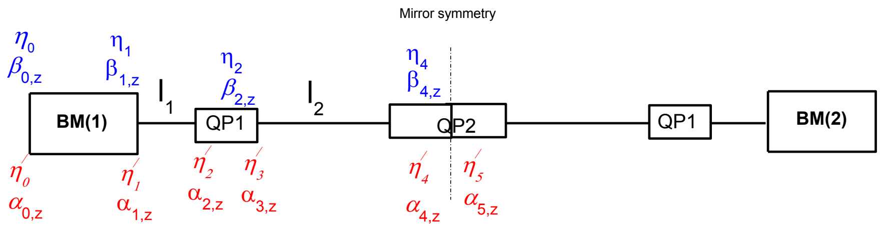

Figure 3. 7 Layout of double bend achromat structure with three quadrupoles (QP1-QP2-QP1). At ith location β, α, η and η' function is denoted by $\beta_{i,z}$ $\alpha_{i,z}$, η_i and η'_i respectively, here i=0 and 1 at entrance and exit of dipole magnet(BM), i=2 and 3 at entrance and exit of QP1, i=4 and 5 at entrance and exit of QP2. Here z=x or y for horizontal or vertical planes respectively.

In the case of QF-QF structure, the gap between the two QFs decides the minimum beam emittance. Further in the vertical plane, focusing action is not available to control the vertical beta function. In this structure, by inclusion of third quadrupole magnet, we will study that whether the gap between two quadrupole magnets is freely adjustable as compared to QF-QF structure and in the vertical plane any control on the twiss parameters are possible. In figure-

3.7 a schematic layout of three quadrupole magnets (QP1-QP2-QP1) structure is shown. Here QP2 is at centre of the achromat with two QP1s placed mirror symmetrically on its either side at a distance of l_2.

At the exit of QP1 $\eta_3^{/}$ is estimated from equation (3.17).

$$\eta_3^{/} = \eta_2 \left\{ -\frac{\alpha_{3,x}}{\beta_{2,x}} + \frac{\alpha_{2,x}}{\beta_{2,x}} + \frac{\eta_2^{/}}{\eta_2} \right\} \tag{3.48}$$

For the theoretical minimum beam emittance, after substituting $\alpha_{2,x} = \alpha_{2,x}^{*}$, $\beta_{2,x} = \beta_{2,x}^{*}$ and $\eta_2^{/}/\eta_2 = 1/(l_1 + \frac{l_b}{2})$ in equation (3.48)

$$\eta_3^{/} = \eta_2 \left\{ \frac{\beta_{2,x}^{*} C_2 - \alpha_{3,x}}{\beta_{2,x}^{*}} \right\} \tag{3.49}$$

Where

$$C_2 = \frac{\beta_{min,x}^2. + \frac{l_b}{8}\left(l_{\ 1} + \frac{5l_b}{8}\right)}{\left[\beta_{min,x}^2. + \left(l_1 + \frac{5l_b}{8}\right)^2\right]\left(l_1 + \frac{l_b}{2}\right)} \tag{3.50}$$

$$C_2 \beta_{2,x}^{*} = \frac{\beta_{min,x}^2 + \frac{l_b}{8}(l_1 + \frac{5l_b}{8})}{\beta_{min,x}(l_1 + \frac{l_b}{2})} \tag{3.51}$$

From equation (3.49) and (3.16), k_{QP1} is given by

$$k_{QP1} = \frac{\eta_3^{/}}{\eta_2} - \frac{\eta_2^{/}}{\eta_2} = \left\{ \frac{\beta_{2,x}^{*} C_2 - \alpha_{3,x}}{\beta_{2,x}^{*}} \right\} - c_3 \tag{3.52}$$

Where $c_3 = \frac{1}{\frac{l_b}{2} + l_1}$. The nature of $\eta_3^{/}$ is decided by $\alpha_{3,x}$ or vice versa. With the help of $\eta_3^{/}$ at entrance of QP2, η_4, $\eta_4^{/}$ are governed by the following relations.

$$\eta_4 = \eta_2 + \eta_3^{/} l_2 \tag{3.53}$$

$$\eta_4^{/} = \eta_3^{/} \tag{3.54}$$

For achromatic condition, it is required that at the exit of QP2 $\alpha_5 = -\alpha_4$, and $\eta_5^{/} = -\eta_4^{/}$. To satisfy these conditions the required integrated strength of QP2 (k_{QP2}) is given by

$$k_{QP2} = -\frac{2\eta_4^{/}}{\eta_4} = -2\left(\frac{\eta_3^{/}}{\eta_2 + \eta_3^{/} l_2}\right) = \frac{2\alpha_{4,x}}{\beta_{4,x}} \tag{3.55}$$

From equation (3.52) and (3.55), k_{QP1} and k_{QP2} are related by following equation

$$k_{QP2} = -\frac{2(k_{QP1} + c_3)}{l_2(k_{QP1} + c_3) + 1} \tag{3.56}$$

The above equation in terms of twiss parameters is rewritten as

$$k_{QP2} = -\frac{2(C_2\beta_{2,x}^{*} - \alpha_{3,x})}{l_2(C_2\beta_{2,x}^{*} - \alpha_{3,x}) + \beta_{2,x}^{*}} \tag{3.57}$$

In thin lens approximation, twiss parameters at QP2 location are estimated by using following relation

$$\beta_{4,x} = \beta_{2,x}^{*} - 2\alpha_{3,x} l_{2,x} + \gamma_{3,x} l_2^2 \tag{3.58}$$

$$\alpha_{4,x} = \alpha_{3,x} - \gamma_{3,x} l_2 \tag{3.59}$$

Accordingly, l_2 can be obtained after substituting the relation of $\beta_{4,x}$ and $\alpha_{4,x,}$ from equation (3.58) and (3.59) into equation (3.55) and we get

$$l_2 = \frac{C_2\beta_{2,x}^{*^2}}{C_2\beta_{2,x}^{*}\alpha_{3,x} + 1} \tag{3.60}$$

From equation (3.60), l_2 is decided by the relation between $\alpha_{3,x}$ and $C_2\beta_{2,x}^{*}$, in which $C_2\beta_{2,x}^{*}$ is a constant. (From equation (3.51). The only parameter, which can be varied is $\alpha_{3,x}$, for different values of $\alpha_{3,x}$, nature and strengths of QP1 and QP2 and l_2 can be estimated. As an example for minimum beam emittance, requirement of l_2, the nature of QP2, for different $\alpha_{3,x}$is discussed below with the help of equation (3.49), (3.52), (3.57) and (3.60). In this example for $l_1 = 0$ following parameters are taken, $\alpha_{2,x}^{*} = -6.45$ (from equation (3.5), $\beta_{2,x}^{*} = 4.13 l_b$ (from equation (3.4) and $C_2\beta_{2,x}^{*} = 1.7$ (from equation (3.51)).

Case-1 QF-QD-QF structure

If $C_2\beta^*_{2,x}$,< $\alpha_{3,x} < C_2\beta^*_{2,x} + \frac{\beta^*_{2,x}}{l_2}$ then from equation (3.52) QP1 is QF. From equation (3.49), at the exit of QP1 the derivative of dispersion function is negative and from equation (3.57) QP2 is QD, thus above structure is QF-QD-QF. In equation (3.60), $\alpha_{3,x}$ is in the denominator, so by keeping a higher value of $\alpha_{3,x}$, l_2 can be reduced. For example if $\alpha_{3,x} = 2C_2\beta^*_{2,x}$ then $l_2 \sim l_b$

Case-2 QF-QF structure

If $\alpha_{3,x} = C_2\beta^*_{2,x}$, then from equation (3.52) QP1 is QF. In this case, from equation (3.49) the derivative of dispersion function is zero. It can be seen from equation (3.57) that at the center of achromat, QP2 is not required. This is the case of QF-QF structure. In this case $l_2 = 1.6l_b$ which is higher than to that of case-1.

Case-3 QF-QF-QF structure

If $-\frac{1}{C_2\beta^*_{2,x}} < \alpha_{3,x} \le C_2\beta^*_{2,x}$, the above range of $\alpha_{3,x}$is decided by equation (3.60) such that l_2 has a finite value. In this case QP1 is QF, from equation (3.52) and at the exit of QP1 (QF), derivative of dispersion function is positive from equation (3.49). From equation (3.57), QP2 is QF. Thus, structure is QF-QF-QF. In this case $\alpha_{3,x}$is smaller as compare to case-1 and 2 so l_2 is larger compared to case-1 and 2. If $\alpha_{3,x} = 0$ then $l_2 = 7.4l_b$ and if $-\frac{1}{C_2\beta^*_{2,x}} < \alpha_{3,x} < 0$ then $l_2 > 7.4l_b$

Case-4 QF-QF-QF/QD-QF-QD structure

If $\alpha_{3,x} \le -\frac{1}{C_2\beta^*_{2,x}}$ then from equation (3.60), l_2 is infinite or negative. In this case, the achromat structure for theoretical minimum beam emittance is not feasible. From equation (3.52), $\alpha_{3,x} \le -0.57$, thus either QP1 is chosen QF ($\alpha_{3,x} > \beta^*_{2,x}(C_2 - C_3)$) or QD ($\alpha_{3,x} < \beta^*_{2,x}(C_2 - C_3)$) minimum beam emittance is not possible. This also makes clear that QD-QF-

QD structure cannot give minimum beam emittance. The above result shows that according to equation (3.56), for a given strength of QP1, a solution of QP2 exists. However, from equation (3.60), stable solution of twiss parameters will not be available for different strength of QP1 and QP2.

A schematic diagram for different cases (case -1, 2 and 3) is shown in figure 3.8. The above figure indicates that in QF-QD-QF structure achromat length remain smaller. In QF-QD-QF structure l_2 can be reduced and a tunability in the vertical plane is also available. In this case, preferred location of SF and SD is close to QF and QD respectively. Due to QD at sextupole location horizontal and vertical plane beta function can be well decoupled. Thus in this structure, it is possible to reduce the strength of chromaticity correcting sextupole magnets, which will be helpful to increase the dynamic aperture. Thus for minimum beam emittance QF-QD-QF structure is better.

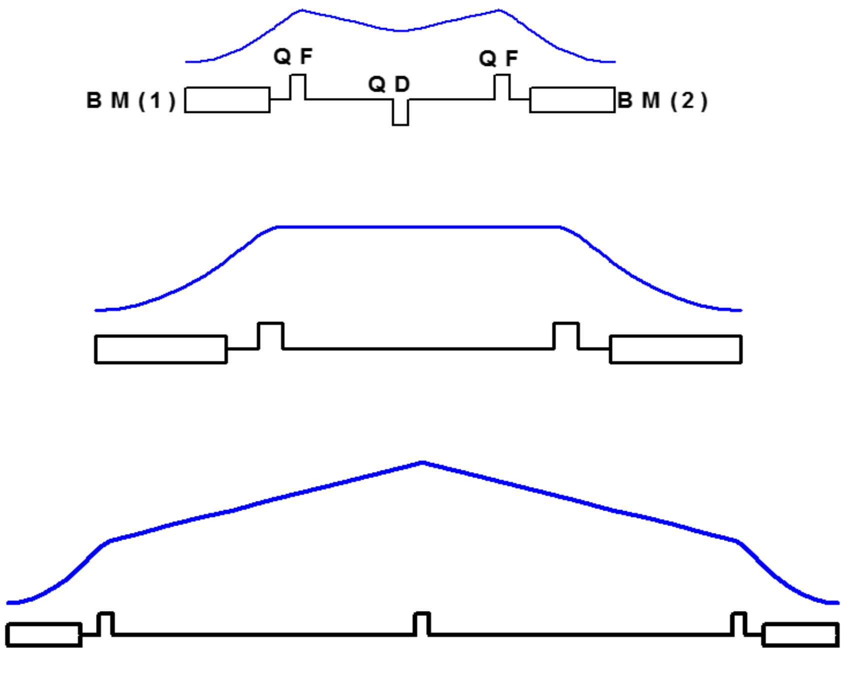

Figure 3. 8 A schematic diagram showing dispersion function in following structure of double bend achromat a) QF-QD-QF b) QF-QF and c) QF-QF-QF. The figure shows that achromat length in QF-QD-QF structure is less than the other two structures.

The integrated strength of QF and QD obtained by using equation (3.52) and (3.56) for different value of l_2 is shown in figure 3.9 for the conditions of Indus-2 as mentioned earlier. The figure shows that for a shorter l_2, the strength of QF and QD are high. For the shorter l_2 strength of QD is very high as compared to the QF strength. The high strength of QD will change the α-function by a large value as a result minimum and maximum vertical beta function will be reduced and increased respectively.

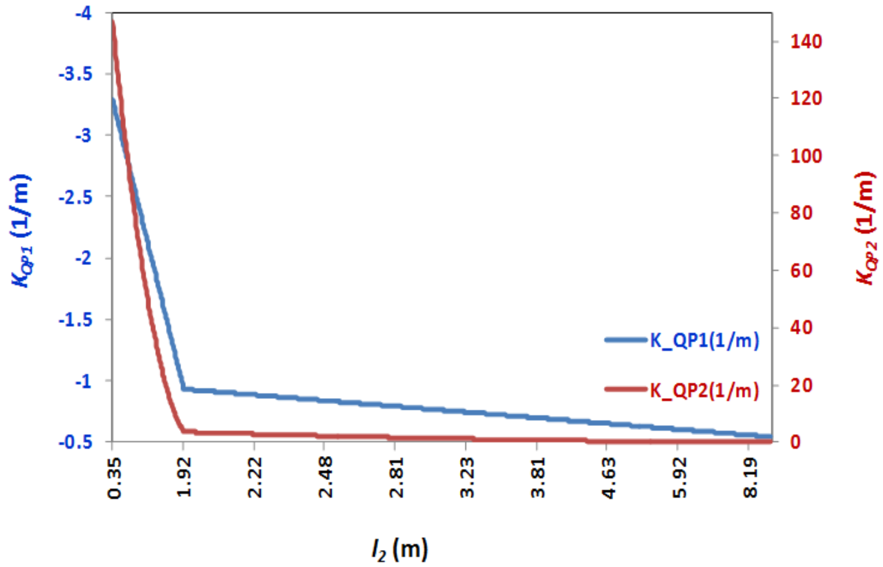

Figure 3. 9 Integrated strength of QF and QD versus l_2 (distance between QF and QD) for Indus-2 conditions (θ_b=22.5°, l_b= 2.18 m and l_1= 0.75 m).The figure shows that for smaller l_2 integrated strength of QF and QD is higher. The calculations have been performed by using equation (3.52) and (3.57).

When $l_2$smaller, strength of QPs is higher as a result beta-functions in both the planes are larger which reduces decoupling of horizontal and vertical plane. Thus the choice of l_2 and strength of QPs are crucial. The strength of QD has to be selected in such a way that vertical beta function at the QF location remains within the limit. At QD location $\alpha_{4,y}$, is given by

$$\alpha_{4,y} = -\frac{k_{QD}\beta_{4,y}}{2} \tag{3.61}$$

The twiss parameters $(\beta_{3,y}, \alpha_{3,y})$ at QF location will be back calculated $(-l_2)$ by following equation

$$\beta_{3,y} = \beta_{4,y}\left\{1 - \frac{k_{QD}l_2}{2}\right\}^2 + \frac{{l_2}^2}{\beta_{4,y}} \tag{3.62}$$

$$\alpha_{3,y} = \alpha_{4,y} + \gamma_{4,y}l_2 \tag{3.63}$$

The initial vertical beta $(\beta_{o,y})$ at the start of achromat is obtained from equation (3.36) after substituting the value of $\beta_{2,y}(\beta_{3,y})$ from equation (3.62) and using following relation of $\alpha_{2,y}$

$$\alpha_{2y} = \alpha_{4,y} + \gamma_{4,y}l_2 - \beta_{2y}k_{QF} \tag{3.64}$$

$$\gamma_{4,y} = \frac{1 + \alpha_{4,y}^2}{\beta_{4,y}} \tag{3.65}$$

To obtain a smaller beam emittance, reasonable value of $\beta_{4,y}$ and k_{QD}should be selected such that initial vertical twiss parameters ($\beta_{o,y}$, $\alpha_{o,y}$) remain within the limits. For this length l_1 and l_2 has to be optimized. In section 3.3, an example of the optimization of l_2 versus beam emittance is discussed.

3.2.4 With four quadrupole magnets

In the case of QD-QF-QD structure stable solutions of twiss parameters are not available for the theoretical minimum emittance. Beside this in the QF-QD-QF structure, achromat length cannot be reduced to small value, due to higher strengths of QF and QD magnet. Now we will study that whether in this structure with the inclusion of an additional quadrupole magnet any flexibility can be obtained.

In four quadrupole magnets structure, to obtain symmetrical solution two QP1 and two QP2 are used to form the achromat. They are placed symmetrically about the center of achromat as shown in figure-3.10. For achromatic condition, strengths of QP1 and QP2 are adjusted such that after QP2, derivative of dispersion function is zero. This relation on the basis of transfer matrix can be written as

$$\begin{bmatrix}\eta_4\\0\end{bmatrix}=\begin{bmatrix}1&0\\k_{QP2}&1\end{bmatrix}\begin{bmatrix}1&l_2\\0&1\end{bmatrix}\begin{bmatrix}1&0\\k_{QP1}&1\end{bmatrix}\begin{bmatrix}1&l_1\\0&1\end{bmatrix}\begin{bmatrix}\eta_1\\\eta_1^{/}\end{bmatrix} \tag{3.66}$$

Where η_4 is the dispersion function at the exit of QP2. From equation (3.66), k_{QP2} and k_{QP1} depend upon each other by following relation

$$k_{QP2}=-\frac{(k_{QP1}+C_3)}{l_2(k_{QP1}+C_3)+1} \tag{3.67}$$

The equation (3.67) can be rewritten as

$$\frac{1}{k_{QP2}}+\frac{1}{k_{QP1}+\frac{1}{\frac{l_b}{2}+l_1}}=-l_2 \tag{3.68}$$

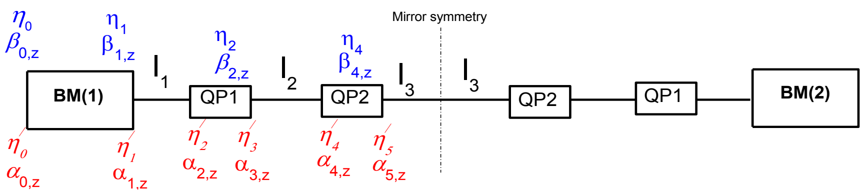

Figure 3. 10 Layout of double bend achromat with four quadrupole magnet structure (QP1-QP2-QP2-QP1). At i^{th} location β, α, η and $\eta^{/}$ function is denoted by $\beta_{i,z}$ $\alpha_{i,z}$, η_i and $\eta_i^{/}$ respectively, here i=0 and 1 at entrance and exit of dipole magnet(BM), i=2 and 3 at entrance and exit of QP1, i=4 and 5 at entrance and exit of QP2. Here z=x or y for horizontal or vertical planes respectively

In this case, for the same k_{QP1}, k_{QP2} is half of three quadrupole magnet structure (equation (3.57)). Now, we will derive an analytical relations for estimating gap (l_3) between two QP2. In this case equation (3.55) can be written as

$$k_{QP2}=-\frac{(\alpha_{5,x}-\alpha_{4,x})}{\beta_{4,x}}=\frac{-\eta_4^{/}}{\eta_2} \tag{3.69}$$

Where

$$\beta_{4,x} = \beta_{2,x} - 2\alpha_{3,x} l_2 + \gamma_{3,x} {l_2}^2 \tag{3.70}$$

The equation (3.69) can be rewritten as

$$\alpha_{5,x} = \alpha_{3,x} - \gamma_{3,x} l_2 + \beta_{4,x} \frac{(k_{QP1} + c_3)}{l_2(k_{QP1} + c_3) + 1} \tag{3.71}$$

$$l_3 = \frac{\alpha_{5,x}\beta_{4,x}}{1 + \alpha_{5,x}^2} \tag{3.72}$$

Here $\alpha_{3,x} = \alpha_{2,x} - k_{QP1}\beta_{2,x}$. At QP2 location, twiss parameters ($\beta_{4,x}$, $\alpha_{5,x}$), k_{QP1} and k_{QP2} are deciding parameters to estimate l_3. By considering twiss parameters for the theoretical minimum beam emittance, l_3 is estimated with the help of equation (3.67), (3.70), (3.71) and (3.72) for two different cases in which different arrangement of QPs are considered.

Case-1 QD-QF-QF-QD structure

If QP1 is QD, from equation (3.67) QP2 is QF. In this arrangement, at exit of QD, $\alpha_{3,x}$ is more negative thus $\beta_{4,x}$ at QF location is higher as compared to $\beta_{2,x}$ of QF-QF structure. The phase advance depends upon beta function from equation (3.39), as a result to obtain required phase advance for the theoretical minimum beam emittance, l_3 is longer as compared to QF-QF structure.

In figure 3.11 an example is shown by considering QD close to dipole magnet and QF 0.75 m away from QD. When strength of QD is zero (QF-QF structure), l_3 is small. As strength of QD increases $\beta_{4,x}$ and l_3 also increases. Thus arrangement of QD-QF-QF-QD is not suitable for the theoretical minimum beam emittance.

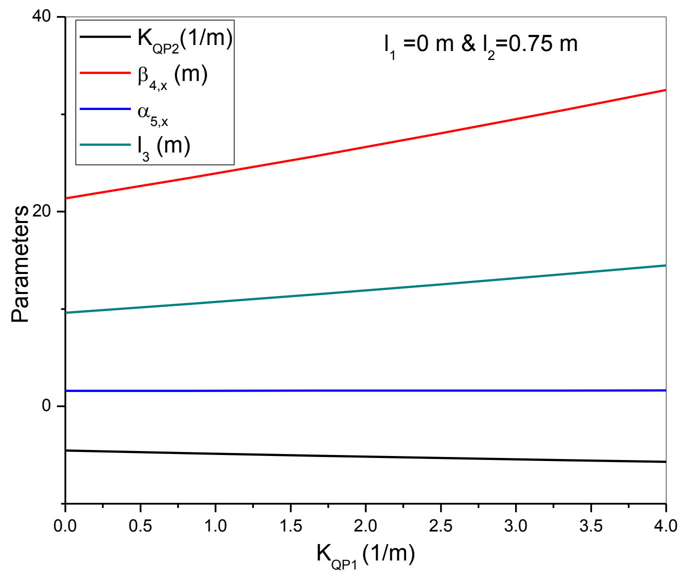

Figure 3. 11 For l_1=0, l_2=0.75 m strength of QD is varied and its effect on the strength of QF, twiss parameters $\beta_{4,x}$, $\alpha_{5,x}$ and on l_3 is shown. In the figure, notation of QF unit is chosen negative. The calculations have been performed by using equation (3.67), (3.70), (3.71) and (3.72).

Case-2 QF-QF-QF-QF/QF-QD-QD-QF structure

If QP1 is QF, for a given strength of QP1 (k_{QP1}), from equation (3.67) QP2 is either QF or QD. The nature of QP2 is dependent upon k_{QP1} and l_2.

Case-2a QF-QF-QF-QF structure

At lower k_{QP1}($|k_{QP1}| \leq \frac{1}{\frac{l_b}{2}+l_1}$), from equation (3.67), QP2 is QF. If $k_{QP1}$is increased then strength of QP2 (k_{QP2}) is reduced. If k_{QP1} is small, due to weak focusing $\alpha_{3,x}$ is negative, thus $\beta_{4,x}$ is higher. As a result, higher value of l_3 is required. If k_{QP1} is equal to the strength as that of QF-QF structure, in that case l_3 is equal to the l_3 of QF-QF structure.

Case-2b QF-QD-QD-QF structure

If k_{QP1} is in the range $\frac{1}{\frac{l_b}{2}+l_1} < |k_{QP1}| < \frac{1}{l_2} + \frac{1}{\frac{l_b}{2}+l_1}$, from equation (3.67) QP2 is QD. If k_{QP1} (QF) is increased then $\alpha_{3,x}$ becomes more positive, as a result $\beta_{4,x}$ is reduced. Thus smaller l_3

is required to obtain the required phase advance. The point at which l_3 is zero, corresponds to QF-QD-QF structure. If k_{QP1} (QF) is further increased then $\beta_{4,x}$ is further reduced and $\alpha_{3,x}$and k_{QP2} (QD) is further increased. At certain point $\alpha_{5,x}$ becomes negative as a result stable solution will not exist.

The advantage of this structure is that in this structure, for the same lengths of l_2, the strengths of QD will be less here compared to QF-QD-QF for the non-zero l_3 case. In this structure an additional space (l_3) is available for installation of insertion devices in the middle of achromat section. As an example in section 3.3, we will discuss the case of Indus-2 with QF-QD-QD-QF structure of the achromat.

3.3 Structure of Indus-2 lattice

In Indus-2, a double bend achromat lattice is adopted. The schematic diagram of its unit cell discussed in section 1.6.3 of Chapter-1, is shown here in figure.3.12. Here we will study its achromat part. The achromat has two 22.5° rectangular dipole magnets, a triplet of quadrupole magnets (QF2-QD3-QF2) to control the dispersion in this section. In the achromat, center of QF2 is kept at 0.75 m away from the exit of dipole magnet(l_1) to provide a sufficient space for SF, steering magnets and beam diagnostics components. Center of QD3 (l_2) is kept 2.66 m away from center of QF2 magnet.

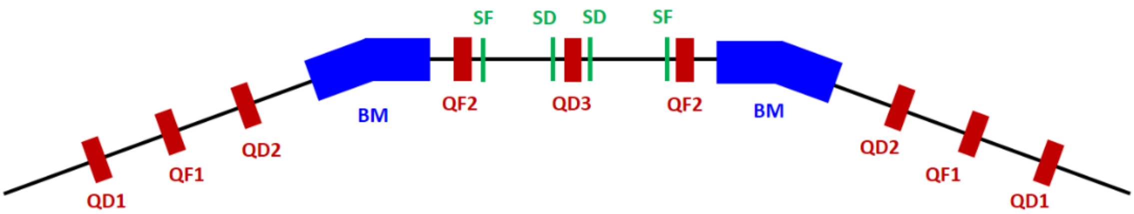

Figure 3. 12 Unit cell of Indus-2 storage ring.

3.3.1 Tunability of Indus-2 lattice with QF-QD-QF structure of the achromat

i) Achromat structure for minimum beam emittance

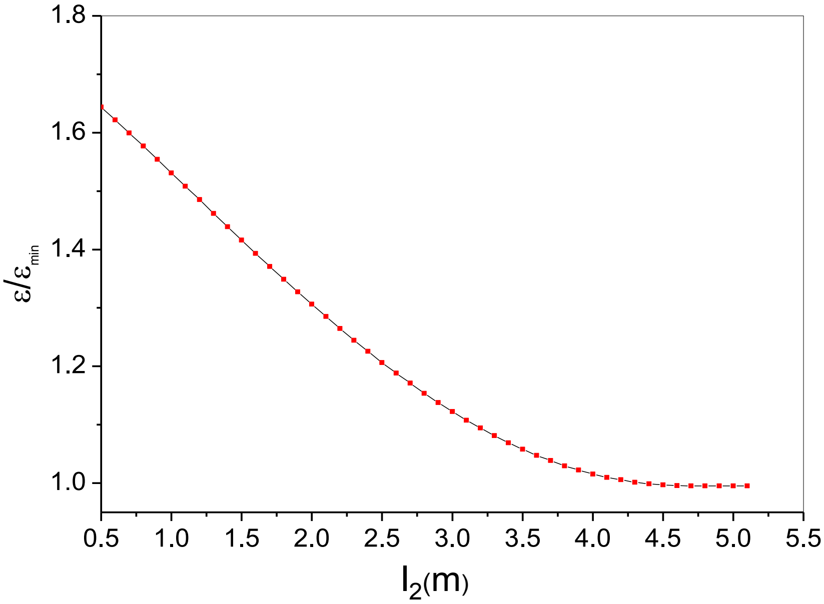

Figure 3. 13 In QF-QD-QF double bend achromat structure, the ratio of achievable beam emittance ($\varepsilon/\varepsilon_{min}$) versus l_2 (distance from QF to QD).

In thin lens approximation, effect of l_2 on beam emittance as well as on the lattice parameters is studied. The minimum achievable beam emittance depends upon the gap (l_2) between QF2 and QD3 as discussed in section 3.2.3. Analytically, different optical solutions of achromat are simulated by keeping different l_2 considering quadrupole magnets as thin lenses for $l_1 = 0.75$ m. For each l_2, quadrupole magnets strengths are estimated with the help of equation (3.52) and (3.57) by considering different initial twiss parameters at the start of achromat. For each solution, β_y-function at the center of the achromat is varied to find out $\beta_{o,y}$ at the start of the achromat by using equations (3.61) to (3.64) and (3.34). In figure 3.13, variation of l_2 vs. ratio of allowable beam emittance ($\varepsilon/\varepsilon_{\min}$) is plotted by considering different twiss parameters at the start of achromat with the help of computer program Achromat [55], in which quadrupole magnets are treated as thin lenses. In this figure, those solutions are accepted for which maximum vertical beta function ($\beta_{o,y}$) does not exceed above 25 m. The figure shows that as l_2 increases, beam emittance decreases. To obtain solution close to the theoretical minimum beam emittance required l_2 is above 4 m. For l_2~4.8m, lattice functions in the achromat are plotted in figure 3.14. The figure shows that to obtain reasonable vertical beta function at the start of achromat, β_y at the center of the achromat has to be kept at a higher value.

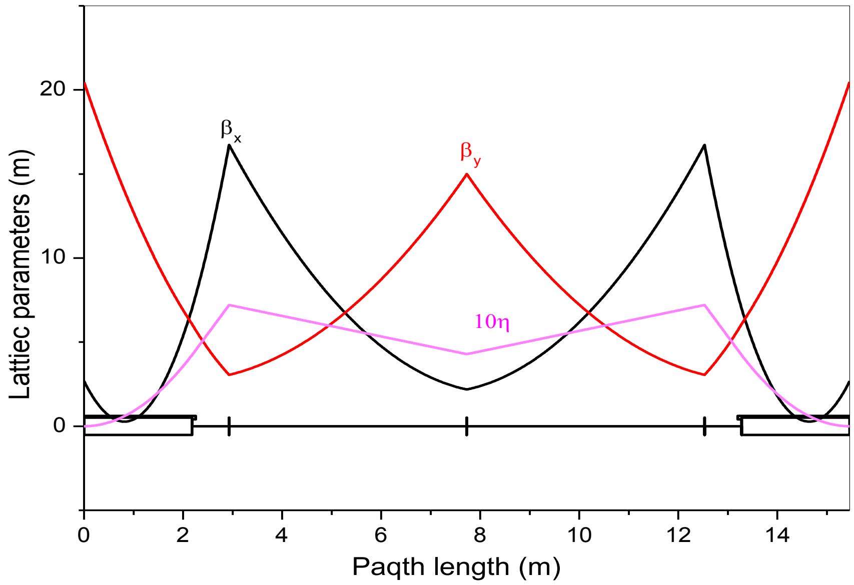

Figure 3. 14 Lattice functions in the double bend achromat for theoretical minimum beam emittance for l_2 (distance from QF to QD) 4.8 m by considering the parameters of Indus-2.

ii) Achromat structure for different length of achromat

The value of l_2 is decided by keeping an eye on requirement of twiss parameters in insertion straight section. As discussed in Chapter-1 the linear and nonlinear beam dynamical effect of insertion devices depends upon the beta function at the location of insertion section. Thus it is desirable to keep smaller value of beta function in both planes (horizontal and vertical) at the center of insertion sections. The beam injection is also carried out in the one of the insertion sections for which a higher value of beam acceptance is required. The linear acceptance of the machine can be increased by keeping horizontal beta -function close to the maximum beta function at the center of insertion section. To satisfy these conflicting requirements of beam injection and insertion devices, horizontal beta function in the insertion section is kept at a moderate value. To obtain moderate solution following constraints are kept during optimization.

1) Beam emittance less than two times of the theoretical minimum beam emittance (72 nmrad)

2) At middle of insertion section (insertion devices and at injection point) 7 m<$\beta_{ins,x}$<15 m and $\beta_{ins,y}$<4 m

3) The horizontal and vertical maximum beta function is less than $\beta_{max,x}$ <25 m and $\beta_{max,y}$ < 20 m respectively.

In addition, a wide tunability of tune point should be available for a given l_2. To obtain the optimum value of l_2, the tune space of optics is studied by taking the finite length of quadrupole magnets (thick lens) with different values of l_2 by using the computer program such as Burhani [56], Achromat [55] and ESRO [57]. For this purpose, strengths of insertion straight section quadrupole magnets are varied for different strengths of achromat quadrupole magnets.

The tune space of the optics is decided on the basis of above mentioned criteria. Under these constraints, the horizontal and vertical tune space of the optics for l_2=2.0 m, l_2=2.5 m, l_2=3.0 m and l_2=3.5 m is shown in Figures-3.15. These result show that tunability is optimum for l_2=2.5 m and 3 m. In case of l_2= 4 m, optical solutions are not possible within above constraints, as in this case maximum horizontal and vertical beta function are well beyond specified limits. Accordingly, Indus-2 lattice has been optimized with l_2=2.66 m. Due to this length, sufficient space is available in Indus-2 to install subsystems components in the ring. Based on this structure various optical solutions [57-63] are studied. The horizontal and vertical tune space of the optics for l_2=2.66 m is shown in the figure 3.16. The figure shows that in the tune space, larger area is available for horizontal and vertical integer tune point above 9.0 and 6.0 respectively.

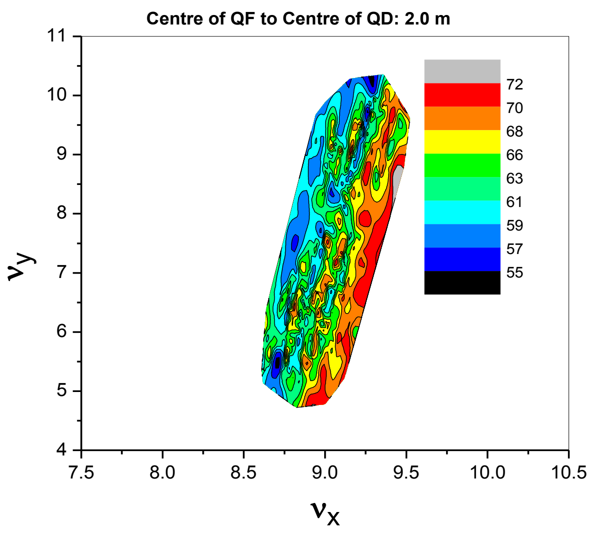

A) ***Tune space for l_2=2.0 m***

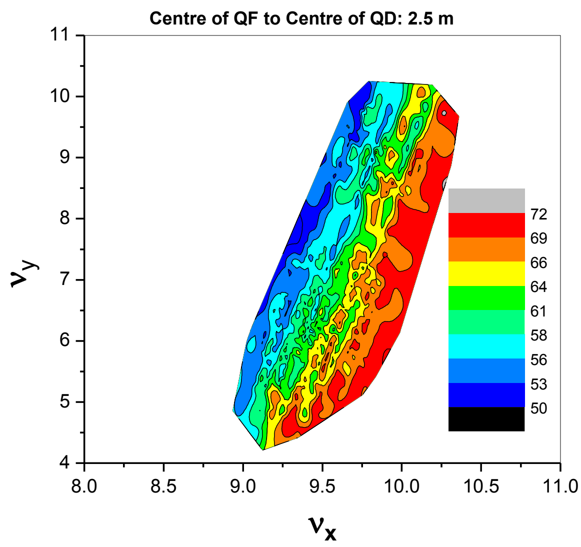

B) ***Tune space for l_2=2.5 m***

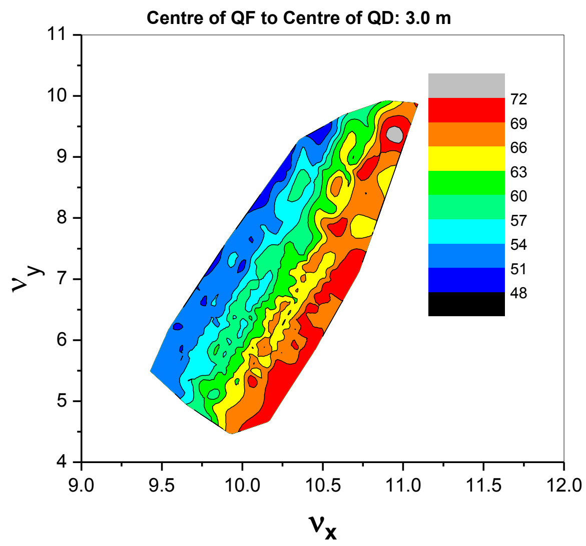

C) ***Tune space for l_2=3.0 m***

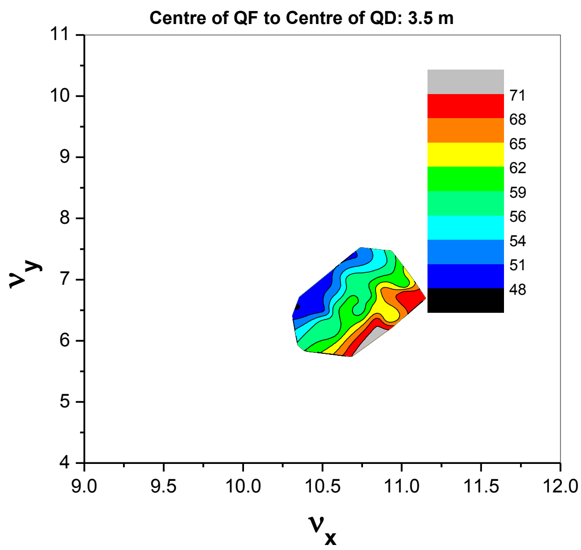

D) ***Tune space for l_2=3.5 m***

Figure 3. 15 In Indus-2 ring, allowable tune point for different length of l_2 (in the achromat between center of QF to center of QD). The simulations are performed with the help of computer program, under following constraint ε<72 nmrad, 7 m<$\beta_{ins,x}$<15 m, $\beta_{ins,y}$<4 m, $\beta_{max,x}$ <25 m and $\beta_{max,y}$< 20 m).

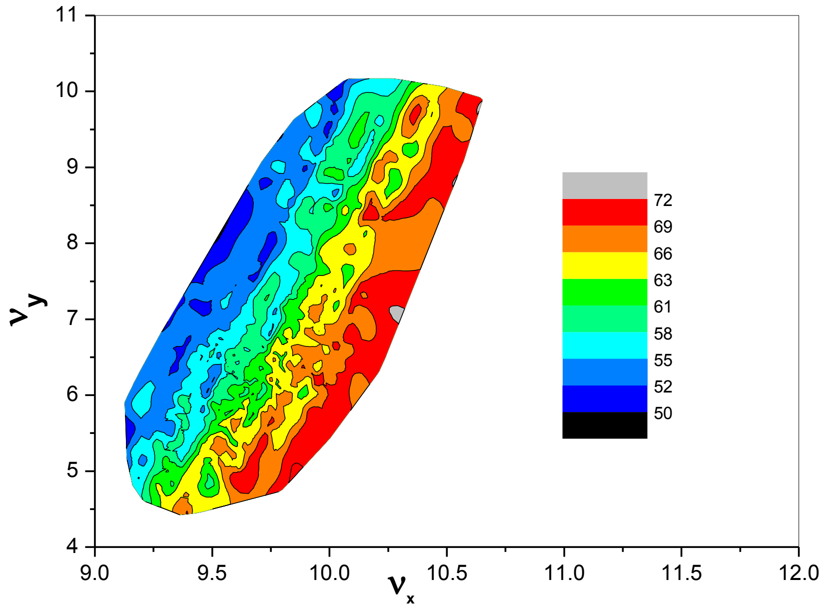

Figure 3. 16 The allowable horizontal versus vertical tune range for the chosen l_2=2.65 m of Indus-2 ring (under following constraint ε<72 nmrad, 7 m<$\beta_{ins,x}$<15 m, $\beta_{ins,y}$<4 m, $\beta_{max,x}$ <25 m and $\beta_{max,y}$< 20 m), the simulations are performed with the help of computer program.

Indus-2 is designed for a beam emittance of ~55 nmrad, which is 1.5 times of the theoretical minimum beam emittance. For the above beam emittance lattice functions for the tune point (ν_x=9.2, ν_y =5.2) and (ν_x=9.3, ν_y =6.2) are shown on figure 3.17 and 3.18.

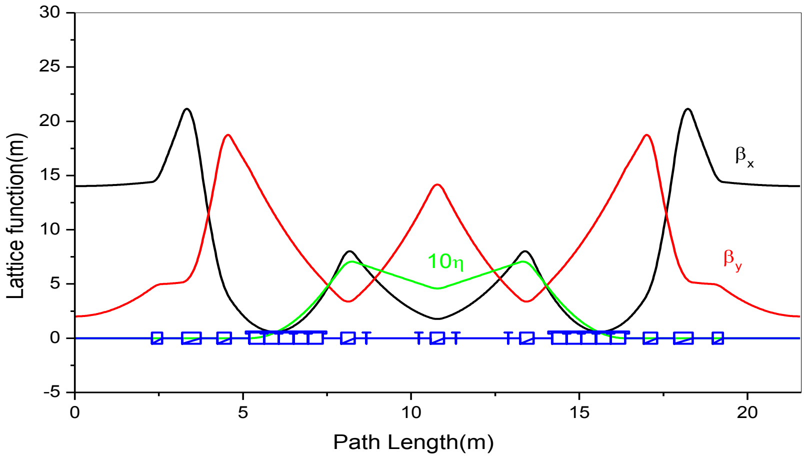

Figure 3. 17 Lattice function of Indus-2 for ε=58 nmrad at(ν_x=9.2, ν_y =5.2).

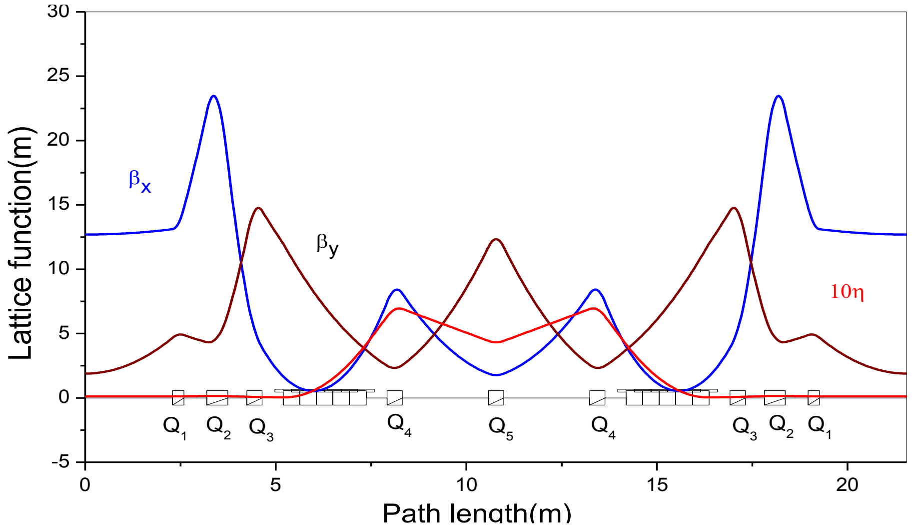

Figure 3. 18 Lattice function of Indus-2 for ε=54 nmrad at(ν_x=9.3, ν_y=6.2).

3.3.2 Tunability of Indus-2 lattice with QF-QD-QD-QF structure of the achromat

The tunability of Indus-2 lattice is also studied. by considering in the achromat part QF-QD-QD-QF instead of QF-QD-QF structure, The gap between QF and center of achromat is kept according to Indus-2 lattice and between QD and center of achromat (l_3) is kept at following values 1) 0.5 m, 2) 1.0 m, 3) 1.5 m and 4) 1.75 m. The tune space of optics is plotted by taking the finite length of quadrupole magnets (thick lens) with the computer program Achromat [55] and ESRO [57].

In the simulations, strength of insertion straight section quadrupole magnets are varied for different strengths of achromat quadrupole magnets. The tune space of the optics is decided on the basis of following constraint ε<72 nmrad, 7 m<$\beta_{ins,x}$<15 m, $\beta_{ins,y}$<4 m, $\beta_{max,x}$ <25 m and $\beta_{max,y}$< 20 m. Under these constraints, the horizontal and vertical tune space for l_3=0.5 m, l_3=1.0 m, l_3=1.5 m and l_3=1.75 m are shown in figure-3.19. These results show that in a wide range of l_2 and l_3 solutions are available for low beam emittance. For l_3=1.75 m, lattice function are plotted in figure 3.20 and 3.21 for the tune point (ν_x=9.3, ν_y =5.2) and (ν_x=9.3, ν_y =6.2) respectively.

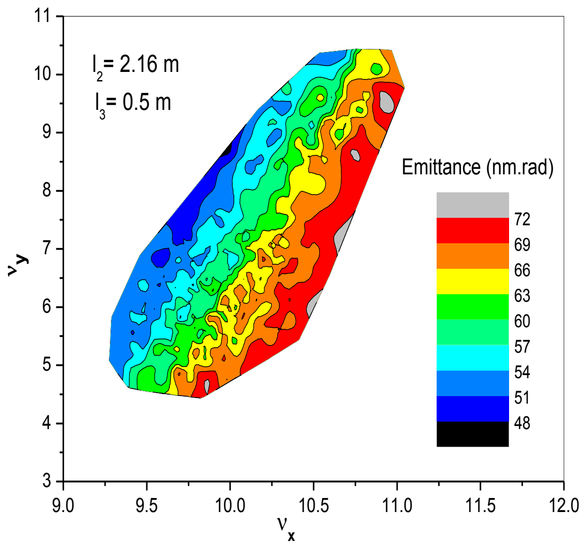

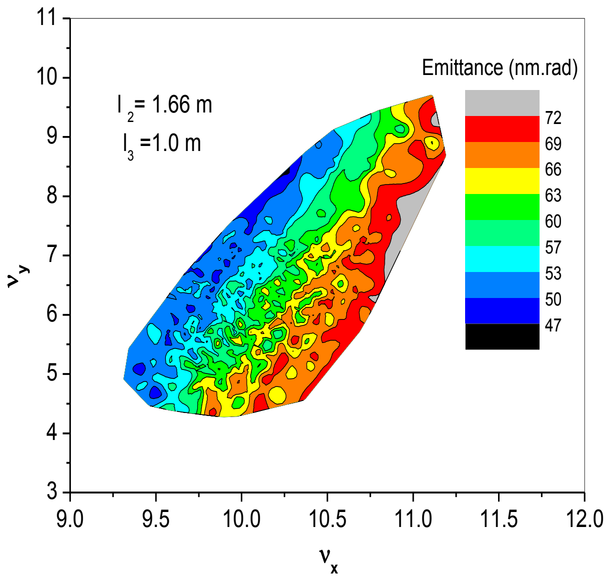

A. Tune space for l_3=0.5 m **B. Tune space for l_3=1.0 m**

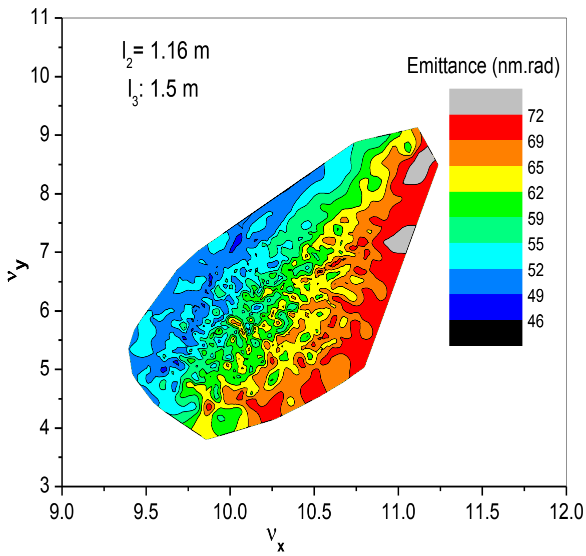

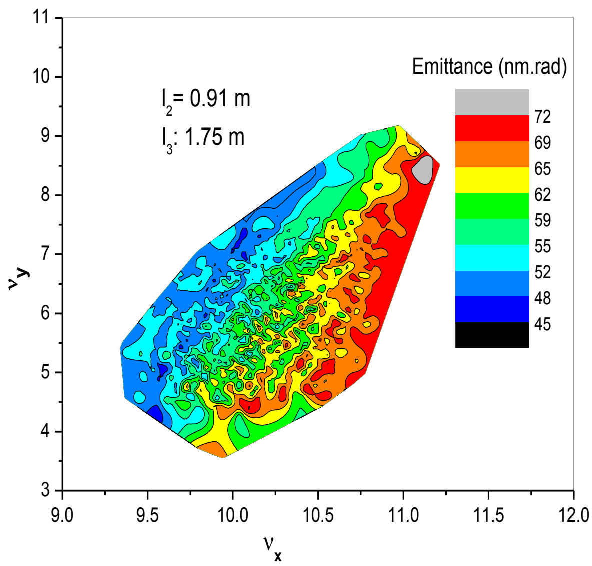

C. Tune space for l_3=1.5 m **D. Tune space for l_3=1.75 m**

Figure 3. 19 In Indus-2 ring, by considering QF-QD-QD-QF structure of the achromat, allowable horizontal versus vertical tune range for different values of gap between center of QD and center of achromat (l_3). For different values of l_3, gap between QF and QD is adjusted such that the length of the achromat should remain constant. The simulations are performed with the help of computer program, under following constraint ε<72 nmrad, 7 m <$\beta_{ins,x}$<15 m, $\beta_{ins,y}$<4 m, $\beta_{max,x}$ <25 m and $\beta_{max,y}$< 20 m).

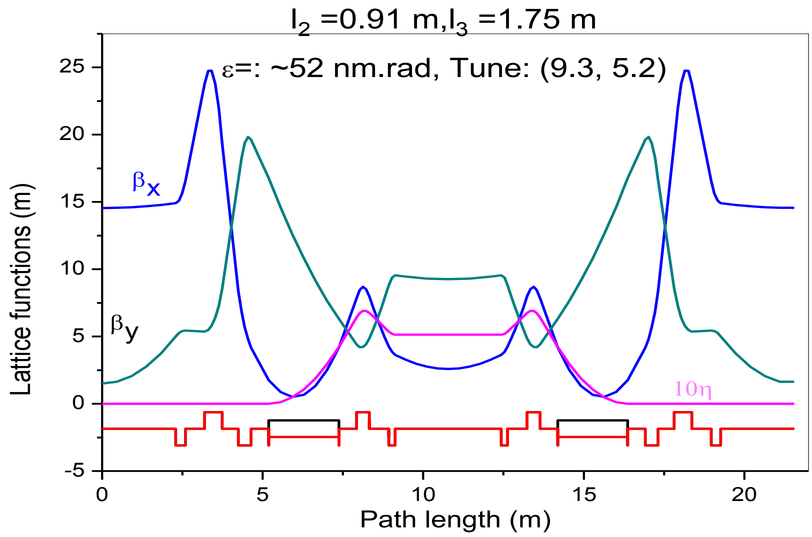

Figure 3. 20 Lattice function of Indus-2 for ε=52 nmrad at(ν_x=9.3, ν_y =5.2) by considering QF-QD-QD-QF structure of the achromat.

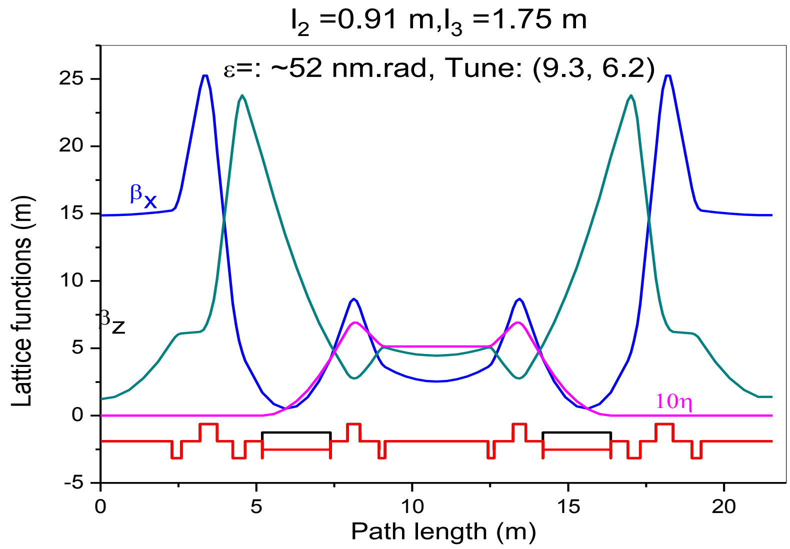

Figure 3. 21 Lattice function of Indus-2 for ε=52 nmrad at(ν_x=9.3, ν_y =6.2) by considering QF-QD-QD-QF structure of the achromat.

The allowable tune space and lattice functions show that it is possible to operate Indus-2 achromat with QF-QD-QD-QF structure. In this structure, gap between two QD can be used for installation of insertion device. The detail study of above structure has to be carried out.

3.4 Conclusions

For different structures of double bend achromat, analytical formulae are presented. In a basic Chasman-Green structure, an analytical relation of beam emittance shows that by increasing the distance between dipole magnet and QF, initially beam emittance reduces afterwards reduction in beam emittance is negligible. In this case, allowable minimum beam emittance is 63% higher than the theoretical minimum beam emittance. In the case of two quadrupole magnet structure (QF-QF structure) by increasing the length of the drift space between QF-QF beam emittance is reduced by a larger value as compared to single QF structure. In this structure, theoretical beam emittance is achievable at the cost of the long length of achromat. Further in this structure, any provision to control the vertical beta function is not available, as a result the utility of above structure is limited. In order to overcome drawback of QF-QF structure, three and four quadrupole structures are discussed. The disadvantage of QF-QF structure is overcome by using the QF-QD-QF/QF-QD-QD-QF structure. In the three quadrupole magnet structure, shorter length of achromat is possible with a higher strength of QF and QD magnets and very high value of initial twiss parameters. In the case of QF-QD-QD-QF structure, strength of QD is reduced at the cost of additional length between the two QDs, this additional length can be used for installation of insertion devices.

In Indus-2, in the achromat part, QF-QD-QF structure is chosen by keeping moderate vertical beta function and moderate achromat length. These studies helped us in understanding and optimizing QF-QD-QF structure for Indus-2 which operates at 1.5 times of the minimum beam emittance. These studies also suggest that in Indus-2, in the achromat section, additional space for insertion devices can be created by changing the present achromat structure of QF-QD-QF into QF-QD-QD-QF structure, for this structure further studies have to be carried out.

The above analytical formulas help to evaluate location of quadrupole magnets, quadrupole magnets strength, variation of twiss parameters and beam emittance before performing time-consuming optics matching.

CHAPTER 4

BEAM EMITTANCE REDUCTION IN INDUS-2

In Indus-2, electron beam is injected in the horizontal plane at a beam energy of 550 MeV. At this injection energy, beam rigidity is low and during the beam injection, the betatron oscillation amplitude of the injected beam remains significantly large for a long time due to longer radial radiation damping time (450 ms).

As explained in Chapter-3, Indus-2 lattice has been optimized in achromatic condition by keeping the beam emittance of ~55 nm.rad, which is ~1.5 times that of the theoretical minimum beam emittance. The beam emittance referred here is the horizontal/radial beam emittance of the ring. In the initial stages of the commissioning, difficulties were faced in accumulating the beam current with the design optics. With this optics, partial beam loss phenomenon was observed during beam accumulation, which was attributed to injection errors arising from the mismatch of kickers [50] and small dynamic aperture [61-63]. In this optics, effects of linear and nonlinear imperfections are high due to high strengths of chromaticity correcting sextupole magnets.

To overcome this problem, Indus-2 was commissioned using a moderate optics [58] having beam emittance of 135 nmrad (~2.5 times that of design beam emittance) at 2.5 GeV. In this optics, dynamic aperture is increased by reducing the strength of sextupole magnets, which is obtained by increasing the dispersion function at its location by breaking achromatic condition. The smaller strength of sextupole magnets will reduce the injected and stored beam oscillations. Using this optics, sensitivity towards linear and nonlinear imperfections are reduced. Effect of injection errors is further reduced with the help of off-momentum beam injection. With off-momentum beam injection, better beam accumulation was observed during beam injection. The tune point in tune space (figure 3.16 of Chapter-3) is chosen such that the optics can be switched over to the optics, which has smaller beam emittance.

In order to operate Indus-2 with a low emittance, we have implemented a scheme, in which the electron beam is injected using the moderate optics at 550 MeV and after accumulation of the required current and increasing the beam energy to final beam energy, the beam emittance is reduced by changing the strengths of quadrupole and sextupole magnets. A similar scheme was also proposed by Miyata et.al [64] in which a lattice is designed in such way that the beam is injected using an optics having a higher beam emittance and after storage of the required current, the emittance is reduced by changing the strengths of quadrupole and sextupole magnets.

An optics providing beam emittance one third of the moderate optics keeping the operating point nearly the same has been evolved by keeping dispersion function nearly zero, in the insertion straight section, where the vertical beta is also less than half of the moderate optics. This optics is termed as low emittance optics. With the help of this optics photon brightness from undulators will be increased by a factor of eight and linear as well as non-linear effects of insertion devices will be reduced by a factor of 2.3 as compared to the moderate optics.

To ensure smooth switch over from the moderate optics to low emittance, a procedure is evolved and executed in a step by step manner. In each step, storage ring's sensitivity to linear and nonlinear imperfections is also controlled in a well-defined way to avoid any partial beam loss. This is done by optimization of the beta function and tune point during the switch over.

In this chapter, we present the studies in dynamical aspects of beam injection with the moderate and low emittance optics to demonstrate that it is easier to inject the beam with the moderate optics. The procedure followed for reduction of the beam emittance, which involves minimization of an objective function maintaining the strict control on the tune and beta functions is also discussed. The results of simulations during switch over from the moderate to low emittance mode and experimental results during its implementation are discussed.

4.1 Dynamic aperture studies

In both horizontal and vertical transverse planes, sufficient dynamic aperture is required for beam injection. In horizontal plane it is required to accommodate the residual oscillation of injected beam. The aperture requirement is further enhanced due to increase in the residual oscillations caused by mismatch between injection kickers. In vertical plane, this is mainly determined by the finite orbit distortion and from injected beam having finite beam size and non-zero initial coordinates (displacement and angle) from the design orbit.

The lattice functions for the moderate and low emittance optics and corresponding dynamic aperture for the tune point (9.27 6.16) at beam injection are shown in figures 4.1, 4.2 and 4.3 respectively. Horizontal and vertical tune are shown in the brackets. The dynamic aperture is computed for one value of radial and vertical damping time (800,000 turns) by considering aperture limit (x = ±32 mm, y = ±17 mm) at 550 MeV using RACETRACK [20]. In this computation, natural chromaticity is corrected up to zero in both the planes with the sextupoles. In the low emittance optics, in both planes dynamic aperture is reduced due to higher strength of chromaticity correcting sextupole magnets. In the vertical plane, vertical acceptance is reduced due to decrease in vertical beta in the center of insertion section and increase $\beta_{y,max}$ .The result shows that in the low emittance optics at x = 13 mm, the dynamic aperture shrinks due to excitation of resonances. Thus, in the low emittance optics, the dynamic aperture is smaller in both horizontal and vertical planes as compared to the moderate optics.

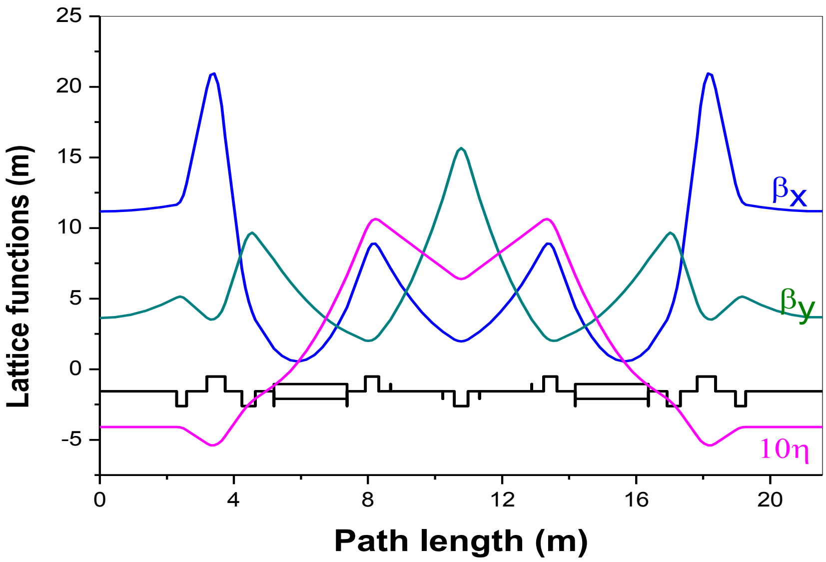

Figure 4. 1 Lattice functions for the moderate optics (Beam emittance 135 nmrad).

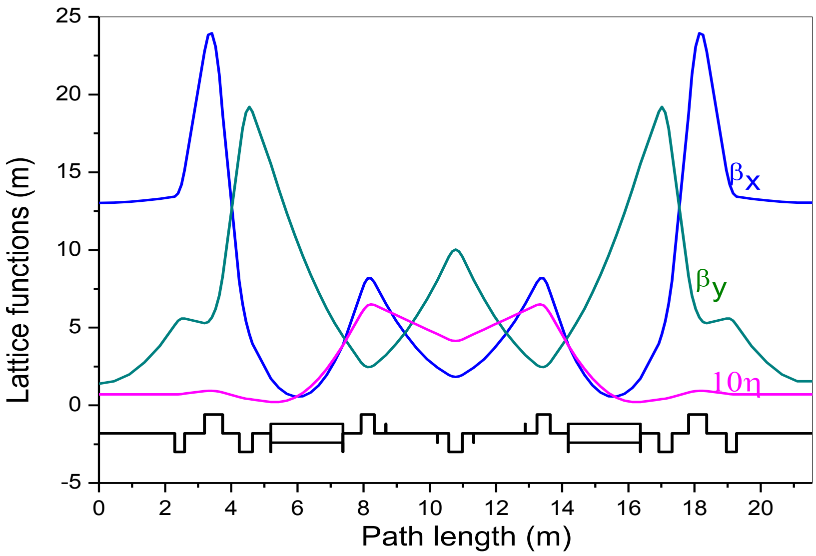

Figure 4. 2: Lattice functions for the low emittance optics (Beam emittance 45 nmrad).

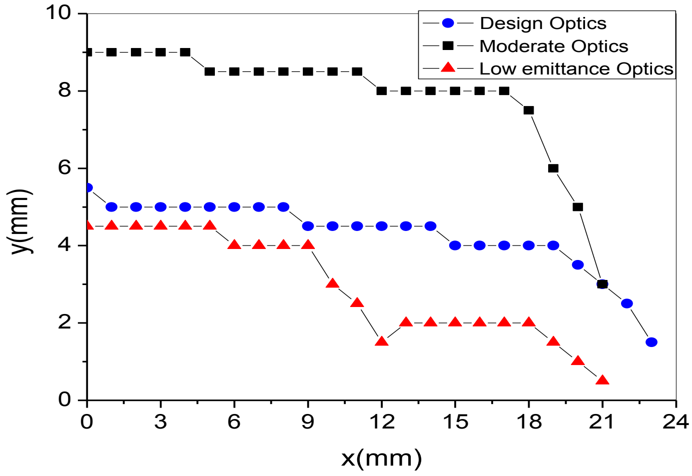

Figure 4. 3 Dynamic aperture for 800,000 turns (one damping time) with the moderate and low beam emittance optics at injection energy (550 MeV) at the tune point (9.27 6.16).

For the moderate optics, required vertical aperture for beam injection is estimated with the help of vertical scrapper movement. The vertical scrapper is located ~2 m away from the center of the 7th insertion straight section. Here, the injection section is considered to be first section. The results of the experiment indicate that minimum aperture required in the vertical plane for beam injection is found to be ±6 mm [66]. During the measurement, rms horizontal and vertical closed orbit after correction are ~1.3 mm and ~0.8 mm respectively. On the other hand, for the low emittance optics closed orbit distortions will be increased due to higher value of amplification of linear imperfection (closed orbit and beta beat) and higher strengths of sextupole magnets. Thus, in the presence of actual linear and nonlinear imperfections, vertical aperture in the low emittance optics, will be reduced by a higher amount as compared to the moderate optics.

4.2 Beam Dynamics at injection energy

4.2.1 Injection scheme

The injection is carried out in the radial plane from the outer side of the ring by using a compensated bump generated by four kicker magnets [67-68] see figure 4.4.

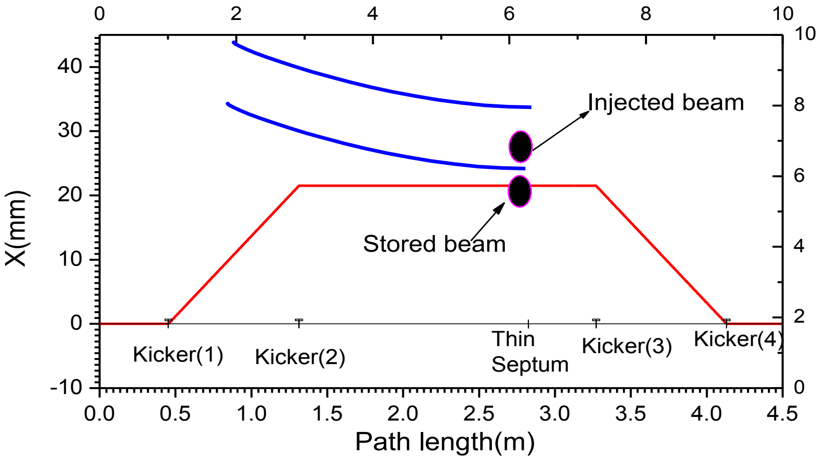

Figure 4. 4 A schematic diagram of beam injection scheme in Indus-2.

During the injection process, the injection bump, which is trapezoidal in shape, generated by the injection kicker magnets, has to be adjusted such that stored beam remains well separated from the septum magnet as well as the residual betatron oscillations of the injected beam remain small. In an ideal case, the amplitude of orbit bump (B) and the location of the septum from the designed orbit (L_s) can be calculated from the following relation [35-37].

$$B = 4\sigma_{i,x} + 2S_c + S_t \tag{4.1}$$

$$L_s = B + 4\sigma_{s,x} + S_c \tag{4.2}$$

Where $\sigma_{i,x}$: Beam size of the injected beam, $\sigma_{s,x}$: Beam size of the stored beam, S_c : septum clearance; septum thickness (S_t)=3.0 mm, injected beam emittance (ε_{xi})= 3.9*10^{-07} mrad and stored beam emittance (ε_{xs})= 2.5*10^{-08} mrad are respectively at 550 MeV. The value of ε_{xs} has been arrived at by taking into consideration a blow-up of emittance due to intrabeam scattering and bunch lengthening [51], which is nearly same for both optics. For the injected beam a blow-up factor of two (2) has also been assumed by considering effect of magnetic field in-homogeneity in the extraction septum [69]of synchrotron and thick and thin septum of Indus-2. [70].

In the case of Indus-2, above relations equation (4.1) and (4.2) are only guidelines and are not exact as pulse shapes of the kicker magnets are nearly half sinusoids and are not exactly identical see table-4.1. They have jitter of ±7 ns with respect to each other, which causes mismatch between pulses.

Table 4. 1 Measured pulse power supply parameters of injection kickers

	Rising time(μs)	**Falling time (μs)**
Kicker(1)	1.3	1.53
Kicker(2)	1.27	1.53
Kicker(3)	1.29	1.60
Kicker(4)	1.29	1.60
The jitter among kickers: ±7 ns		

In the presence of mismatch between the injection kicker pulses, the injection bump is not closed, as a result the residual betatron oscillations of injected and stored beam are increased. Thus a part of injected or stored beam or both beams may be lost during injection process. These losses can be reduced by using a combination of following methods 1) reducing the nonlinear forces / strengths of sextupole magnets using a moderate optics and 2) with the help of negative orbit displacement at the septum location or with the smaller injection bump or combination of both.

In the case of a negative orbit displacement or a lower bump, higher dynamic aperture is required to accommodate increased residual betatron oscillation of the injected beam. As mentioned earlier higher dynamic aperture is available with the moderate optics.

More flexibility can be obtained by employing an off-momentum beam injection ($\Delta p/p$). In off-momentum beam injection, injected beam oscillations can be partially reduced during the injection as shown by Shoji et. al. [71]. They have demonstrated that the reduced betatron oscillation helps in the storage of the ring .In order to carry out off-momentum beam injection a finite value of dispersion function (η_{ins}) is required at the injection point. For off-momentum beam injection, the center of injected beam position at the septum location [35-37] is given by

$$X = x_{cod,sep} + \eta_{ins}\frac{\Delta p}{p} + x_{bump}\cos\left(\frac{2\pi n T_r}{T_k}\right) + x_{residual}\cos(2\pi n \nu_x) \tag{4.3}$$

$$with\ x_{residual} = \left(x_c - x_{bump} - \eta_{ins}\frac{\Delta p}{p} - x_{cod,sep}\right)$$

Where x_{bump} represents the magnitude of orbit bump (generated by injection kicker magnets), $x_{cod,sep}$ denotes orbit displacement at the septum location, x_c injected beam center from the design orbit, $x_{residual}$ amplitude of residual betatron oscillation, ν_x horizontal tune, n number of turns of the stored particles in the ring, with maximum value of bump at n =0 (injection time), T_r revolution period of the ring and T_k fall time of the kicker pulse. During initial few turns $x_{residual}$ will be reduced and injected beam center is shifted by $\eta_{ins}\frac{\Delta p}{p}$, afterwards the oscillation will be increased due to synchrotron-betatron oscillations.

For the moderate optics, at the point of beam injection, dispersion function is -0.4 m, whereas it is negligibly small for the low emittance optics. It is possible to reduce residual horizontal betatron oscillations of the injected beam with off-momentum beam injection for the moderate optics. On the other hand for the low emittance optics, these oscillations are not much reduced due to very small dispersion function.

4.2.2 Effect of mismatch between injection kickers

Tracking studies have been carried out with the modified computer code RACETRACK for the moderate and low beam emittance optics at the tune point (9.27, 6.16). In these studies, beam size is taken to be 1.5 times that of the rms beam size of the injected beam. In the calculations, inner side of septum location is fixed at 15 mm from the design orbit. It is worth mentioning here that in the ring, the distance of the septum from the design orbit had to be reduced from 21 mm to 15 mm to enable viewing of the beam on the beam profile monitors due to the aperture limitations of these monitors. Consequently, this has reduced the aperture for beam oscillations in the ring. Currently, the beam position indicators installed in the ring, do not have a provision for the turn-by-turn beam position measurement.

Injected and stored beam tracking is done by including the mismatch between the kickers (as given in table 4.1) and neglecting the mismatch (no jitter and equal pulse lengths, having rise time of 1.2 μs and fall time of 1.6 μs). The turn by turn tracking simulations of the injected and stored beam have been done by considering the injection beam bump of 9.6 mm. For the bump of 9.6 mm, injection simulation results for the low emittance and moderate optics in the presence of mismatch between injection kickers are plotted in figure 4.5 and 4.6 respectively. These figures show that in the low emittance mode, a part of the stored beam hits the septum magnet, whereas for the moderate optics, injected and stored beam, do not hit the septum magnet. A comparative analysis is summarized in table 4.2, with and without mismatch between the injection kickers. The effect of the mismatch among kickers is smaller for the moderate optics as compared to the low emittance optics. It is attributed to the smaller strength of chromaticity correcting sextupole magnets, which is nearly half of the low emittance optics. This results in a less distortion of the transverse betatron phase space. This is also manifested as smaller amplitude dependent tune shift in this optics as compared to the low emittance optics as shown in figure 4. 7. The stored beam experiences the angular kick from the kickers for five turns, whereas the injected beam for three turns (revolution time in the storage ring 575 ns) respectively. Thus residual oscillations of stored beam are increased by higher amounts as compared to the injected beam (table-4.2).

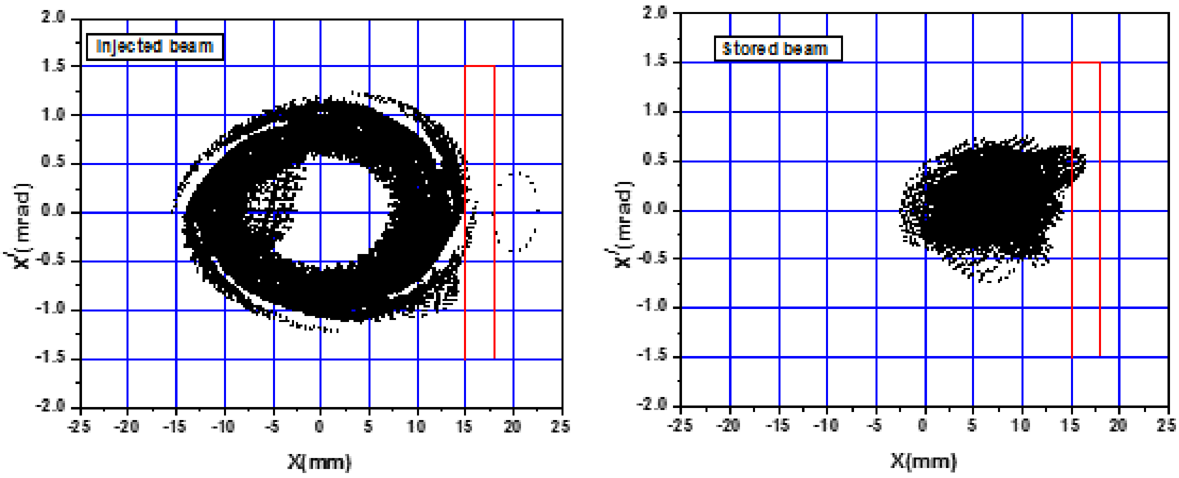

A) Injected beam oscillation B) Stored beam oscillation

Figure 4. 5 For the low emittance optics a) injected and b) stored beam oscillations for thirty and six turns, respectively in the presence of mismatch between injection kickers (table 4.1). The injection bump of 9.6 mm is generated by matching the starting point of injection kickers.

Table 4. 2: The maximum oscillations of injected and stored beam in the moderate and low beam emittance optics with and without mismatch between injection kickers

Δp/p=0, Bump=9.6 mm	**Without mismatch**		**With mismatch**	
Optics	A_+ (mm)	S_+ (mm)	A_+ (mm)	S_+ (mm)
Low emittance	13.0	12.1	15.5	16.5
Moderate	13.0	11.5	14.5	15.1

Where A_+ and S_+ represents the maximum displacement towards the septum magnet of injected and stored beam.

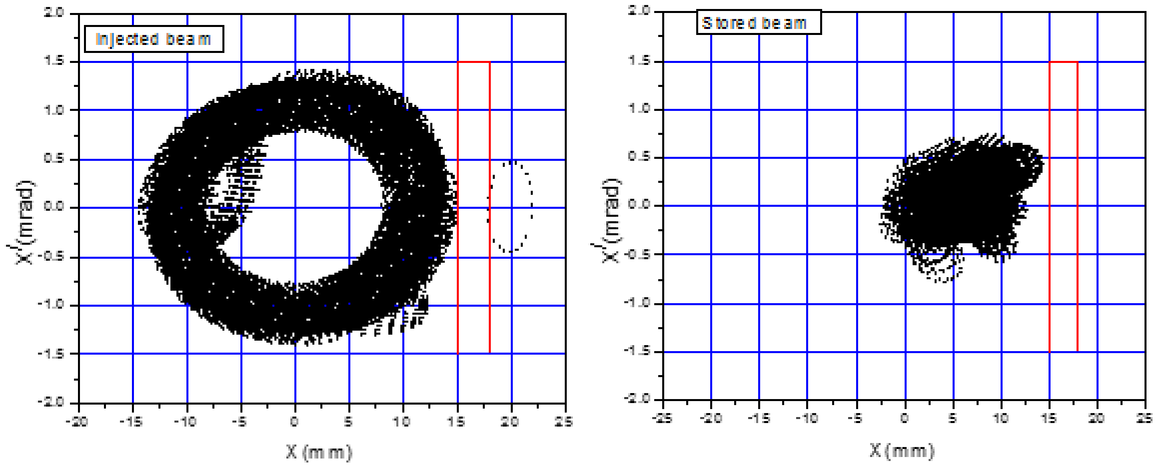

A) Injected beam oscillation B) Stored beam oscillation

Figure 4. 6 For the moderate optics a) injected and b) stored beam oscillations for thirty and six turns respectively in the presence of mismatch between injection kickers (table 4.1). The injection bump of 9.6 mm is generated by matching the starting point of injection kickers.

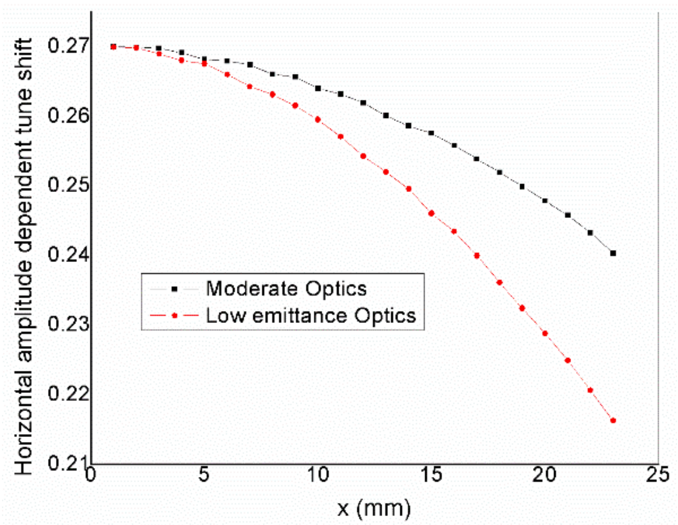

Figure 4. 7 The amplitude dependent tune shifts in horizontal plane w.r.t. horizontal beam position for the moderate and low emittance optics.

For the low emittance optics, due to mismatch between the injection kickers, residual betatron oscillation in horizontal plane is higher as compared to the moderate optics. These aspects make the beam injection very difficult with the low emittance optics.

4.2.3 Commissioning experience with moderate optics

During the commissioning with the moderate optics, smooth beam injection took place when a negative DC bump of ~4.5 mm was generated in the injection section using orbit corrector magnets. This negative orbit displacement helps in keeping the injected and stored beam away from the septum for the same value of the injection bump. An additional advantage of the negative orbit displacement is that it increases the horizontal aperture available for betatron oscillation by 4.5 mm in the injection section (the horizontal aperture at other places in the ring is 32 mm). Accordingly, the dynamic aperture on the other side of septum will also be increased. When the injection bump was 12.3 mm, the injection efficiency was ~40 % and this is increased to ~80 % with off-momentum injection (-0.9 %) achieved by synchronously increasing the magnet currents of all storage ring magnets. Injection efficiency is estimated with respect to transmitted beam current in Indus-2. In the moderate optics shown in figure 4.1, dispersion function is negative thus for off-momentum beam injection, stored beam energy is kept ~0.9 % higher than that injected beam energy. For both on and off-momentum beam injection, fast decay of stored beam was observed. This fast decay was arrested by increasing the separation of the stored beam from the septum magnet. This was done by reducing the injection bump from ~12.3 mm to ~9.6 mm. For the smaller bump, for on-momentum beam injection, injection was not possible and for off-momentum injection rate was 40 %. For higher bump, the fast decay of stored beam current is attributed to the beam going close to the septum magnet. On reducing the bump to 9.6 mm, improvement in beam lifetime of the stored beam was observed.

The turn by turn tracking simulations of the injected and stored beam have been done to understand the above findings in the presence of mismatch between injection kicker pulses. In simulations, the injection beam bump of 12.3 mm and 9.6 mm for on and off-momentum electrons (-0.9 %) are considered by including the mismatch between injection kickers. In order to estimate the fraction of the injected pulse length, which can be accepted, these studies include tracking of electrons which are injected at the synchronous phase and also those which are displaced in time scale (0.25 ns, and 0.5 ns) with respect to the synchronous phase. The simulation results are presented in table-4.3, which contains the maximum displacement of the injected beam on the septum side (A_+) and on the other side of the septum (A_-) during the first 10 turns and during initial 200 turns. The tracking of the beam up to 200 turns has been done to account for the synchrotron oscillations as the period of one synchrotron oscillation is ~50 turns at 700 kV RF voltage [72] and the energy acceptance is ~2%.

This table shows that for the bump of 12.3 mm, on-momentum injected beam having pulse length up to 0.25 ns is accepted. On the other hand for the same bump, off-momentum electrons up to 0.5 ns pulse length are accepted. This indicates why injection improves with off-momentum beam injection. For 12.3 mm bump, the stored beam goes close to the septum magnet. On reducing the bump to 9.6 mm, the on-momentum beam is not accepted much because it goes close to the septum magnet and thus injection is not possible.

For this bump, off-momentum beam with pulse length equal to ~0.25 ns is accepted and since the stored beam remains far away from the septum magnet. Acceptance of shorter pulse length explains why there is a reduction in the injection efficiency when the bump is reduced from 12.3 mm to 9.6 mm.

Table 4. 3: The maximum displacement towards and opposite side of the septum magnet for on and off-momentum beam injection with the moderate optics. In simulation following parameters are kept, $x_{cod,sep}$=-4.5 mm, horizontal beta function (β_{xi}) of injected beam is 8 m.

Case	**Bump (mm), pulse length (ns)**	**A_+, A_- (mm) (0-10 turns)**	**A_+, A_- (mm) (0-200 turns)**	**S_+ (mm)**
On-momentum	12.3, 0	12.6 - 21.3	12.6 - 21.3	14.0
	12.3, 0.25	14.1 - 19.1	14.3 - 24.5	
	12.3, 0.5	15.0 - 18.0	16.0 - 27.3	
	9.6, 0	14.7 - 23.2	14.7 - 23.2	10.6
	9.6, 0.25	16.3 - 20.9	16.5 - 26.6	
	9.6, 0.5	17.2 - 19.8	17.9 - 29.7	
Off-momentum	12.3, 0	12.0 - 16.1	12.1 - 22.8	14.0
($\Delta p/p$ =-0.9%)	12.3, 0.25	12.9 - 13.9	12.9 - 23.9	
	12.3, 0.5	13.9 - 12.5	14.0 - 26.6	
	9.6, 0	14.2 - 18.2	14.3 - 24.9	10.6
	9.6, 0.25	15.1 - 16.0	15.1 - 26.4	
	9.6, 0.5	16.3 - 14.6	16.3 - 28.6	

Where A_+ represents the maximum displacement towards the septum magnet and A_- is the maximum displacement on the side opposite to the septum magnet from the design orbit. Pulse length 0 indicates the synchronous particle.

4.3 Procedure for optimization during operation

The horizontal beam emittance (discussed in Chapter-1) is given by

$$\varepsilon = C_q \gamma_0^2 \frac{\langle H \rangle}{j_x \rho} \tag{4.4}$$

Here $\langle H \rangle = \int \left(\gamma_x \eta^2 + 2\alpha_x \eta \eta^{/} + \beta_x {\eta^{/}}^2 \right) ds/2\pi\rho$, s is the longitudinal distance in a bending magnet at which twiss parameters beta, alpha, dispersion function and derivative of dispersion function are $\beta_x, \alpha_x,\ \eta$ and $\eta^{/}$, respectively on the horizontal plane, $\gamma_x = \frac{1+\alpha_x^2}{\beta_x}$, C_q is the compton wavelength of the electron, γ_o is the reduced energy of the electrons. ρ is the bending radius and j_x is the horizontal partition number.

The beam emittance can be reduced by reducing the $\langle H \rangle$ function. To do this, profiles of β_x and η in the bending magnets have to be optimized by varying the strength of quadrupole magnets. The strength of quadrupole magnets are optimized such that beta function at the center of insertion section satisfies the requirement of insertion devices and beam injection.

In the double bend achromat for achromatic condition in the insertion section, dispersion function and its derivative at first bending magnet and at the exit of second magnet should be zero (figure 1.3 of Chapter-1). This condition can be satisfied by choosing a proper phase advance between the two bending magnets (discussed in section 3.1 of Chapter-3), for which proper strengths of quadrupole are required between the two bending magnet. The requirement of phase advance also depends upon the initial twiss parameters at the start of bending magnet. The initial twiss parameters at the start of bending magnet will be governed by the insertion straight section quadrupoles. Thus the strength of quadrupole magnets of insertion and achromat sections are simultaneously adjusted in a gradual manner to reduce the beam emittance by adjusting $\beta_{ins,x}$ (horizontal beta function at center of the insertion straight section) or $\beta_{ins,y}$ or both keeping the tune point as required. In the usual method of optical matching, a nonlinear system of equations is solved by Newton-Raphson method [73], in which the number of variables are kept equivalent to number of matching parameters. Since the optimization has to be done in the presence of the beam, this method provides limited flexibility in optimization.

For the proper optimization, we solve a system of linear equations so that the trend of change of optics can be regulated. In this method, the number of variables can be kept higher than the number of matching parameters. Another advantage of this method is that during its execution, if the observed closed orbit distortion (COD), β-asymmetry (beta-beat) and tunes are higher than the values predicted theoretically, then the necessary corrections (for COD and β-asymmetry) are implemented. The detailed description of the method is given below

In order to obtain the required beta functions and tunes simultaneously, while exploring the possibility of reducing the emittance, an objective function is constructed and it is optimized by using least square and Lagrangian multiplier method [74]. This function is given by equation (4.5), which is minimized by differentiating it with respect to small perturbations in quadrupole magnet strengths (Δk). In this objective function, first two terms $((B_{z,ij}\Delta k_j), z = x, y)$ show β-asymmetry generated by the quadrupole magnets all over the ring in horizontal (*x*) and vertical (*y*) planes respectively. Here *i* is the location at which change in beta function is considered. The index *j* denotes the quadrupole magnet whose strength is to be varied. The next two terms (S_1, S_2) given by equation (4.6) are related to the required tune shift and contribution of different quadrupole magnets to the tune shift ($A_{z,j}\Delta k_j$) in *x* and *y* plane respectively. The remaining two terms (S_3, S_4) are given by equation (4.7). These are related to the required β-asymmetry and contribution of different quadrupole magnets to the β-asymmetry at a particular azimuthal location in ($B_{z,lj}\Delta k_j$) in *x* and *y* plane respectively.

$$S=\sum_{i=1}^{m}\left[\left\{\sum_{j}B_{x,ij}\Delta k_j\right\}^2+\left\{\sum_{j}B_{y,ij}\Delta k_j\right\}^2\right]+\lambda_1 S_1+\lambda_2 S_2+\lambda_3 S_3+\lambda_4 S_4 \tag{4.5}$$

$$\left.\begin{array}{l} S_1=\Delta\nu_x^{required}+\sum_{j=1}^{n}A_{x,j}\Delta k_j=0.0 \\ S_2=\Delta\nu_y^{required}+\sum_{j=1}^{n}A_{y,j}\Delta k_j=0.0 \end{array}\right] \tag{4.6}$$

$$\left.\begin{array}{l} S_3=\left(\dfrac{\beta_{l,x}^{required}-\beta_{l,x}}{\beta_{l,x}}\right)+\sum_{j=1}^{n}B_{x,lj}\Delta k_j=0.0 \\ S_4=\left(\dfrac{\beta_{l,y}^{required}-\beta_{l,y}}{\beta_{l,y}}\right)+\sum_{j=1}^{n}B_{y,lj}\Delta k_j=0.0 \end{array}\right] \tag{4.7}$$

In equation (4.5) the parameters λ_1, λ_2, λ_3 and λ_4 are Lagrangian undetermined multipliers, $\beta_{l,z}$ indicates beta function at a particular azimuthal location, $\beta_{l,z}^{required}$ indicates required beta function at a particular azimuthal location l and $\Delta\nu_z^{required}$ indicates required tune shift. The upper limit in the summation *n* and *m* denote the number of quadrupole magnets whose strengths are varied and the number of observation points respectively.

Here we use thin lens approximation to define the changes in beta and tune values. $B_{z,ij}$ and $A_{z,j}$ are related to the change in the strength of j[th] quadrupole magnet through equations (4.8) and (4.9). These coefficients are calculated using these equations by considering small perturbations in quadrupole magnet strengths (Δk_j). In the first order and thin lens approximation they are given by [12],

$$B_{z,ij}\Delta K_j=\left(\frac{\Delta\beta_z}{\beta_z}\right)_i=\frac{1}{2\sin(2\pi\nu_z)}\beta_{j,z}.\cos\{2\nu_z(\pi-|\mu_{j,z}-\mu_{i,z}|)\}\Delta k_j \tag{4.8}$$

$$A_{z,j}\Delta k_j=\Delta\nu_z=\frac{1}{4\pi}\beta_{j,z}\Delta k_j \tag{4.9}$$

Here $\mu_{i,z}=\int\frac{ds}{\nu_z\beta_{i,z}}$

In order to minimize the function S (equation (4.5)), it is differentiated with respect to Δk_j s

$$\frac{\partial S}{\partial(\Delta k_j)} = 0.0 \tag{4.10}$$

From equations (4.6), (4.7) and (4.10) we get n+4 equations and n +4 unknowns **(** Δk_1 **,** Δk_2 **,** Δk_3 **,...,** Δk_n **,** λ_1**,** λ_2 **,** λ_3 and λ_4 **).** By solving these equations numerically using Guass elimination method [75], the required changes in Δk of n quadrupole magnets are obtained.

In order to minimize the difference between the strength of quadrupole magnets obtained using thin lens approximation and corresponding strength of real quadrupole magnets, $\beta_{l,z}^{required}$ and $\Delta\nu_z^{required}$ are changed in small steps. In each step, the quadrupole magnet strengths obtained from above method are put into a standard computer code such as RACETRACK. The code RACETRACK is used to convert thin lens calculations into thick lens optics, new twiss parameters are used in next step calculations in which $\beta_{l,z}^{required}$ and $\Delta\nu_z^{required}$ are again changed by small amounts. This procedure is repeated several times.

To find out the trends of optics in each step, beam emittance, strengths of sextupole magnets, amplification factors for COD at $\beta_{\max,z}$ location, β-asymmetry and amplitude dependent tune shifts due to sextupole magnets are calculated. During the switch over the strengths of quadrupole magnets need to be varied such that β-asymmetry and COD [11-12] generated are not increased enormously otherwise there can be a loss of the stored beam. The amplification factor for COD due to the misalignment of quadrupole magnets and β-asymmetry due to quadrupole magnet field errors are estimated by using equation (4.11) and (4.12).

$$\left\langle \frac{z_{CO}}{\Delta z} \right\rangle_{\beta_{\max,z}} = \frac{\sqrt{\beta_{\max,z}}}{2\sqrt{2}\left|\sin \pi\nu_z\right|}\left[\sum_j \beta_{j,z} k_j^2\right]^{1/2} \tag{4.11}$$

$$\left\langle \frac{\Delta\beta_z/\beta_z}{\Delta k/k} \right\rangle = \frac{1}{2\sqrt{2}\left|\sin 2\pi\nu_z\right|}\left[\sum_j \left(\beta_{j,z}k_j\right)^2\right]^{1/2} \tag{4.12}$$

Here $Z_{co} = X_{co}$ *or* Y_{co} (horizontal or vertical COD), Δz rms quadrupole magnet misalignment, k_j denotes the integrated strength of j^{th} quadrupole magnet and $\beta_{\max,z}$ is the maximum betatron function in the ring.

The strength of sextupole magnets also need to be changed in synchronism with quadrupole magnets. Amplitude dependent tune shift [18] as expressed by equation (4.13) is an important parameter influencing the dynamic aperture. It is also calculated at each step during the switch over process. This is calculated by considering the requirement of dynamic aperture for beam lifetime, which is roughly ten times of the beam sizes.

$$\left.\begin{aligned} \delta\nu_x &= C_{11}2J_x + C_{12}2J_y \\ \delta\nu_y &= C_{21}2J_x + C_{22}2J_y \end{aligned}\right] \tag{4.13}$$

Here $J_z = z^2 / 2\beta_z\cos^2\phi_z$ J_z and ϕ_z denote the action and corresponding angle variables in transverse planes. The four coefficients $C_{ij}\,(i,j=1,2)$ are expressed in the harmonic expansion

4.4 Implementation

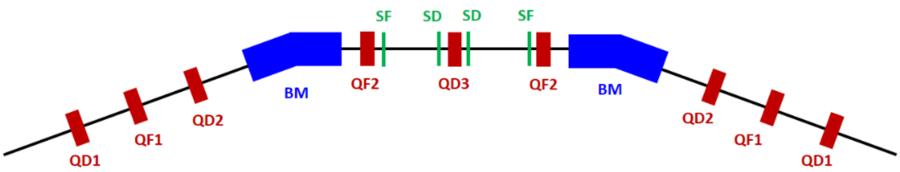

Figure 4. 8 Unit cell of the storage ring in Indus-2, in this unit cell quadrupole magnets and chromaticity correcting sextupole magnets arrangement are shown.

The schematic diagram of Inuds-2 unit cell discussed in subsection 1:6:3 of Chapter-1 is shown here in figure 4.8. In the lattice, five quadrupole magnet families are available for reducing the beam emittance, maintaining the tune point nearly unchanged. The optimization is carried out by using the modified computer code Burhani [56]. The emittance change over procedure is carried out under the following constraints

(1) Transverse betatron tune point remains constant or controlled as per requirement, so that partial beam loss, which may take place due to excitation of resonances can be avoided,

(2) Sensitivity of the beam optics to linear and nonlinear imperfections is as smooth as possible,

(3) The horizontal ($\beta_{ins,x}$) /vertical beta ($\beta_{ins,y}$) at the center of long insertion straight section are also adjusted to reduce the beam dynamical effect of insertion devices,

(4) Chromaticity correcting sextupoles strengths are adjusted as per natural chromaticities of the optics.

It was observed that in the insertion section among three quadrupole (QD1-QF1-QD2) only two quadrupoles should be used for optimization. Since, defocusing quadrupoles QD1 and QD2 are close to each other, as a result during optimization if both families (QD1 and QD2) are used, then their variations of strength are irregular. Thus only four quadrupole (QD1, QF1, QF2, QD3/ QD2, QF1, QF2, QD3) families are available for optimization.

4.4.1 Optimization and Implementation

Initially, the beam emittance reduction was tried at 2.0 GeV, since closed orbit distortions were significant at this energy thus the beam emittance could be reduced to half of the moderate optics [65]. Later on the ring was operated at 2.5 GeV with better correction of the orbit. At this energy i.e. at 2.5 GeV, in the moderate optics, measured horizontal tune, ν_x =9.20, which nearly matches with the theoretical tune. On the other hand, the measured vertical tune, ν_y =6.14, is less than the theoretical tune 6.20. The measured beta beat (β-asymmetry) in the horizontal and vertical planes is ~10-15 % [72]. COD is corrected with rms values of ~1.35 and ~0.7 mm in horizontal and vertical plane respectively.

In the moderate optics, dispersion function in the insertion section is ~ -0.4 m. In the low emittance optics, the dispersion function is nearly zero and $\beta_{y,\text{ins}}$ is ~1.4 m. Since the tune points are nearly the same in both the optics, there is a possibility of switching over the operation from the moderate optics to low emittance optics, resulting in a smaller beam emittance and smaller $\beta_{y,\text{ins}}$.

To proceed to the optics giving smaller $\beta_{y,\text{ins}}$ and reduction in beam emittance, various combinations of quadrupole magnets have been simulated. From these simulations, it is observed that a combination of three quadrupole magnets namely QD2 of the insertion section and QF2 and QD3 of achromat section are suitable for approaching the required optics. It is noticed that when $\beta_{y,ins}$ is reduced from 3.5 m to 1.4 m, the beam emittance is reduced from 135 nmard to 45 nmrad. $\beta_{x,ins}$ is kept as a free parameter because the reduction in its value requires a large change in horizontal tune. The strength of sextupole magnets are increased by a large amount during the switch over process due to increase in the natural chromaticity, change in dispersion function and change in de-coupling between beta functions at their locations. So during this process, the sextupole strengths are required to be varied synchronously in a well-defined manner.

When the tune point is kept constant during the switchover process, percentage change in amplification factors of COD and β-asymmetry from the moderate to low emittance optics are higher as compared to that when horizontal and vertical tunes are increased by 0.07 and 0.05 respectively. These results are shown in table 4.4. It is, thus, better to slowly change the tunes during reduction of the beam emittance.

During the above optimization process, percentage change in amplification factors of COD and β-asymmetry, quadrupole and sextupole magnet strengths with respect to the beam emittance are shown in the figure 4.9 and 4.10. A comparison between the moderate and low emittance optics in terms of main parameters is tabulated in table 4.5

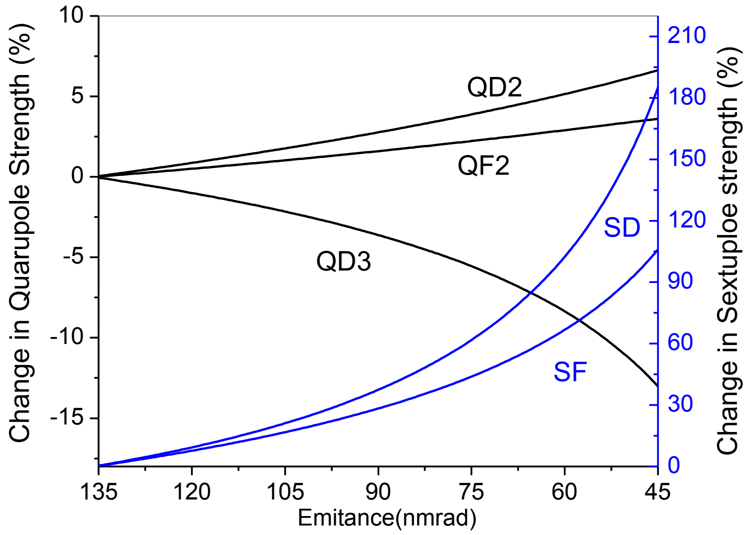

Figure 4. 9 Variation of % change in strength of quadrupole and sextupole magnets with beam emittance.

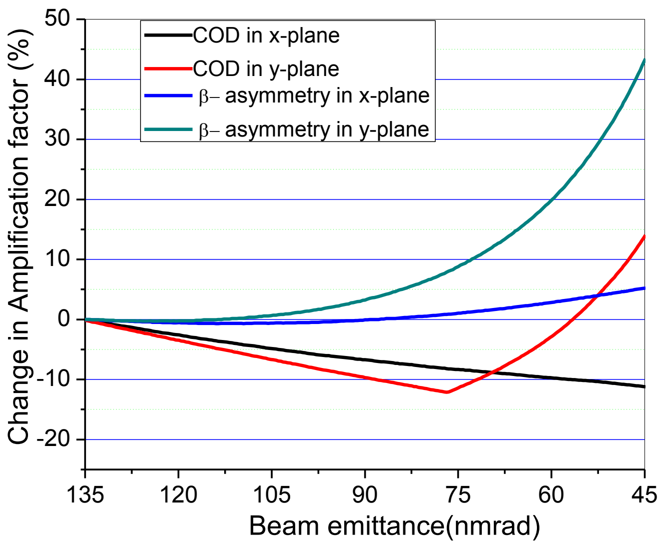

Figure 4. 10 Variation of % change in amplification factors of COD, β-asymmetry in horizontal and vertical plane with beam emittance.

Table 4. 4. Percentage change in amplification factor from the moderate to low emittance optics, when tune point are kept constant or changed

$(\Delta\nu_x, \Delta\nu_y)$ **during switch over**	$\left\langle \frac{x_{CO}}{\Delta x} \right\rangle$	$\left\langle \frac{y_{CO}}{\Delta y} \right\rangle$	$\left\langle \frac{\Delta\beta_x/\beta_x}{\Delta k/k} \right\rangle$	$\left\langle \frac{\Delta\beta_y/\beta_y}{\Delta k/k} \right\rangle$
(0.0, 0.0)	13%	61%	13%	79%
(0.07, 0.05)	-11%	12%	5%	43%

Table 4. 5: Comparison between the moderate and low emittance optics

Parameters	**Moderate Optics**	**Low Emittance Optics**
$\beta_{x,\max}$, $\beta_{y,\max}$, $\eta_{\max}$ (m)	19.8, 14.8, 1.05	22.7, 18.8, 0.65
$\beta_{x,ins}$ $\beta_{y,ins}$, η_{ins} (m)	11.1, 3.6, -0.41	13, 1.4, 0.07
ν_x, ν_y	(9.19, 6.2)	(9.26, 6.25)
ε@ 2.5 GeV (nmrad)	135	45
ξ_x, ξ_y (Natural chromaticities)	-20, -9	-22, -13
$\partial\nu_x$	$-64x^2 - 68y^2$	$-118x^2 - 321y^2$
$\partial\nu_y$	$-24x^2 + 31y^2$	$-41x^2 - 197y^2$
Momentum compaction	$7*10^{-03}$	$4*10^{-03}$

Here x and y denotes the initial amplitude of betatron oscillations in horizontal and vertical plane respectively.

The amplitude dependent tune shift due to sextupoles for ten times of the beam size (at the center of insertion section), during the switch over process are plotted in figure 4.11. As evident from figure 4.11, the amplitude dependent tune shift in the low emittance optics is much smaller as compared to the moderate optics primarily due to changes in the beam size with beam emittance.

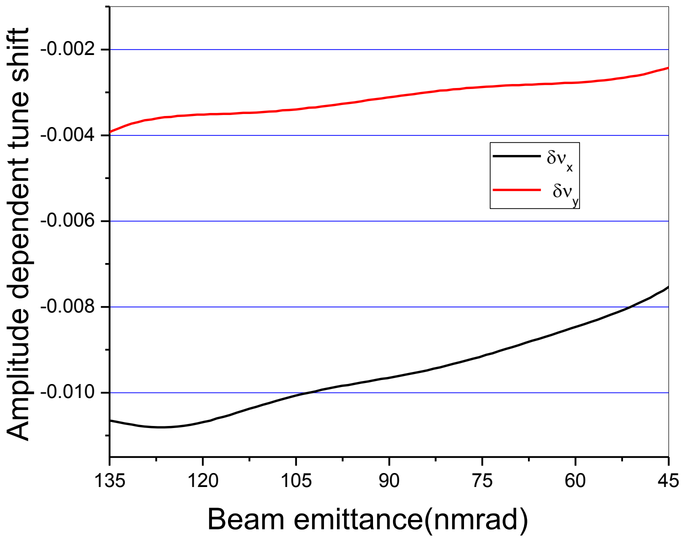

Figure 4. 11 Variation of horizontal and vertical amplitude dependent tune shift with beam emittance.

4.4.2 Implementation of switch over procedure

Nearly 110 mA beam current was initially stored at 2.5 GeV using the moderate optics. Here, two third of the ring (200/291 bunches) was filled with ~0.55 mA current/bunch to overcome ion trapping effects. Thereafter, the strength of quadrupole and sextupole magnets were changed synchronously as shown in figure 4.9. For this, a look up table was generated and applied to the software [76]. The time taken for the changeover is less than few minutes as shown in figure 4.12. The switch over procedure was temporarily halted at 66 nmrad to measure beam lifetime for about 2 minutes. It is evident from this figure that during the process of switch over there is no drastic change in the decay rate of the beam current and the beam lifetime seems to increase by ~20 %. The beam life time in Indus-2 is primarily governed by the vacuum [43, 77]. Our estimate indicates that due to the reduction of vertical dynamic aperture (as shown in figure 4.3), the beam lifetime should decrease nearly by 7 %. The anomaly between the observed and estimated values is attributed to the uncertainty in the available transverse apertures, DCCT noise and in the coupling constant between the two planes. However, this is still a matter of study.

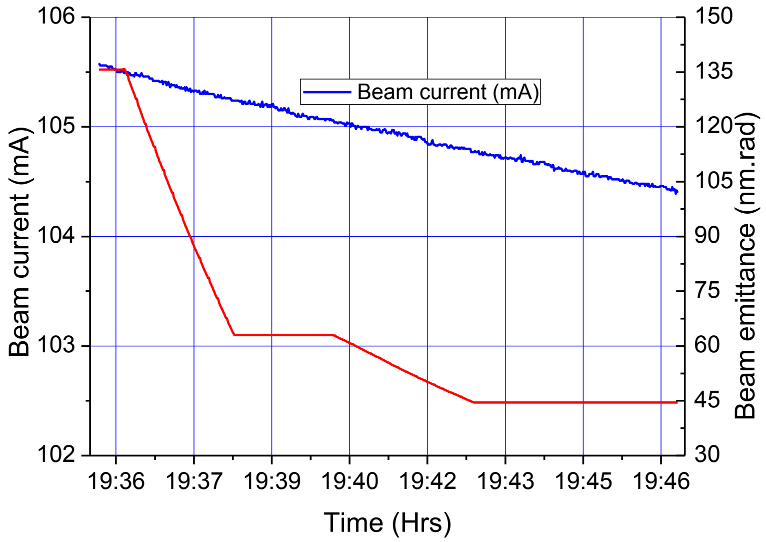

Figure 4. 12 The reduction of beam emittance (estimated), beam lifetime and beam current with time (during switch over)

During the switch over process, variation of rms COD calculated using BPI data with the estimated beam emittance is shown in figure 4.13. This figure shows that, in vertical plane, rms COD is increased whereas in horizontal plane, it is slightly decreased. These results are in agreement with the theoretical predictions. The variation of difference between the measured and theoretical tune in each plane is shown in figure 4.14. This figure shows that in both the planes, the difference varies smoothly up to ~100 nmrad, afterwards in vertical plane it starts to increase. This may be attributed due to the increase in β- asymmetry or increase in rms COD.

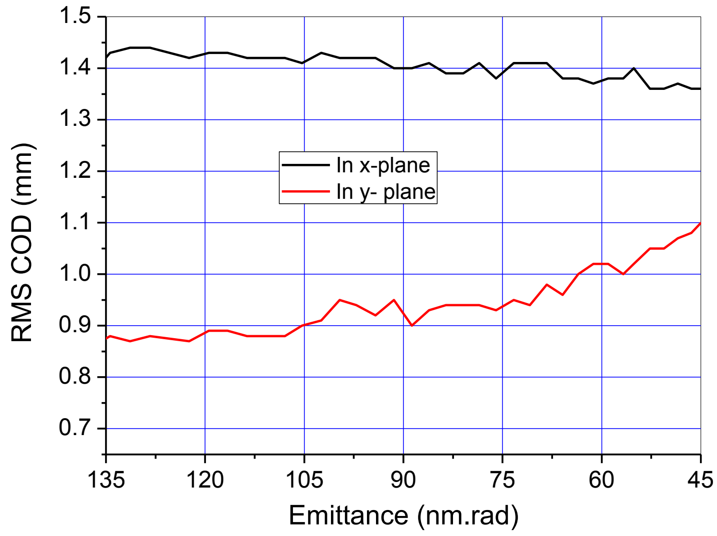

Figure 4. 13 Variation of measured horizontal and vertical rms COD with estimated beam emittance.

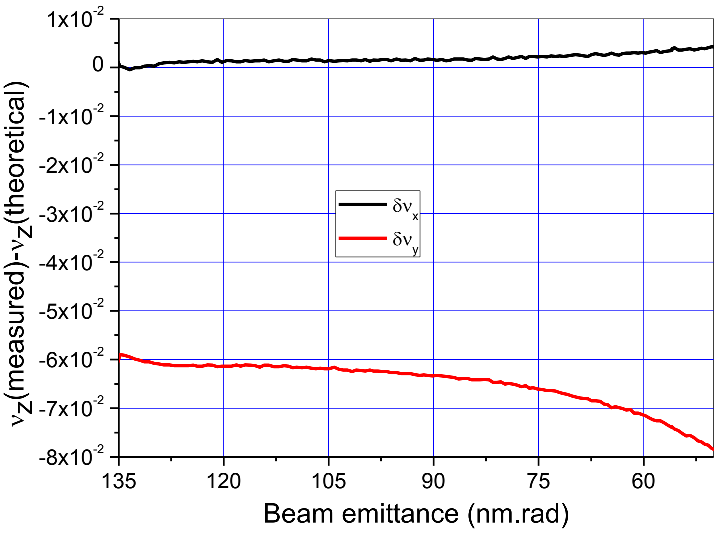

Figure 4. 14 Variation of difference in horizontal and vertical tune between measured and estimated with beam emittance.

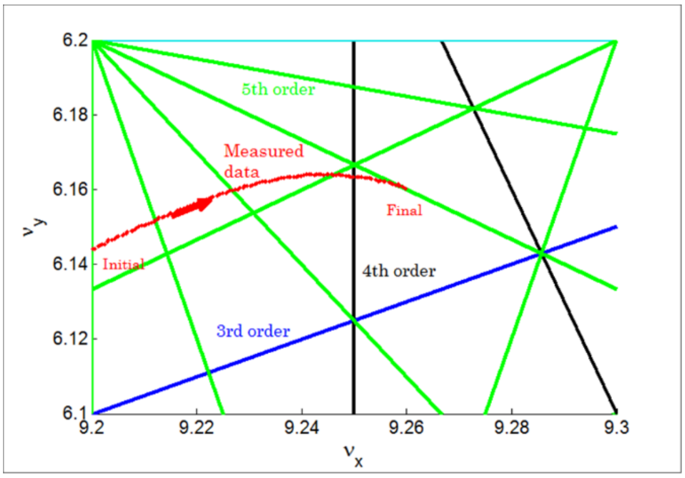

Figure 4. 15 Movement of tune point in resonance diagram during switch over

Movement of the tune points during switch over process is plotted in the resonance diagram (figure 4.15), which is plotted by considering single periodicity of the lattice and resonances up to 5th order. The tune diagram shows that during the switch over process, tune point crosses 4th and 5th order resonances. No additional loss of beam as shown in figure 4.15 is observed during this process.

There is a provision to measure beam size of the circulating beam using X-ray and pin hole camera. A beamline known as X-ray diagnostic beamline has been setup on a dipole magnet. The horizontal and vertical beam sizes measured at the x-ray diagnostic beamline installed at a bending magnet [78] whole setup with the moderate and low emittance optics are tabulated in table 4.6. There is a good agreement between the theoretical and measured values of beam size in horizontal plane. In the moderate optics, coupling between horizontal and vertical plane is 0.7 % [72]. In the low emittance optics, the measured vertical beam size is ~20 % higher than the beam size estimated taking the above value of coupling. This difference may be due to increase in β-asymmetry, uncertainty in the transverse coupling and effect of beam instabilities in vertical plane.

Table 4. 6. A comparison between measured and theoretical beam size at the moderate and low emittance optics

	Moderate Optics	**Low emittance Optics**
Theoretical beam size (rms)	*x*: 430 µm, *y*: 65 µm	*x*: 225 µm, *y*: 51 µm
Measured beam sizes (rms)	*x*: 440±10 µm, *y*: 68±3 µm	*x*:230±10 µm, *y*: 68±3 µm

4.5 Conclusions

The moderate optics is employed for the storage of the beam in Indus-2 at 550 MeV taking advantage of the negative dispersion function and using the negative DC orbit bump with the off-momentum beam (~0.9 %). At 2.5 GeV, the beam emittance is reduced by switching over the ring operation from the moderate to low emittance optics. Lagrangian multiplier method is used for changing the optics. Here an objective function employing a least square method with Lagrangian multiplier is evolved to calculate the strength of quadrupole and sextupole magnets required during transition from the moderate to low emittance optics. By using this method, the beam emittance in Indus-2 at 2.5 GeV is successfully reduced to one third without any additional loss of beam. The method followed here can be implemented for the synchrotron radiation sources, where it is difficult to store electron beam at the low emittance.

CHAPTER 5

EFFECT OF WAVELENGTH SHIFTER ON BEAM DYNAMICS

Introduction

In an electron storage ring, insertion devices are used to enhance the spectral flux/brightness of the synchrotron radiation sources. In which, a wavelength shifter is used to reduce the critical wavelength of the emitted synchrotron radiation spectrum. In Indus-1, a wavelength shifter with peak field of 3T is considered to shift its critical wavelength from 61 A^o to 31 A^o. The schematic location of wavelength shifter and lattice functions of the storage ring is shown in figure 5.1 and 5.2 respectively.

Insertion devices, adversely affcet the linear and nonlinear beam dynamics of electrons, as discussed in Chapter-1. They cause distortion of the betatron functions, linear and non-linear (amplitude dependent) tune shift. These effects are inversely proportional to square of the beam energy. In Indus-1, at 450 MeV these effects are significant. The beam lifetime is short in Indus-1 therefore the wavelength shifter should be kept on during beam injection. During beam injection, injected and stored beam oscillation amplitude remains large due to single kicker multi-turn injection scheme. In the presence of this device, oscillations of injected and stored beam will be further increased and dynamic aperture of the ring may also be reduced due to its linear and nonlinear forces. With these changes, it may be difficult to store the beam current. Thus it is essential to study effects of the device on the beam dynamics,

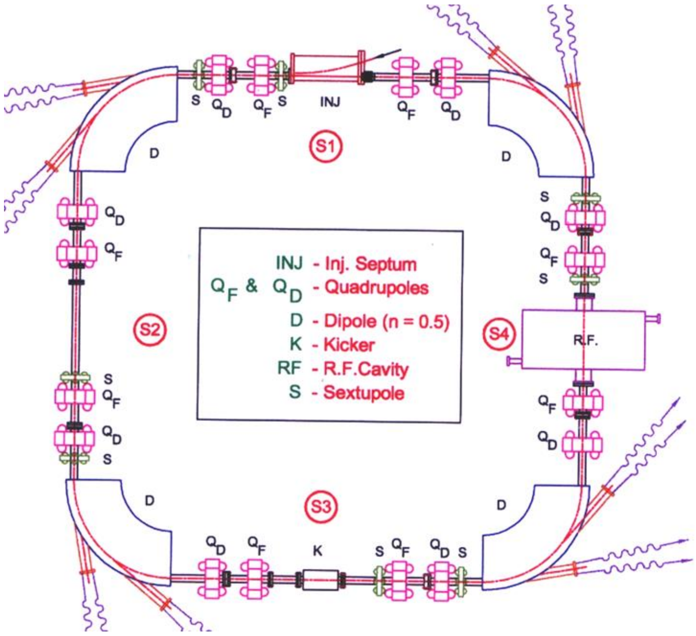

Figure 5. 1 A schematic layout of Indus-1 ring, S2 section is kept to accommodate a wavelength shifter.

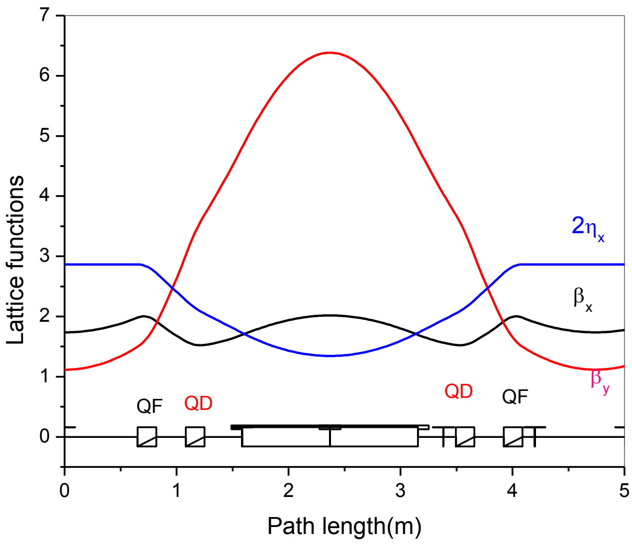

Figure 5. 2 The lattice functions of Indus-1 ring

The effect of insertion devices on beam dynamics was studied by L. Smith[39], in which equations of motion were obtained from the Hamiltonian with Halbach's magnetic field model (sinusoidal magnetic field) for sinusoidal electron beam trajectory. As discussed in Chapter-1, the equations of motion obtained from Hamiltonian, show that for this device quadrupole and octupole like component has to be taken into consideration, the oscillating magnetic fields such as sextupole, decapole etc are negligible, when these terms are averaged over a period.

The magnetic field of a wavelength shifter is generally complicated [79]. If transverse horizontal magnetic field component is present in wavelength shifter then orbit bump in it will give an additional linear and nonlinear component [80-82] in comparison to oscillating trajectory. However, it is helpful to express its magnetic field as a sinusoidal function. Here we will discuss the wavelength shifter, which has three magnet poles. In this structure, electron beam trajectory is a compensated bump. The Hamiltonian, studied by L. Smith is derived for the compensated electron beam trajectory transformation by assuming wavelength shifter magnetic field in terms of a sinusoidal function. Using this Hamiltonian various linear and nonlinear forces (components) are estimated, which are arising due to compensated orbit bump in the sextupole and decapole component.

5.1A Hamiltonian for wavelength shifter

5.1.1 Magnetic Field

The components of transverse magnetic field in a wavelength shifter can be obtained from Halbach's [40] expression, by taking a large number of harmonics into account. This model has been used for wigglers [83, 84] and is used here for the wavelength shifter to express the magnetic field as follows

$$
\begin{aligned}
\frac{B_{mx}}{B_m} &= \sum_{p,n} \frac{pk_{mx}}{k_{my,np}} c_{m,pn} \sinh(pk_{mx}x)\sinh(k_{my,np}y)\sin nk_{mz}(z-\phi_m) \\
\frac{B_{my}}{B_m} &= \sum_{p,n} c_{m,pn} \cosh(pk_{mx}x)\cosh(k_{my,np}y)\sin nk_{mz}(z-\phi_m) \\
\frac{B_{mz}}{B_m} &= -\sum_{p,n} \frac{k_m}{k_{my,np}} c_{m,pn} \cosh(pk_{mx}x)\sinh(k_{my,np}y)\cos nk_{mz}(z-\phi_m) \\
&-p^2k_{mx}^2 + n^2k_{mz}^2 = k_{my,np}^2
\end{aligned}
\tag{5.1}
$$

Here x, y, z are horizontal, vertical and beam directions respectively, $k_{mz} = \pi / d_m$, m denotes pole number 1,2 and 3, d_m is used to represent corresponding pole length, $C_{m,pn}$ indicates the amplitudes of p[th] and n[th] harmonic, B_m is the peak magnetic field, and ϕ_m is phase $(\phi_1 = 0, \phi_2 = d_1, \phi_3 = d_1 + d_2)$ for different pole. The side and main pole magnetic field and length are adjusted such that the first and second field integral of magnetic field along the beam axis is zero and higher order multipole components are small.

For an ideal wavelength shifter with infinitely wide pole k_{mx} tends to zero, and field is independent of *x*. However, if the field distribution is known with the width of poles $\pm L_x$,(L_x half of the pole width) we can define the horizontal periodicity as $k_x = 2\pi / L_x$. With a two dimensional Fourier transform, the coefficients $C_{m,pn}$ can be obtained from the field data in x-z plane. In general, a real field has an infinite number of modes and these are obtained from the coefficients of Fourier transform. If fitted field does not correspond exactly to the field map then small corrections [84] to the higher order coefficients can greatly improve the correspondence between the fitted field and the mapped field.

To simplify the Hamiltonian for the wavelength shifter, single harmonics (p=1, n=1) of magnetic field along with $B_1 = B_3 = -\frac{B_2 d_2}{2 d_1}$, $(d_1 = d_2 = d_3 = d)$, $C_{m,11} = 1$, $k_{1x} = k_{2x} = k_{3x}$ $k_{my,11}$ is defined as k_{my} and $k_{1z} = k_{2z} = k_{3z} = k$. Where B_2 is peak magnetic field and d is magnetic pole length. In real practice, these Hamiltonian has to be sum over all harmonics of magnetic field. In figure 5.3 magnetic field profile of a 3T wavelength shifter is shown.

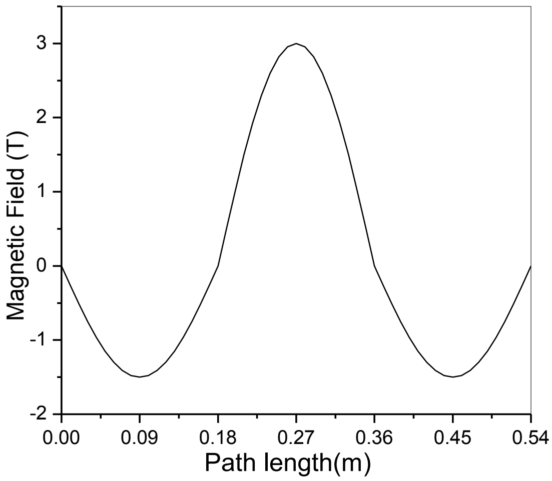

Figure 5. 3 Profile of magnetic field in a 3T wavelength shifter, which is generated by three dipole magnets.

5.1.2 Electron beam trajectory

The equation of motion for the first pole in the horizontal plane, with $\cosh k_x x \sim 1$ is:

$$\frac{d^2x}{ds^2} = \frac{B_2}{2B\rho} \sin k(s-\phi_1) \tag{5.2}$$

Here $B\rho = 3.333E(\mathrm{GeV})$

The first and second integral of equation (5. 2) is

$$\frac{dx}{ds} = -\frac{B_2}{2kB\rho}[\cos k(s-\phi_1)-1] \tag{5.3}$$

$$x = -\frac{B_2}{2kB\rho}\left[\frac{\sin k(s-\phi_1)}{k} - s\right] \tag{5.4}$$

Similarly for the second pole and third pole, we can write

$$x = \frac{B_2}{kB\rho}\left[\frac{\sin k(s-\phi_2)}{k} + \frac{d}{2}\right] \tag{5.5}$$

$$x = -\frac{B_2}{2kB\rho}\left[\frac{\sin k(s-\phi_3)}{k} + s - 3d\right] \tag{5.6}$$

In equations (5.4-5.6), on right hand side the second additional term is arising due to compensated electron bump trajectory.

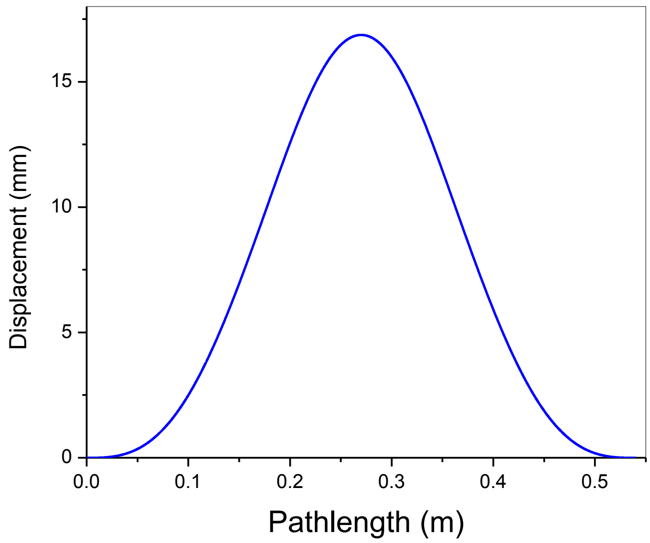

Figure 5. 4 Electron beam trajectory in the presence of the 3T wavelength shifter

The electron beam trajectory in the presence of magnetic field of 3T wavelength shifter (as shown in figure 5.3) is plotted in figure 5.4, with the help of equations (5.4), (5.5) and (5.6).

5.1.3 A Hamiltonian for Betatron motion

The Hamiltonian of the motion [39] of an electron under above magnetic field can be written as,

$$H = \frac{1}{2}[p_z^2 + (p_x - A_{mx}\cos k_m(z-\phi_m))^2 + (p_y - A_{my}\cos k_m(z-\phi_m))^2] \qquad (5.7)$$

Here: $A_{mx} = -\frac{B_m}{k_m B\rho}\cosh k_{mx}x\cosh k_{my}y, \quad A_{my} = \frac{B_m k_{mx}}{k_{my}}\frac{\sinh k_{mx}x\sinh k_{my}y}{k_m B\rho}$

A canonical transformation is required to change variables from (x, y, z) to (x_β, y_β, s) where s is distance along the equilibrium orbit, x_β is a displacement in the (x, z) plane perpendicular to the equilibrium orbit and $y_\beta = y$ is the vertical displacement from the equilibrium orbit. Transformation between variables for first pole, second pole and third pole can be written as

For the first pole

$$x = x_e + z_e^{/} x_\beta = x_e - \frac{B_2}{2kB\rho}\left[\frac{\sin k(s-\phi_1)}{k} - s\right] \sim x_e - a_1 \tag{5.8}$$

Here $a_1 = \frac{B_2}{2kB\rho}\left[\frac{\sin k(s-\phi_1)}{k} - s\right]$

$$z = s - x_e^{'} x_\beta = s - x_e^{/} \frac{B_2}{2kB\rho}\left[\frac{\sin k(s-\phi_1)}{k} - s\right] \sim s \tag{5.9}$$

For the second pole

$$x \sim x_e + \frac{B_2}{kB\rho}\left[\frac{\sin k(s-\phi_2)}{k} + \frac{d}{2}\right] \sim x_e - a_2 \tag{5.10}$$

Here $a_2 = -\frac{B_2}{kB\rho}\left[\frac{\sin k(s-\phi_2)}{k} + \frac{d}{2}\right]$

$$z = s - \frac{B_2}{kB\rho}\left[\frac{\sin k(s-\phi_2)}{k} + \frac{d}{2}\right] x_e^{'} \sim s \tag{5.11}$$

For the third pole

$$x \sim x_e - \frac{B_2}{2kB\rho}\left[\frac{\sin k(s-\phi_3)}{k} + s - 3d\right] \sim x_e - a_3 \tag{5.12}$$

Here $a_3 = \frac{B_2}{2kB\rho}\left[\frac{\sin k(s-\phi_3)}{k} + s - 3d\right]$

$$z = z_e - \frac{B_2}{2kB\rho}\left[\frac{\sin k(s-\phi_3)}{k} + s - 3.d\right] x_e^{'} \sim s \tag{5.13}$$

And the canonical momentum transformation can be written as

$$p_x = z_e^{'} p_{x_\beta} + \frac{x_e^{/}}{(1+\Omega x_\beta)} p_s \tag{5.14}$$

$$p_y = p_{y_\beta} \tag{5.15}$$

$$p_z = \frac{z_e^{/}}{(1+\Omega x_\beta)} p_s - x_e^{/} p_{x_\beta} \tag{5.16}$$

Here x_e, x_e', z_e, z_e' are regarded as a function of 's' and $\Omega = \frac{B_m}{B\rho}\sin k(s-\phi_m)$. For simplicity drop the subscript e and β .

In equation (5.7), after canonical transformation and hyperbolic functions are expanded up to fourth order in x and y. The equation of motions are governed by

$$x' = \frac{\partial H}{\partial p_x} \tag{5.17}$$

$$p_x' = -\frac{\partial H}{\partial x} \tag{5.18}$$

$$y' = \frac{\partial H}{\partial p_y} \tag{5.19}$$

$$p_y' = -\frac{\partial H}{\partial y} \tag{5.20}$$

In presence of wavelength shifter equation of motion is given by

$$\begin{aligned} x'' = &-\frac{B_m^2 k_{mx}^2}{2k_m{}^2 B^2 \rho^2}\left[(x-a_m)+\frac{1}{6}k_{mx}^2(x-a_m)^3+\frac{1}{2}k_{my}^2(x-a_m)y^2\right] \\ &+\frac{B_m \cos k_m(s-\phi_m)}{k_m B\rho}yy' k_{mx}^2\left[a_m+\frac{k_{my}^2 y^2}{6}+\frac{k_{mx}^2(x-a_m)^2}{2}\right] \\ &+\frac{B_m \sin k_m(s-\phi_m)}{B\rho}\left[\frac{k_{my}^2 y^2}{2}+\frac{k_{my}^2 y^4}{24}+\frac{k_{mx}^2(x-a_m)^2}{2}+\frac{k_{mx}^2 k_{my}^2(x-a_m)^2 y^2}{4}+\frac{k_{xm}^4(x-a_m)^4}{24}\right] \end{aligned} \tag{5.21}$$

$$\begin{aligned} y'' = &-\frac{B_m^2 k_{my}^2}{2k_m^2 B^2 \rho^2}\left[y+\frac{1}{2}k_{mx}^2(x-a_m)^2 y+\frac{1}{6}k_{my}^2 y^3\right] \\ &-\frac{B_m \cos k_m(s-\phi_m)k_{my}^2 yx'}{k_m B\rho}\left[1+\frac{1}{2}k_{my}^2 y+\frac{1}{2}k_{mx}^2(x-a_m)^2\right] \\ &-\frac{B_m \sin k_m(s-\phi_m)}{B\rho}k_{mx}^2 y\left[(x-a_m)+\frac{1}{6}k_{my}^2(x-a_m)y^2+\frac{1}{6}k_{mx}^4(x-a_m)^3 y\right] \end{aligned} \tag{5.22}$$

In the wavelength shifter, trajectory of the electron beam is a compensated bump thus oscillating sink_m(s-c_m) and cosk_m(s-c_m) terms are retained in equation (5.21) and (5.22), where these terms are neglected in the case of wigglers and undulators (discussed in Chapter-1). These terms are averaged over the length of wavelength shifter, and will give quadrupole, sextupole and octupole magnet like terms, which are discussed below.

i) Quadrupole magnet components:

In the horizontal plane, for a side pole, quadrupole magnet component due to edge focussing and orbit offset into the sextupole magnet component will cancel each other, thus only main pole has to be considered. In vertical plane, edge focusing of the side and main pole both has to be taken into account.

$$x'' = -\frac{2B_2^2 k_{2x}^2}{(B\rho)^2 k_2^2} x \tag{5.23}$$

$$y'' = -\frac{3B_2^2}{4(B\rho)^2} y - \frac{2B_2^2 k_{2x}^2}{(B\rho)^2 k_2^2} y \tag{5.24}$$

These components will distort the beta functions and produce the linear tune-shifts. The distortions of the beta functions around the ring will cause a change in beam sizes and that can affect the users, reduce beam lifetime and break the symmetry of chromaticity correcting sextupoles, as a result additional resonances will be excited. The linear tune-shifts can derive the machine operation close to a resonance.

ii) Sextupole magnet components:

These terms are determined by averaging oscillating terms of the Hamiltonian. In addition, orbit offset in the octupole magnet will also generate sextupole like magnet components, their contributions remain small so these terms are not taken into account.

$$x'' = \frac{B_2(k_{1x}^2 - k_{2x}^2)}{k_m B\rho}(x^2 - y^2) \tag{5.25}$$

$$y'' = -\frac{2B_2(k_{1x}^2 - k_{2x}^2)}{k_m B\rho} xy \tag{5.26}$$

If coupling coefficients for side and main pole are equal ($k_{1x} = k_{2x} = k_{3x}$), then sextupole magnet components will be vanished, on the other hand it has to be taken into account. These components will generate amplitude dependent tune shift, which may lead to reduction in the dynamic aperture.

iii) Octupole magnet like components:

These terms are determined by the non-oscillating and oscillating terms of the equations (5.21) and (5.22). In oscillating terms, these arise due to the orbit offset in the decapole magnet like component. In vertical plane contributions of these terms are small, thus they are not considered. However, in horizontal plane these terms are considered. In the device, strength of octupole magnet like components are higher than to the components of insertion device [39].

$$x'' = -\frac{B^2{}_2 k_{1x}^2}{4{k_1}^2 B^2 \rho^2}\left[\frac{1}{3}k_{1x}^2 x^3 + k_{1y}^2 xy^2 - \frac{1}{2}k_{1x}^2 xy^2\right] - \frac{B_2^2}{4k_1^2 (B\rho)^2} k_{1x}^2 k_{1y}^2 xy^2 \qquad (5.27)$$

$$- \frac{B^2{}_2 k_{2x}^2}{2{k_2}^2 B^2 \rho^2}\left[\frac{1}{3}k_{2x}^2 x^3 + k_{2y}^2 xy^2 - \frac{1}{2}k_{2x}^2 xy^2\right] + \frac{2}{3}\frac{B_2^2}{k_2^2 (B\rho)^2} k_{2x}^2 k_{2y}^2 xy^2$$

$$y'' = -\frac{B_2^2 k_{1y}^2}{4k_1^2 B^2 \rho^2}\left[k_{1x}^2 (yx^2) + \frac{1}{6}k_{1y}^2 y^3\right] - \frac{B_2^2 k_{2y}^2}{2k_2^2 B^2 \rho^2}\left[k_{2x}^2 (yx^2) + \frac{1}{6}k_{2y}^2 y^3\right] \qquad (5.28)$$

The octupole magnet like components will generate non-linear effects and will produce the amplitude-dependent tune-shifts and excite its own intrinsic resonances that can lead to degradation of dynamic aperture.

5.2 Studies for Indus-1

The parameters of the wavelength shifter taken here are B_2 (peak magnetic field) = 3T, coupling coefficients $(k_{mx}/k_{my})^2 = -0.03$, number of poles ($m$) =3, total magnetic length =0.54 m, $k_{1x} = k_{2x} = k_{3x} = k_x$ and $k_1 = k_2 = k_2 = k$. A detailed study has been carried out for Indus-1 for present operating tune point $\nu_x = 1.69$ and. $\nu_y = 1.28$. The wavelength shifter is divided into a number of hard edge rectangular magnets having field index to model the horizontal and vertical focusing caused by the wavelength shifter as shown in equation (5.23) and (5.24). For optics and tracking calculations, a wavelength shifter model [8] was used in which each wavelength shifter pole was simulated by a constant field dipole with gap between the poles. The dipole pole field, $B_p=B_o\pi/4$ and pole length $L_p=4\lambda/\pi^2$ were set to produce the same bending and focussing effect as the actual wavelength shifter. To estimate the edge focussing due to finite k_x, dipole field index into the central dipole is modelled by defining a field index $n = -\frac{\rho}{B}\left(\frac{dB_y}{dx}\right) = -2\frac{B_2^2}{(B\rho)^2}\left(\frac{k_{2x}^2}{k_2^2}\right)$. The model yields the linear tune shifts and β-asymmetry in the wavelength shifter. These parameters are presented in table 5.1. The change due to nonlinear component (octupole magnet like) is calculated using a thin lens transport matrix. The kick is derived by integrating the equation of motion (equation 5.27 and 5.28) over the length of the device.

Table 5. 1: wavelength shifter model for computer simulations

Component	Length (m)	Bending radius(m)	Focusing strength	Field index(n)
Side dipole	0.146	1.2732394	-0.6168 m^{-2}	0.0
Drift	0.034			
Central pole	0.146	0.6366197	-2.4674 m^{-2}	0.247
Drift	0.034			
Side dipole	0.146	1.2732394	-0.6168 m^{-2}	0.0

5.2.1 Linear effect compensation

If wavelength shifter have both k_{mx} and k_{my} component then in horizontal and vertical planes, β-asymmetry as well as linear tune shift will take place. It is required to correct both tunes and β-asymmetry for smooth operation. To locally compensate these effects, it is required that the strength of quadrupole magnets should be varied symmetrically to maintain the symmetry of the lattice. For this, four quadrupole magnet pairs are required. In this configuration, only two pairs of quadrupole magnets are available. With these two variables, four parameters cannot be corrected. The various options of compensation such as local beta/global tunes [85-86], global beta and tunes using different combinations of quadrupole magnets were studied using computer program Burhani [56], it is found that it is not possible to compensate both simultaneously.

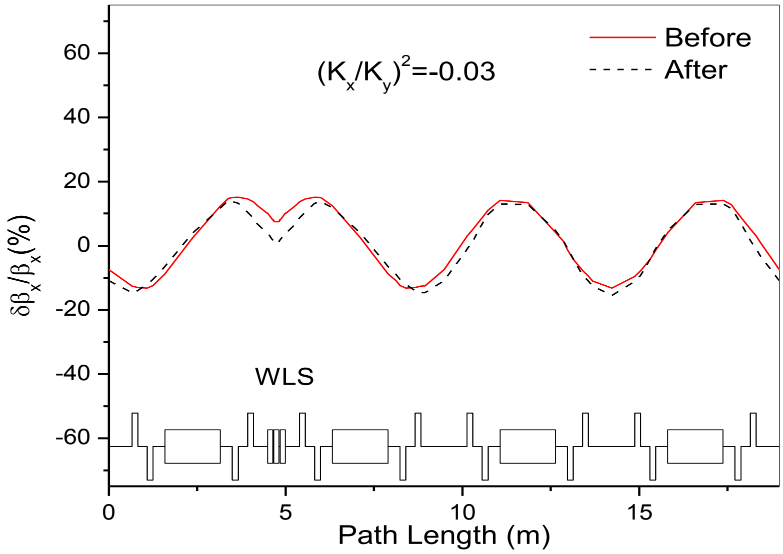

Figure 5. 5 In horizontal plane, β-asymmetry after global tune correction

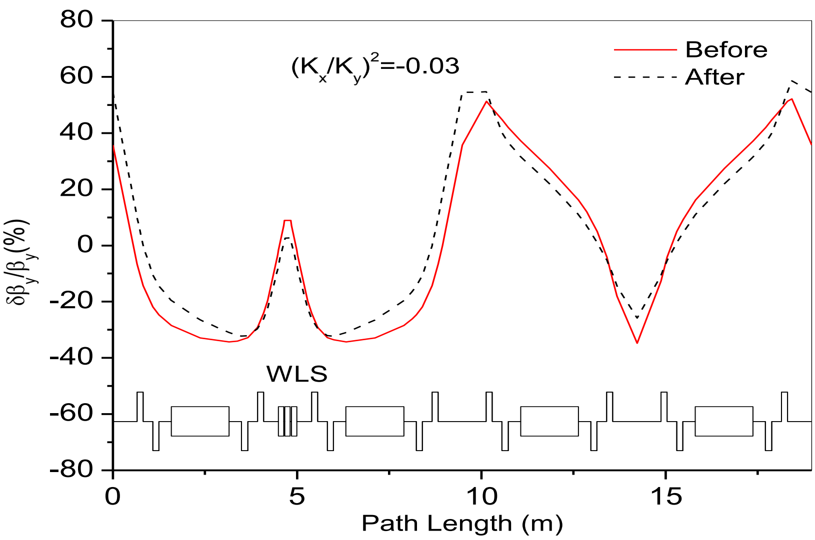

Figure 5. 6 In vertical plane, β-asymmetry after global tune correction

The global tunes correction does not offer good solution as it leaves the large β-asymmetry (figure 5.5 and 5.6). The β-asymmetry in both planes are compensated by α-matching (except in region of the device), using neighbouring focussing (QF) and defocusing (QD) quadrupole magnet, which are adjacent to the device. The α-matching changes the linear tunes by a large amount. Therefore, the scheme, in which first α-matching is done by using neighbouring QF and QD families and then linear tunes are compensated globally with remaining families of QF and QD, was studied (figure 5.7 and 5.8). The scheme offers a promising solution in which beta function is well corrected in the dipole magnet, where synchrotron radiation is taped. The detail results are summarized in table-5.2

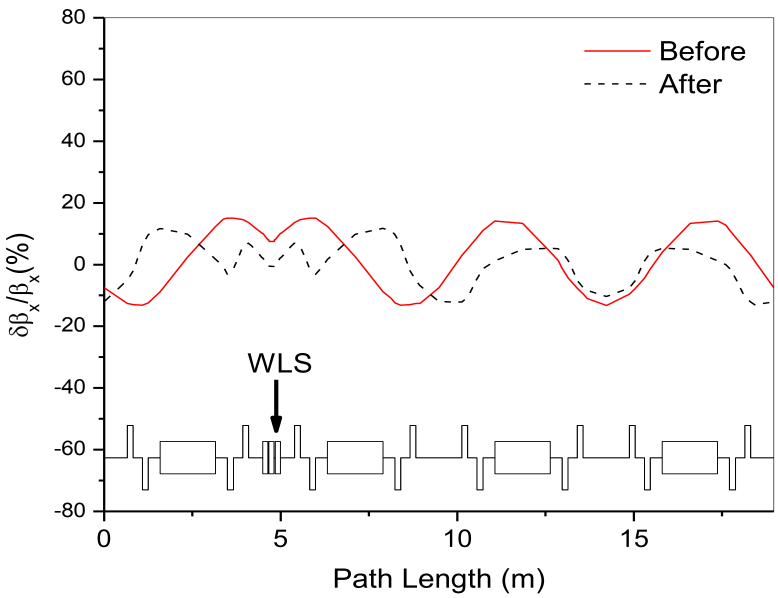

Figure 5. 7: In horizontal plane, β-asymmetry after α-matching and tune correction

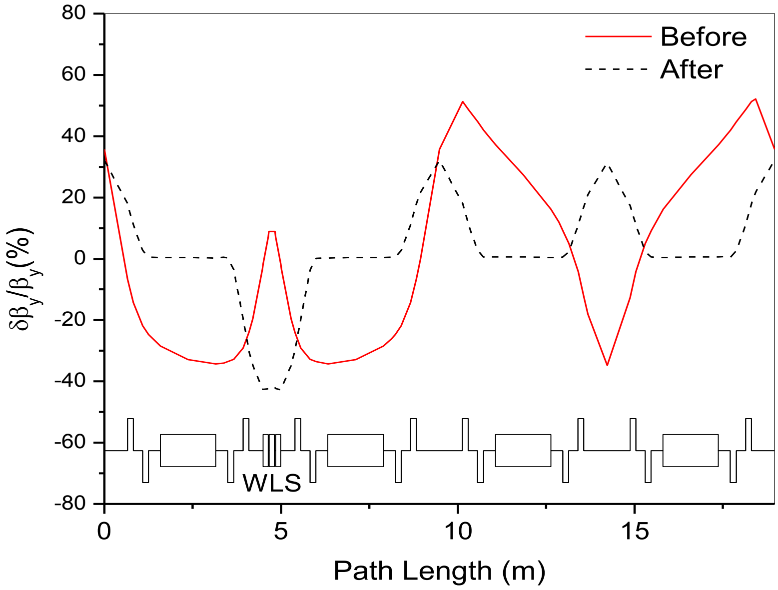

Figure 5. 8: In vertical plane, β -asymmetry after α-matching and tune correction

Table 5. 2: linear distortions caused by the magnetic profile of wavelength shifter

Correction	$\Delta\nu_x$	$\Delta\nu_y$	$(\delta\beta/\beta)_{xrms}$	$(\delta\beta/\beta)_{yrms}$
Before	-0.02	0.06	10.39	27.47
Only Tune	0.0	0.0	9.36	27.47
α Matching and tune	0.0	0.0	6.78	23.87

5.2.2 Dynamic aperture

In the presence of the wavelength shifter symmetry of the lattice will be broken as a result various resonances will be excited. In the figure resonance diagram is plotted by considering periodicity of the lattice equal to four (figure 5.9) and one (figure 5.10).

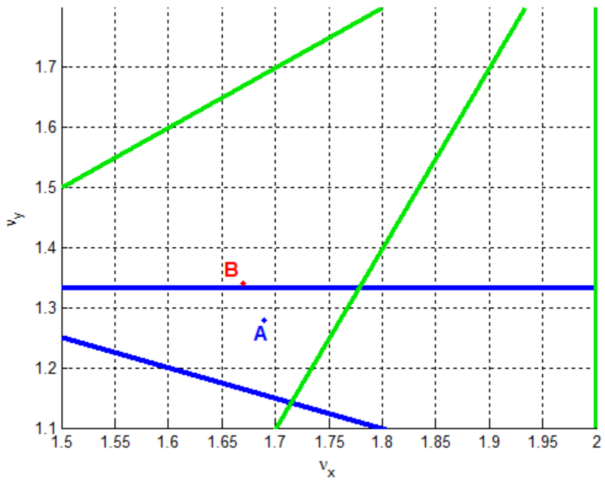

Figure 5. 9 Tune diagram up-to 4th order considering four periodicity of the ring. Blue and green colour indicates 3rd and 4th order resonances respectively. The points A and B indicate tune point for a bare lattice and in the presence of wavelength shifter.

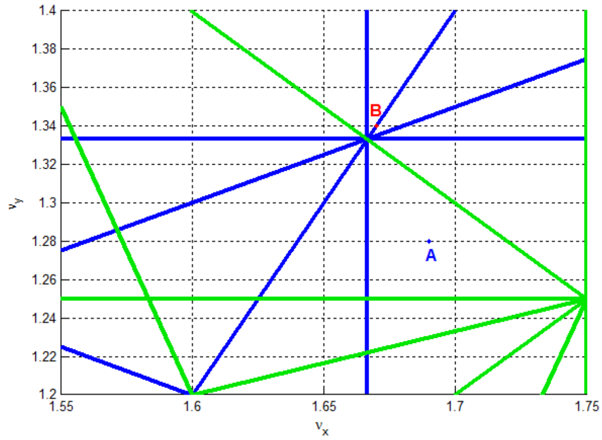

Figure 5. 10: Tune diagram considering single periodicity of the ring. Blue and green color indicates 3rd and 4th order resonances respectively. The points A and B indicate tune point for a bare lattice and in the presence of wavelength shifter.

The dynamic aperture simulations are plotted for on-momentum electrons, after 100,000 turns in the following cases

a) For bare lattice

b) In presence of wavelength shifter

1. Without any correction
2. After tune correction with octupole magnet like component of wavelength shifter
3. After both corrections (α-matching and tune) without octupole magnet like component of wavelength shifter and
4. After both corrections (α-matching and tune) with octupole magnet like component of wavelength shifter.

The simulated result shows that without any linear correction, the dynamic aperture reduces nearly 50%, see figure 5.11, since horizontal tune (1.67) is shifted near to third order resonance see figure 5.10. The tune point (1.67, 1.34) is also near to fourth order resonances.

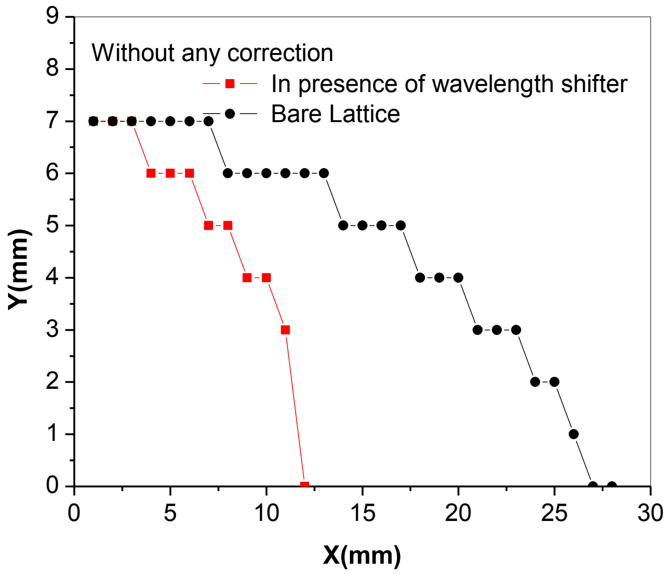

Figure 5. 11 Dynamic Aperture for bare lattice and in presence of wavelength shifter (without any correction)

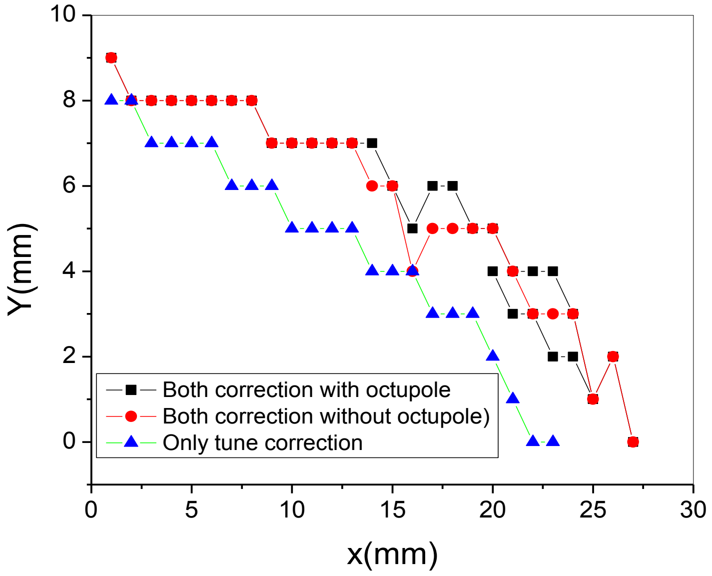

Figure 5. 12 Dynamic Aperture after following correction 1) after tune correction and 2) α-matching and tune correction

After global tune correction, the dynamic aperture improves significantly and after the both corrections (α-matching and tune), the dynamic aperture is further increased. In horizontal plane, it is increased from 21 mm to 26 mm, see figure 5.12. Similarly in the vertical plane, the dynamic aperture is improved, for example at the following coordinates $(x, x', y, y') = (20, 0, 4, 0)$, in the case of global tune correction fourth order island formation takes place (as shown in figure 5.13) and after the both corrections island formation does not take place (as shown in figure 5.14).

The dynamic aperture is also simulated with and without octupole like magnet component of the wavelength shifter in the case of both (α-matching and tune) corrections. The results show that reduction in dynamic aperture due to octupole like magnet component of the device is quite small, see figure 5.12.

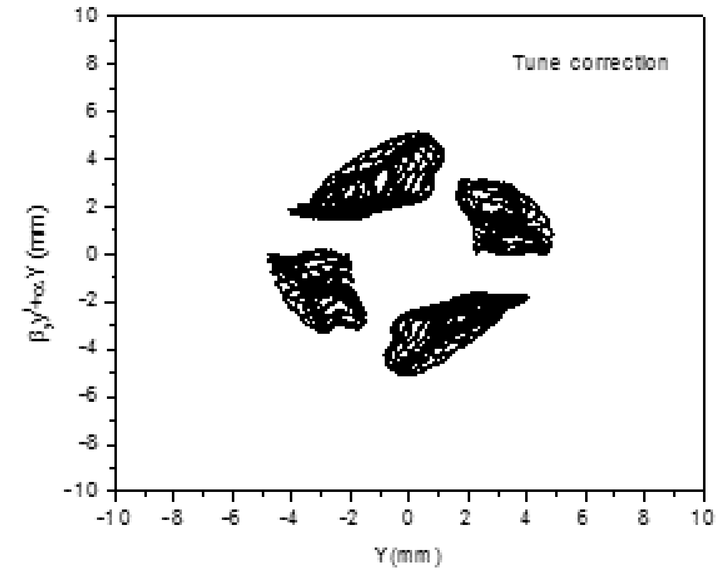

Figure 5. 13: In vertical plane, phase space plot after tune correction

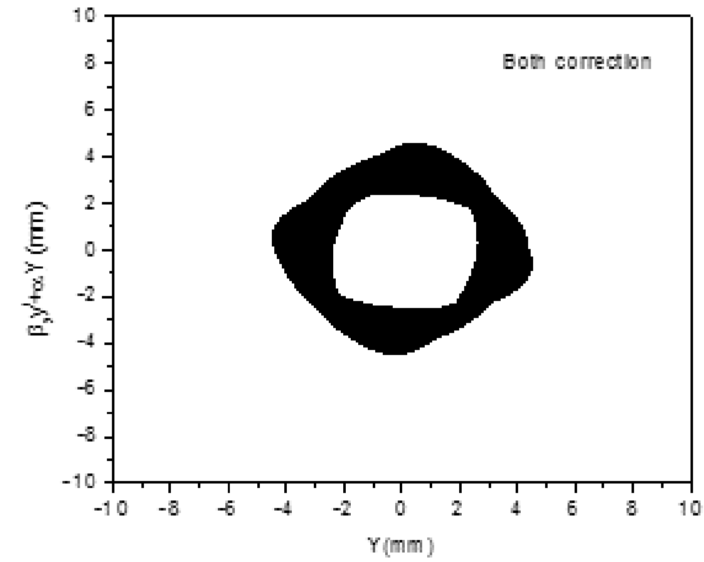

Figure 5. 14: In vertical plane, phase space plot after both corrections (α-matching and tune).

5.2.3 Injection simulation

In Indus–1, a single kicker multi-turn injection scheme [49] is adopted in the horizontal plane. In this scheme, the injection septum and injection kicker magnet are located at symmetry points of the ring diametrically opposite to each other, so that maximum of orbit bump (x_b) occurs at the center of the straight section, in which the injection septum magnet is placed. Two bunches (separated by 30ns) extracted from the synchrotron are injected into Indus-1. The locations of the injected bunches on the injection kicker are shown in the figure 5.15. The injection kicker magnetic field reaches to peak value in 1.2 μS following a sinusoidal shape and it decays exponentially with fall time of 150 nS. The first and second bunch is on the top and falling edge of injection kicker respectively. The first bunch experiences higher bump in comparison to the second bunch. Thus for the second bunch, injected beam oscillations and residual oscillations after beam injection will remain higher in comparison to the first bunch.

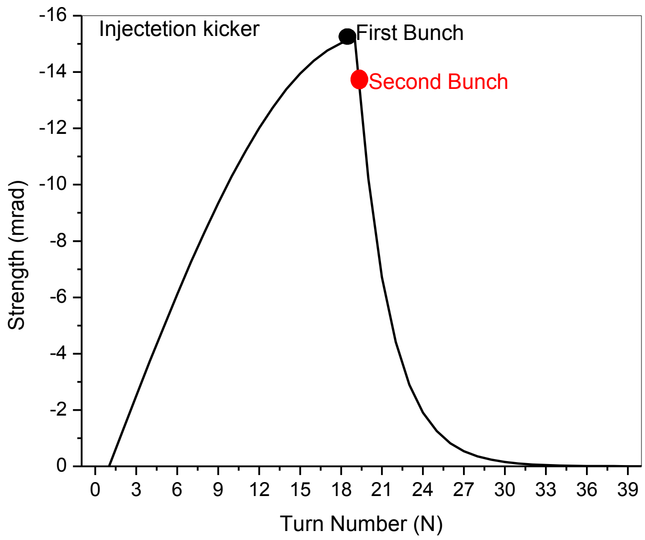

Figure 5. 15: Spatial distribution of first and second bunch of injected beam with respect to the strength of injection kicker magnet.

Now, we will derive a relation to estimate the strength of the injection kicker. For a periodic lattice, the transfer matrix [8-13] from the injection kicker magnet to injection septum can be written as

$$\begin{pmatrix} x_b \\ x_{b1} \end{pmatrix} = \begin{pmatrix} a_{11} & a_{12} \\ a_{21} & a_{22} \end{pmatrix} \begin{pmatrix} x_{ki} \\ x_{ki1} \end{pmatrix} \tag{5.29}$$

With $\Delta\mu = \mu_{s,x} - \mu_{ki,x}$, $a_{11} = \sqrt{\frac{\beta_{s,x}}{\beta_{ki,x}}}(\cos\Delta\mu_x + \alpha_{ki,x}\sin\Delta\mu_x)$, $a_{12} = \sqrt{\beta_{s,x}\beta_{ki,x}}\sin\Delta\mu_x$

$$a_{21} = -\sqrt{\frac{1}{\beta_{s,x}\beta_{ki,x}}}\left\{(\alpha_{s,x} - \alpha_{ki,x})\cos\Delta\mu_x + (1+\alpha_{s,x}\alpha_{ki,x})\sin\Delta\mu_x\right\} \text{ and } a_{22} = \sqrt{\frac{\beta_{s,x}}{\beta_{ki,x}}}(\cos\Delta\mu_x + \alpha_{ki,x}\sin\Delta\mu_x)$$

After one turn, transfer matrix at the injection kicker magnet location can be written as

$$\begin{pmatrix} x_k^o \\ x_{k1}^o \end{pmatrix} = \begin{pmatrix} b_{11} & b_{12} \\ b_{21} & b_{22} \end{pmatrix}\begin{pmatrix} x_k^i \\ x_{k1}^i \end{pmatrix} \tag{5.30}$$

$b_{11} = \cos 2\pi\nu_x + \alpha_{ki}\sin 2\pi\nu_x$, $b_{12} = \beta_{ki,x}\sin 2\pi\nu_x$, $b_{21} = -\gamma_{ki,x}\sin 2\pi\nu_x$ and

$b_{22} = \cos 2\pi\nu_x + \alpha_{ki,x}\sin 2\pi\nu_x$

To satisfy closed orbit condition, the transfer matrix has to satisfy following condition

$$\begin{pmatrix} x_k^i \\ -x_{k1}^i \end{pmatrix} = \begin{pmatrix} b_{11} & b_{12} \\ b_{21} & b_{22} \end{pmatrix}\begin{pmatrix} x_k^i \\ x_{k1}^i \end{pmatrix} \tag{5.31}$$

By solving the above expression, the kicker strength can be written as

$$\text{Strength} = \frac{\mathrm{x_b}}{\{\mathrm{b_{12}a_{11}} + a_{12}(1-b_{11})\}}\left[(1-\mathrm{b_{11}}) - \mathrm{b_{21}b_{12}} + b_{22}(1-b_{11})\right] \tag{5.32}$$

Now we will study the effect of wavelength shifter on the injection dynamics. In the presence of this device (having finite k_x), at the injection septum magnet, symmetry of beta function will be broken and orbit bump, which is generated by the injection kicker magnets will be distorted.

At the injection septum magnet placed at 21 mm from the design orbit maximum oscillation amplitude of injected and stored bunches are tabulated in table 5.3 and 5.4 for the bare lattice and after both α-matching and globally tune correction. For these calculations, 16 mm orbit bump is produced the kicker magnet as shown in figure 5.16.

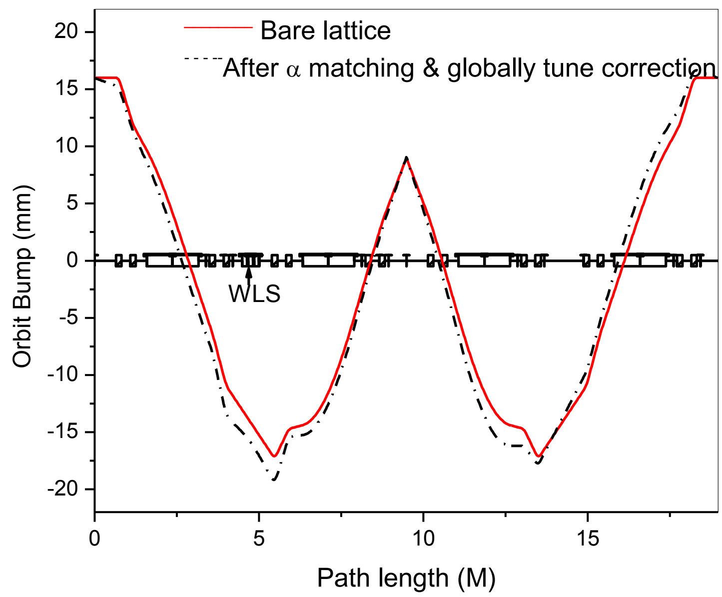

Figure 5. 16: The bumped closed orbit for bare lattice and after both correction (α-matching and tune correction)

Table 5. 3: For bare lattice amplitude of beam oscillation during beam injection

	Injected Beam Oscillation (mm)			**Stored Beam Oscillation (mm)**		
Bunch	Max at septum	Max. and Min. at other places	Residual oscillation	Max at septum	Max. and Min. at other place	Residual oscillation
First	15.0	18.1-29.1	±12.6	16.60	16.7- 17.1	±4.8
Second	17.4	19.7 -29.1	±16.2	16.14	16.2-16.7	±6.5

Table 5. 4: During beam injection, amplitude of beam oscillation after the both corrections (α- matching & tune)

	Injected Beam Oscillation (mm)			**Stored Beam Oscillation (mm)**		
Bunch	Max at septum	Max. and Min. at other place	Residual oscillation	Max at septum	Max. and Min. at other place	Residual oscillation
First	15.7	18.7-31.3	±13.3	16.47	17.2 -18.0	±5.2
Second	17.9	20.3-31.3	±17.7	16.05	16.6-17.4	±7.1

After both correction (α-Matching and global tune correction), maximum and minimum injected beam oscillation over the ring (20.3, -31.3) is slightly higher in comparison to the bare lattice (19.7, -29.1). The above result indicates that in the horizontal plane dynamic aperture requirement is 20 mm for beam injection. In vertical plane, dynamic aperture requirement is 4 mm, which is mainly determined by the finite orbit distortion and from injected beam having finite beam size and non-zero initial coordinates (displacement and angle) from the design orbit. It is discussed in sub section 5.2.3 that the above mentioned dynamic aperture is available after both corrections (α-matching and tune correction). Thus it is possible to operate wavelength shifter in Indus-1 during bema injection after both corrections.

The dynamic aperture requirement can be further reduced with the help of off-momentum injection. In which, by injecting positive off-momentum electrons (+0.1%), injected beam oscillations can be reduced (18.8, -28.3). For these electrons, oscillation amplitude of injected bunches as well as stored bunches are shown in the figure 5.17 and 5.18 and these oscillations are tabulated in table-5.5.

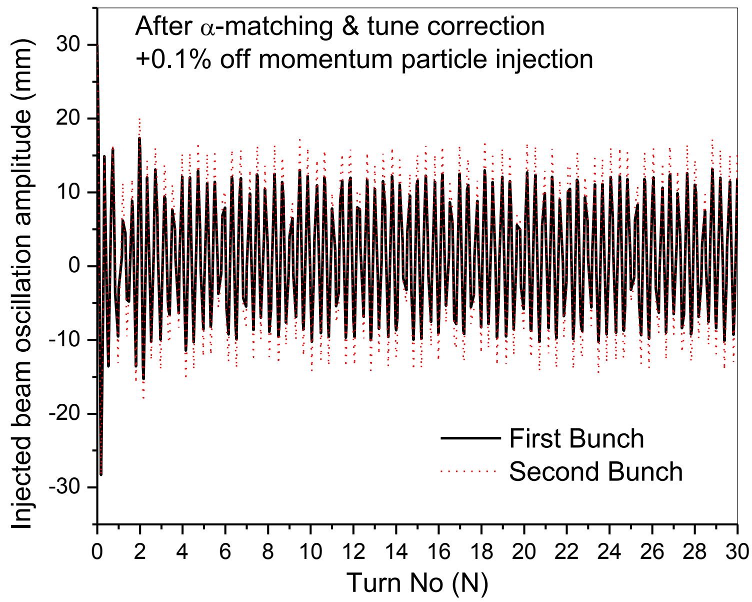

Figure 5. 17: After the both corrections (α-matching and tune correction), injected Beam oscillation during beam injection with +0.1% off-momentum beam injection.

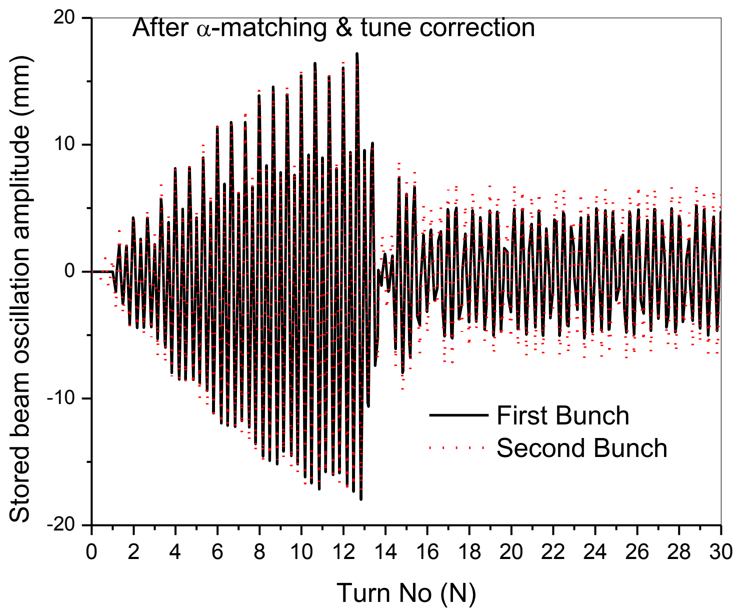

Figure 5. 18: After the both corrections (α-matching and tune correction), stored beam oscillation during beam injection.

Table 5. 5 During beam injection, amplitude of beam oscillation for +0.1% off-momentum injection after both correction (α- matching and tune)

	Injected Beam Oscillation (mm)		
Bunch	**Max at septum**	**Max. and Min. at other place**	**Residual oscillation**
First	15.8	18.8-28.3	13.1-10.1
Second	18.1	19.1-28.3	17.2-14.3

5.3 Conclusion

The derived Hamiltonian for the wavelength shifter generates an extra term for quadrupole, and octupole magnet like component, which arises due to orbit offset into the wavelength shifter. The sextupole magnet component has to be taken into consideration, if side pole and main pole coupling coefficients differ with each other. In order to operate the wavelength shifter in Indus-1, local β correction/ partial and total global tunes correction may be required.

CHAPTER 6

SUMMARY AND CONCLUSIONS

In Chapter-1, basics of beam dynamics of synchrotron /storage ring including topic such as beam injection, beam optics and effect of insertion devices on beam dynamics are discussed. In Chapter-2, beam injection into the synchrotron is discussed and it is explained that why the synchrotron (common injector for Indus-1 and Indus-2) performance in terms of accelerated beam current was found better in the uncompensated orbit bump scheme as compared to the compensated orbit bump scheme. In the synchrotron, at the injection septum magnet, twiss parameters in the plane of beam injection have large values, as a result in the compensated bump injection scheme, amplitude of residual oscillations of the subsequent turns increase with a higher amount than the bump reduction rate. In the uncompensated bump scheme, it is possible to generate higher value of the bump and bump slope at the injection point, which helps in constraining the amplitude of residual oscillations for a short pulse (pulse duration equal to few times the revolution period of the synchrotron). This condition is not achievable with the three kicker compensated bump scheme. Consequently in the uncompensated bump scheme amplitude of residual oscillation of the accepted slices remain smaller as compared to the compensated bump injection scheme and this helps in achieving a higher beam current.

In Chapter-3, a double bend achromat lattice with various types of achromats such as a single QF or combination of QFs and QDs are discussed from point of view of achieving the theoretical minimum beam emittance. This structure contains either a single QF or combination of QFs and QDs to form the achromat. An analytical approach assuming quadrupoles as thin lenses have been followed for studying these structures. It is shown that with single QF structure, the theoretical minimum beam emittance is not possible. The theoretical minimum beam emittance in a given structure is possible with following combinations of quadrupole magnets QF-QF/QF-QD-QF/QF-QF-QF/QF-QF-QF-QF/QF-QD-QD-QF/QD-QF-QF-QD. This is shown that for smaller length of an achromat having QF-QD-QF and QF-QD-QD-QF structures are suitable for obtaining the minimum beam emittance.

Achromat of Indus-2 i.e. QF-QD-QF is also studied. The tunability of Indus-2 lattice for obtaining smaller beam emittance under the given constraints of optical parameters is studied by choosing different lengths of achromat. It is found that the chosen length of Indus-2 achromat is around the beam emittance of 55nmrad, which is 1.5 times of the theoretical minimum beam emittance. Initial studies indicate that in the achromat section, an additional space for insertion devices can be created by modifying the present achromat structure from QF-QD-QF to QF-QD-QD-QF.

In Chapter-4, studies carried out to reduce the beam emittance are presented. The commissioning experience of Indus-2, which is commissioned by using the moderate optics is discussed. It is shown that why it is easier to inject the beam with the moderate optics as compared to the low emittance optics. The advantage of an off-momentum beam injection is also highlighted. In order to operate the Indus-2 with the low emittance optics, a procedure is evolved and implemented at the final beam energy to reduce the beam emittance and vertical beta function by controlling the linear and nonlinear imperfections in a well-defined way to avoid any fast decay of beam current. Here an objective function employing a least square method with Lagrangian multipliers is evolved to calculate the strength of quadrupole and sextupole magnets required during transition from the moderate to low emittance optics. By using this method, the beam emittance in Indus-2 at 2.5 GeV is successfully reduced to its one third value without any additional loss of beam

In Chapter-5, a Hamiltonian for wavelength shifter is derived by considering compensated electron beam trajectory transformation. Based on this Hamiltonian, linear and non-linear forces are estimated. The result shows that in the wavelength shifter, the compensated electron beam trajectory gives additional quadrupole, sextupole and octupole components in comparison to the oscillating electron beam trajectory of the insertion devices. Based on this, effects on beam dynamical parameters are studied by considering the case of Indus-1.

Future work

1. In the synchrotron, dynamic acceptance is small, a significant beam current loss takes place in initial part of beam energy ramping. Within this region, tune point is not constant and its variation is not smooth. In the region dynamic acceptance can be partially improved by optimizing the tune point. In the present setup, facility is not available to change the tune point during the beam energy ramping process. In order to get flexibility in optimization, a new ramping scheme should be studied.
2. The double bend achromat lattice should be studied by considering a gradient or alternate gradient in the dipole magnet
3. In Indus-2, at the low beam emittance, closed orbit distortion, beta-beat as well as transverse coupling need to be properly corrected. Afterwards these corrections, the procedure, evolved here to reduce the beam emittance in Indus-2 should be used for further reducing the beam emittance by allowing finite dispersion function in the insertion section.
4. In the Indus-2 additional space for installation of insertion devices can be created by modifying the present achromat QF-QD-QF structure with QF-QD-QD-QF structure. Initial few results of this structure are presented, further detailed studies have to be carried out.
5. In Indus-2, a wavelength shifter having five poles will be used to provide a fixed source

point. In order to predict the linear and nonlinear effects of this wavelength shifter on the electron beam motion, the Hamiltonian will be derived for the double bump trajectory.

REFERENCES

[1] H. Winick, G. Brown, K. Halbach, and J. Harris, “Synchrotron radiation: wiggler and undulator magnets”, Physics Today 34, No. 5 (1981).

[2] James A Clarke, "The science and technology of undulators and wigglers”, Oxford, (2004).

[3]P. L. Hartman, “Early Experimental Work on Synchrotron Radiation”, Synchrotron Radiation News 1, No. 4 (1988).

[4] E. Karantzoulis, “Elettra 2.0-The Next Machine”, International Particle Accelerator Conference -2015, Richmond, May (2015).

[5] Y.Cai et al, “A baseline design for pep-x an ultra-low emittance storage ring”, International Particle Accelerator Conference -2010, Japan (2010).

[6] M. Bei, M. Borl and Y. Cai,P. Elleaume, R. Gerig, K. Harkay, L. Emery, A. Hutton, R. Hettel, R. Nagaoka, D. Robin and C. Steier, “The potential of an ultimate storage ring for future light sources”, Nucl. Instrum. Methods Phys. Res Sect. A 622 (2010).

[7] J. A. Thorpe, "Elementary Topics in Differential Geometry", Springer (1979).

[8] H. Widemann, “Particle Accelerator Physics volume I and II”, Springer, Berlin, Heidelberg (1995)

[9] S. Tuner, editor, “Proceedings of the 1992 CERN Accelerator School”, Finland, CERN, 94-01 (1994).

[10] E. D. Courant and H. S. Snyder, "Theory of alternating gradient synchrotron", Annals of Physics, 281(2000).

[11] S. Y. Lee, "Accelerator Physics", World Scientific (1999).

[12] M. Sands, "The Physics of Electron Storage Ring", SLAC-121 (1979).

[13] Philip J. Bryant and Kjell Johnsen, "The Principles of Circular Accelerators and Storage Rings", Cambridge University Press (1993).

[14]. R. H. Helm, M.J. Lee, P. L. Morton and M. Sands, "Evaluation of synchrotron radiation integrals", IEEE. Trans. Nucl. Sci. NS-20 (1973).

[15]. K. Ohmi, K. Hirata and K. Oide, "From the beam envelope matrix to synchrotron radiation integrals", Physical Review E 49(1) (1994).

[16]. T. Rubenheimer, "The generation and acceleration of low emittance flat beams for future linear colliders", SLAC-R-387 (1991).

[17] A. Verdier, "Chromaticity", Proceedings of CERN Accelerator School: 5th Advanced Accelerator Physics Course, p. 7, CERN 95-06 (1995).

[18] Ryutaro Nagaoka, Katsuhisa Yoshida and Masahiro Hara, "Non linear dynamics with sextupoles in low emittance light storage rings", Nucl. Instrum. Methods Phys. Res Sect. A 302, 9-26 (199l).

[19] S. Tazzari, "Apertures for Injection", Internal report, ESRP-IRM-4/83 (1983).

[20] A. Wrulich, "RACETRACK; A computer code for the simulation of the non-linear particle motion in accelerators," DESY 84-026 (1984).

[21] F. Christoph Iselin, "The MAD Program: Physical Methods Manual", CERN/SL/92 (AP) (1994).

[22] R. Maier, "High Brilliance Lattices", CERN Accelerator School, CERN 89-01 (1989).

[23] A. Streun, "Lattices for light sources", CERN Accelerator School, p55-82, CERN-2005-012 (2005).

[24] R. Chasman, G. Green and E. Rowe, "Preliminary design of a dedicated synchrotron facility" IEEE Trans. Nucl. Sci NS-22, 1765 (1975).

[25] A Jackson, "A comparison of the Chasman-Green and triple bend achromat lattices", Particle Accelerators, Vol. 22, pp. 111-128 (1987).

[26] D. Einfeld and M. Plesko, “A Modified QBA optics for low emittance storage rings” Nucl. Instrum. Methods Phys. Res Sect A 335, 402 (1993).

[27] H. Tarawneh, M Eriksson, L-J Lindgrena and B Anderberg, “MAX-IV lattice, dynamic properties and magnet system” Nucl. Instrum. Methods Phys. Res Sect. A 508 480 (2003).

[28] L. Emery, C. Chaves, Carl William Cork and Pan Wang, “The 1.2 GeV High Brightness Photon source at the Stanford photon Research Laboratory”, Particle Accelerator Conference,Washington DC (1987).

[29] M. Somer, “Optimization of the emittance of Electron storage rings”, LAL/RT/83-15 (1983).

[30] L.C. Teng, “Minimum emittance lattice for synchrotron radiation storage ring”, ANL/FNAL, LS-17 (1985).

[31] G. Wustefeld, “The minimization of natural emittance in the triple bend achromat”, BESSY TB 108/87 (1987).

[32] D. Trbojevic and E. Courant, “Low emittance lattices for electron storage rings revisited”, in: Proceedings of European Particle Accelerator Conference-94, p1000 (1994).

[33] S. Y. Lee, “Emittance optimization in three and multiple bend achromats”, Physical review E, 54, 2 (1996).

[34] E. Karantzoulis, A. Carniel, S. Krecic and C. Pasotti “Elettra status and upgrades”, Proceedings of International Particle Accelerator Conference, Busan, Korea (2016).

[35] G. H. Rees, “Injection”, Proceedings of the General Course of CERN Accelerator School, CERN, 94-01,p737 (1994).

[36] C. Bovet, D. Lamotte and R. Le Bail, “Macroparticle computer simulation of multi-turn injection into the CERN PS booster” Proceedings of the 8th International Conference on High Energy Accelerators, CERN, Geneva, P-102 (1971).

[37] L. C. Teng, “Booster injection and extraction”, BNL-26709 (1979).

[38] Taeyeon Lee and Moohyun Yoon, “A method for deriving the Hamiltonians of Insertion devices”, Nucl. Instrum. Methods Phys. Res Sect A 349, pp.316-320 (1994).

[39] Lloyd Smith, “Effects of wigglers and undulators on beam dynamics”, Report No. LBL-21391, ESG-18 (1986).

[40] K. Halbach, “Fields of undulators and wigglers,” Nucl. Instrum. Methods Phys. Res Sect A 187, pp 109-177 (1981).

[41] S. Tuner, editor, “Fifth Advanced Accelerator Physics Course”, Proceedings of the 1995 CERN Accelerator School Greece, CERN 95-06 Vol II (1995).

[42] G. Singh, D Angal-Kalinin, D. D. Bhawalkar, A. A. Fakhri, A. D. Ghodke, Pradeep Kant, Pradeep Kumar, P.K. Nema, A. S. Raja Rao, G. K. Sahoo and B Singh, “Commissioning status of Indus-1 SR facility”, Indian Journal of Pure and Applied Physics Vol. 39 1-2; pp. 96-103 (2001).

[43] D Angal-Kalinin, A Banerji, P R Hannurkar, M G Karmarkar, S Kotaiah, S P Mhaskar, P K Nema, S S Prabhu, M Pravin Kumar, S S Ramamurthi, S K Shukla, G Singh, H C Soni, and B J Vaidya, “ Synchrotron radiation source Indus-1”, Current Science 82(3) (2002).

[44] G Singh, G. K. Sahoo, D Angal, B Singh, A. D. Ghodke and Pradeep Kant. “Synchrotron Radiation Source INDUS-2”, Indian Journal of Pure and Applied Physics Vol.35, 183 (1997).

[45] “Technical report of Synchrotron radiation source Indus-2”, Center for Advanced Technology, Indore, India (1998).

[46] P R Hannurkar, S K Deb, A C Thakurta, T A Puntambekar, S R Tiwari, M R Lad, Pravin Fatnani, R S Shinde, A D Ghodke, R Sridhar, P Shrivastava, R K Sahu, R M Pandey, Jishnu Dwivedi, G. Singh, and P D Gupta “Indus Synchrotron Radiation Sources: A national Facility”, Indian Nuclear Society News Vol.10, No. 3&4 (2013).

[47] B. Singh, G. Singh and S. S. Ramamurthi, “Injection into the synchrotron for Indus-1 and Indus-2”, Indian Journal Physics 65A (6), pp. 471-478 (1991).

[48] Ali Akbar Fakhri, S.K. Prajapati and Gurnam Singh, "Injection experiment in Booster", Report no. RRCAT-09/01 (2009).

[49] B.Singh and G. Singh "Modified injection scheme for Indus-1", Report no. CAT/98-3 (1998).

[50] Ali Akbar Fakhri and Gurnam Singh, "Injection optimization for Indus-2", Asian Particle Accelerator Conference 2007, Indore, pp-146-148 (2007).

[51] Deepa Angel Kalanin and Gurnam Singh, "Beam Lifetimes and Filling schemes for Synchrotron Radiation Source Indus-2", European Particle Accelerator Conference, Paris, pp. 641-643 (2002).

[52] H.C. Soni and S. S.Ramamurthi, "Microtron injector for booster synchrotron of SR facility", Proceedings of International Conference on Synchrotron Radiation sources, Indore, p 181(1992).

[53] J Murphy "Synchrotron Light Source Data Book" BNL 42333, Ver. 4.0 (1996).

[54] G Vignola "Preliminary design of a dedicated 6-GeV synchrotron radiation storage ring" Nucl. Instrum. Methods Phys. Res Sect. A 236, 12 (1985).

[55] G.Singh, G.K. Sahoo, Pradeep Kant and S.S. Ramamurthi, "Study of achromat of INDUS-2 lattice", Presented at 3rd National seminar on Physics and Technology of Particle Accelerators and Their Applications (PATPAA-93), IUC, Calcutta Centre, November 25-27 (1993).

[56] A. A. Fakhri, B. Singh and G. Singh, "The effects of insertion devices on betatron functions and linear betatron tunes and method of their correction for the storage ring" Indus-2", CAT/98-6 (1998).

[57] G.K. Sahoo and G. Singh "Design studies of Indus-2 storage ring lattice using the code ESRO", Indian Journal of Pure and Applied Physics, 37, 371 (1999)

[58] Ali Akbar Fakhri and Gurnam Singh. "Optics for commissioning and routine operation of Indus-2", Report no. CAT/2005-15(2005).

[59] Ali Akbar Fakhri and A.D.Ghodke "Electron Beam Optics Of Indus-2 In Presence Of Insertion Devices", Indian Particle Accelerator Conference-2013, Paper ID 74, VECC, Kolkata, Nov., 19-22 (2013).

[60] G.K.Sahoo, D. K. Vats and G. Singh "Alternate high and low β configuration of Indus-2" Indian Particle Accelerator Conference-2003, CAT, Indore, pp –30-31(2003).

[61] Ali Akbar Fakhri, Pradeep Kant and Gurnam Singh "Tune Point for Indus-2" Indian Particle Accelerator Conference-2006, BARC, Mumbai pp-199-200 (2006).

[62] Ali Akbar Fakhri, Pradeep Kant and Gurnam Singh, "Explorations of various tune points for moderate optics of Indus-2 lattice", CAT/2005-16 (2005).

[63] Ali Akbar Fakhri, Sanjay Kumar Prajapati and Gurnam Singh, "Dynamic aperture results for Indus-2", CAT/2005-17 (2005).

[64] Kenji Miyata and Masatsugu Nishi, "New Operation Scheme for Low Emittance Storage Rings", Nucl. Instrum. Methods Phys. Res Sect. A 279, 640-645 (1989).

[65] Ali Akbar Fakhri, P. Kant, A. D. Ghodke and G.Singh, "Low emittance electron beam optics commissioning in Indus-2", Indian Particle Accelerator Conference-2011, Paper ID 171, IUAC, Delhi, Feb., 15-18 (2011).

[66]. R.S.Saini, Pradeep Kumar, A.A.Fakhri, Akhilesh Karnewar, A. Holikatti and A.D. Ghodke, "Experiment to find out available vertical aperture for Insertion devices in Indus-2", technical report for beam dynamics laboratory (2014).

[67].B. Singh, G. Singh and S. S. Ramamurthi "Scheme of Injection for Indus-2" CAT/I/93-3 (1993)

[68] A. A. Fakhri, and G. Singh, "Injection studies for Indus-2", CAT/2003-26 (2003).

[69] S. Jena, Ali Akbar Fakhri and A.D.Ghodke, "Beam Dynamics Requirement for Proposed Booster Extraction Septum Magnet", Indian Particle Accelerator Conference -2013, Paper ID 72, VECC, Kolkata, Nov., 19-22 (2013).

[70] Pradeep Kant, Ali Akbar Fakhri and A.D.Ghodke, "Field error tolerances of eddy current thin septum for Indus-2", Indian Particle Accelerator Conference 2013, Paper ID 78, VECC, Kolkata, Nov., 19-22 (2013).

[71] Y. Shoji, Y. Minagawa and Y. Takemura, "Off-energy injection into new Subaru", International Particle Accelerator Conference 2013, Shanghai, pp. 1913-1915 (2013).

[72] A. D. Ghodke, Riyasat Husain, Pradeep Kumar, Surendra Yadav and T. A. Puntambeker "Measurement of parameters in Indus-2 synchrotron radiation source", Rev. Sci. Instrum., 83, 10303 (2012).

[73] W. H. Press, S.A. Teukolsky William T. Vetterling, Brian P. Flanneryet, "Numerical recipes in fortran 77 The art of scientific computing", 2nd edition, Cambridge Uni Press (1992).

[74] Masahiro Katoh, Ichiro Honjo and Yukihide Kamiya, "Effect of insertion devices on betatron functions and their correction in the low emittance mode of the photon factory storage ring", Report No. KEK-86-12 (1987).

[75] M. L. James, G. M. smith and J.C. Wolford "Applied numerical methods for digital computation with fortran and CSMP", 2nd edition, pp 176-180, Harper International edition, Harper and Row publishers, New York (1977).

[76] R. K. Agrawal, A.Chauhan, G. Singh,K. Saifee, M. Seema, P. Fatnani, R. Husain and Y. Sheth, "Implementation and Experience of Energy Ramping for Indus-2", Asian Particle Accelerator Conference 2007, Indore, pp. 443–445 (2007).

[77] Pradeep kumar, A.D.Ghodke, Akhilesh Karrnewae, A. C. Holikatti, Surendra Yadav, T. A. Puntambeker, Gurnam Singh and Pitambr Singh., "Measurements of aperture and beam

lifetime using movable beam scraper s in Indus-2 electron storage ring", Rev. Sci. Instrum., 84, 123301 (2013).

[78] Akash Deep Garg, A.K. Karnewar, A. Ojha, B.B. Shrivastava, A.C. Holikatti, T.A. Puntambekar and C.P. Navathe, "Design of x-ray diagnostic beam line for a synchrotron radiation source and measurement results", Nucl. Instrum. Methods Phys. Res Sect. A 754, 15–23 (2014).

[79] Taeyeon Lee and Moohyun Yoon "A method for deriving the Hamiltonians of Insertion devices" Nucl. Instrum. Methods Phys. Res Sect. A 349 pp.316-320 (1994).

[80] V.V. Anashin P. D. Voblyi, E.S. Gluskin, N. I. Zubkov, P.M. Ivanov, P. P. Ilyinsky, V.N. Korchuganov, G.N. Kulipanov, N. A. Mezentsev, S.P. Petrov, A. N. Skrinsky, A. S. Soklov, E.M. Trakhtenberg and V. Ushakov. "Superconduting "Snake" or the dedicated SR source Siberia-1", Nucl. Instrum. Methods Phys. Res Sect. A 246 pp.99-104 (1986).

[81] N.V. Smolyakov "Focusing properties of a plane wiggler magnetic field" Nucl. Instrum. Methods Phys. Res Sect. A 308 pp.83-85 (1991).

[82] P. Beloshitsky, E. Levichev, I. Meshkov and I. Tikova "Effect of superconducting wiggler on the DELSY beam dynamics" Nucl. Instrum. Methods Phys. Res Sect. A 524 (2004).

[83] A. Wolski,"Symplectic Integrators for Nonlinear Wiggler Fields," LCC-0062, CBP-tech Note 228 (2001).

[84] Y.K. Wu, E. Forest, and D.S. Robin "Explicit symplectic integrator for s-dependent magnetic field" Physical Review E 68 pp.046502-1 046502-8 (2003).

[85] Ali Akbar Fakhri and Gurnam Singh, "A Hamiltonian for wavelength shifter and its effect on Indus-1", CAT/2004-23 (2004).

[86] Ali Akbar Fakhri and Gurnam Singh "A Hamiltonian for Wavelength Shifter and its studies on INDUS-1", Asian Particle Accelerator Conference Indore (2007).